Validation Study of Fire Dynamics Simulator

Master Thesis
Jess Grotum Nielsen (TEPE4-1002)
Department of Energy Technology
Aalborg University
June 4th 2013

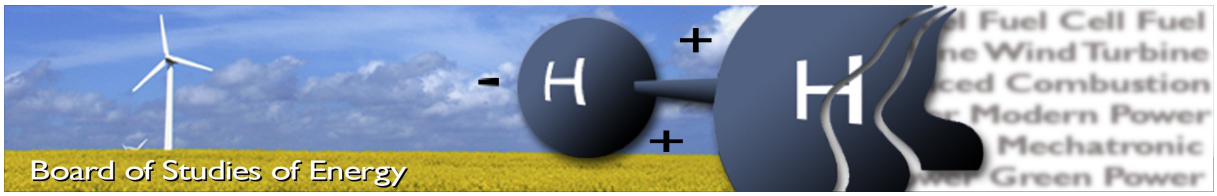

Title:	Validation Study of Fire Dynamics Simulator
Semester:	10^{th}
Semester theme:	Master thesis
Project period:	01.02.13 to 04.06.13
ECTS:	30
Supervisor:	Peter V. Nielsen and Li Liu
Project group:	Jess Grotum Nielsen (TEPE4-1002)

SYNOPSIS:

From the 1^{st} of June 2004 the building regulations was changed from only prescriptive fire protection to also include a function based option. With the function based fire protection, CFD simulation can be used to document the fire protection level. In order to use CFD for fire simulations it must be ensured that the CFD software is capable of modelling the real world, which is studied in a validation investigation.

The purpose of this report is to investigates Fire Dynamincs Simulators (FDS) ability to simulate the NFSC2 experiemt. A sufficient setup of FDS is determined in a parameter study, where different parameters impact on the results and computational time are judged. The recommended setup from the parameter study is used to a validation study of FDS with the NFSC2 experiment.

Based on the results seen in the parameter studies and in the validation studies, it is found that FDS is capable of reproducing the transient fire induced phenomenon from the NFSC2 experiment, in the most cases within the expected accuracy and in many cases within the experimental uncertainty with a prescribed HRR.

Jess Grotum Nielsen

Copies:	4
Pages, total:	96 pages
Appendices:	18 pages
Supplements:	CD-ROM attatched

Preface

This Master's thesis is written by Jess Grotum Nielsen (TEPE4-1002) of the 10^{th} semester Thermal Energy and Process Engineering at Aalborg University. The master thesis performes a validation study of Fire Dynamics Simulator, which is a computational fluid dynamics program develop for modelling of fire scenarios.

During the project periode several people has help with knowledge sharing, discussion of results, ect. Therefore, I would like to give a speciale thanks to the following persons:

- Hans La Cour-Harbo, Fire consultant / Section leader - Orbicon
- Anders Brosbøl, Section leader - Beredskabscenter Aalborg, Dept. Fire & Safety
- Dr. Kevin B. McGrattan, Mathematician at Fire Research Division - NIST
- Simo Hostikka, Principal Scientist, Team Leader - VTT Technical Research Centre of Finland

Reader's guide

The main report of the Master's thesis shows all the results obtained through the studies. The attaced appendices are used for additional calculations and information about the subject. Therefore, reading the appendices might be useful to give a full understanding of the subject investigated in this master thesis.

The Harvard referencing method is used for source references throughout the report. In the text a reference is given by [Surname, Year] the reference is then listed in alphabetic order in the bibliography in the end of the report. A nomenclature is included in the beginning of the report which shows the acronyms and the symbols used in the report. The Figures, Tables and Equations are sequentially numbered according to the chapter.

Structure of Master's Thesis

The structure of the Master's thesis is illustrated and described in Figure 1.

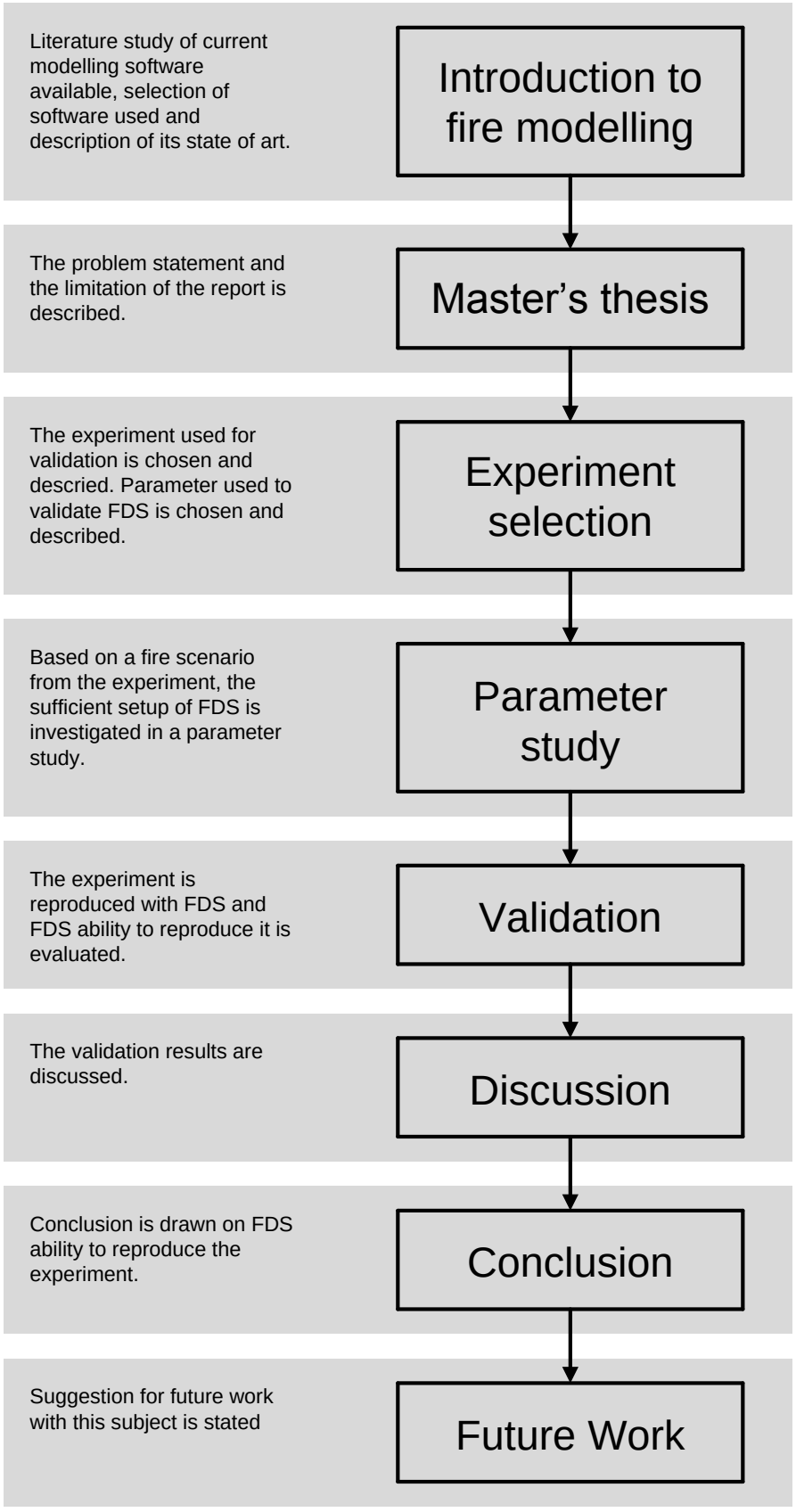

Figure 1. Flow diagram of the structure of the master thesis master project.

Summery

From the 1st of June 2004 the building regulations was changed from only prescriptive fire protection to also include a function based option. The advantage of using the function based fire protection is that it allows the architect and consulting engineer to make a new building layout and architecture, they just have to show the fire protection is sufficient with for eaxmple CFD fire simulation.

In order for the consulting engineer to use CFD for fire simulations he must ensure that the CFD software used is capable of modelling the real world which is studied in a validation investigation. These validation are typically collected in validation guide where the consulting engineer can find a similar case as the new design case he want to use CFD on. Therefore, this report is the documentation of the validation study performed on Fire Dynamics Simulator (FDS). FDS is chosen beacuse it is the most commonly used software in Danmark for CFD fire simulations.

The purpose with this validation study is to determines FDS ability to reproduce the fire induced phenomenon experienced in the "Experimental Study of the Localized Room Fires - NFSC2 Test Series" experiment from VTT Technical Research Centre of Finland.

The NFSC2 experiment was performed by Simo Hostikka, Matti Kokkala and Jukka Vaari from VTT. This experimental study consists of two series of full scale fire tests, which were produced in order to produce well-documented data for CFD code verification. The fire test which is used in this report is an experimental series which consist of 21 tests in a 10 x 7 x5 m3 test room with a 2.4 x 3.0 m2 opening to ambient. During the 21 tests the fire size and locations were varied to investigate its impact on the gas temperature, wall temperature, etc. From the NFSC2 experiment fire scenarion one is chosen as the reference scenario for the parameter study.

The purpose with the parameter study is to determine a sufficient setup for the validation study of the NFSC2 experiment. The sufficient setup is determined with a parameter variation study. The parameter simulation results are compared with the experimental results and based on this comparison a conclusion is made for the particular parameter. The table below shows the investigated parameter and the conclusion made in each study which together is the recommended setup for validation of FDS

Parameter	**Conclusion**
Heat release rate	Combustion eff. 0.85
Pool size	Equivalent circumference
Radiation model	1 band (grey gas model)
Radiation domain	100 angles
Computational domain	Room, 3.2 m extension
Flow mesh	8.0 cm

The recommended setup is then used to validate FDS against fire scenario one and two of the NFSC2 experiment. The two fire scenarios are compared by the hot gas layer (HGL) height, HGL upper temperature and the ceiling jet temperature. The validation study of FDS shows that it has the ability to reproduce the experimental results with in the expected difference of 10-20% and in many cases when the

fire is burning the relative difference is below 10%. When the fire is extinguish higher difference between the results are seen for the HGL height in both fire scenario one and two, where the relative difference is up to approximately 45% in fire scenario two.

Based on the results seen in the parameter studies and in the validation studies, it is found that FDS is capable of reproducing the transient fire induced phenomenon from the NFSC2 experiment, in the most cases within the expected accuracy and in many cases within the experimental uncertainty.

Contents

Nomenclature

Acronym	Description
CFD	Computational Fluid Dynamics
DNS	Direct Numerical Simulation
FDS	Fire Dynamics Simulator
HGL	Hot Gas Layer
HRR	Heat Release Rate
NFSC2	Experimental Study of the Localized Room Fires - NFSC2 Test Series
NIST	National Institute of Standards and Technology
RANS	Reynolds-Averaged Navier-Stokes
VTT	VTT Technical Research Centre of Finland

Symbol	Description	Unit
r	Stoichiometric ratio	[-]
$\dot{Q}$	Peak heat release rate	[kW]
$\dot{Q}$	Heat release rate	[kW]
$\dot{Q}$	Total heat release rate	[kW]
$\dot{m}_f$	Mass flux of fuel	$\left[\frac{kg}{s\ m^2}\right]$
$\dot{m}_{O_2}$	Mass flux of fuel	$\left[\frac{kg}{s\ m^2}\right]$
A_O	Area of the compartment opening	$[m^2]$
H_O	Height of the opening	[m]
ρ	Density of the air,	$\left[\frac{kg}{m^3}\right]$
$\dot{V}$	Volume flow of air into the compartment	$\left[\frac{m^3}{s}\right]$
χ	Efficiency of the combustion	[-]
$\dot{m}$	Mass loss rate	$\left[\frac{kg}{s}\right]$
ΔH_c	Heat of combustion	$\left[\frac{MJ}{kg}\right]$
ϵ	Relative difference	[-]
M_p	Model peak value	
M_0	Model start value	
E_p	Experimental peak value	
E_0	Experimental start value	
s	Unit direction vector of the intensity	
$\nabla\ I_\lambda(x,s)$	The derive radiation intensity at wavelength λ in cell x and in the s direction	$\left[\frac{W}{m^3}\right]$
$\kappa(x,\lambda)$	Absorption coefficient in cell x for wavelength λ	$\left[\frac{1}{m}\right]$
$I_b(x)$	Radiation intensity source term in cell x	$\left[\frac{W}{m^2}\right]$
$I_\lambda(x,s)$	Radiation intensity at wavelength λ in cell x and in the s direction	$\left[\frac{W}{m^2}\right]$
$\nabla\ I_n(x,s)$	The derive radiation intensity at band n in cell x and in the s direction	$\left[\frac{W}{m^3}\right]$
$\kappa(x,n)$	Absorption coefficient in cell x for band n	$\left[\frac{1}{m}\right]$
$I_{b,n}(x)$	Radiation intensity source term for band n in cell x	$\left[\frac{W}{m^2}\right]$
$I_n(x,s)$	Radiation intensity at band n in cell x and in the s direction	$\left[\frac{W}{m^2}\right]$
I(x,s)	Total intensity in cell x in the s direction	$\left[\frac{W}{m^3}\right]$
D	Diameter of the fuel source	[m]
L	Mean flame height	[m]
$\dot{Q}_c$	Convective heat release rate	[kW]
$\dot{Q}_c$	Convective heat release rate	[kW]
$\dot{m}_c$	Plume mass flow	$\left[\frac{kg}{s}\right]$
z	Height where the plume mass flow is determined	[m]
P	Perimeter of the fire	[m]

Introduction to Smoke and Fire Simulation

1

This chapter is an introduction to the subjects concerning validation/benchmark test of computational fluid dynamic (CFD) fire simulations. The chapter opens with a description of the use of CFD fire simulation in Denmark according to the Danish building regulations. It continues with an introduction to fire dynamics and CFD fire simulations, where the turbulence models will be described together with the available CFD software. Finally the chapter finish off with a description of Fire Dynamic Simulator (FDS) which is the chosen CFD software for the validation/benchmark test. The term fire simulation are used through out the report and it covers the both simulations of fire and simulation of smoke movement.

1.1 Fire Protection in Denmark

The building regulation has demands to the fire protection level in building to prevent personal injuries and building damages. The main focus in the building regulations is on person evacuation and safety. Therefore, the focus in the building regulations is on smoke management, evacuation and fire protection. Smoke management is a ventilation form where the smoke and heat is removed from the building as fast as possible without any discomfort for the people that are being evacuated. This also improves the working condition for the fire brigade, decreases the damages on the building and decreases the fire spread [Nielsen, 2010].

Even though the building regulations has demands on the fire protection level an average of 77 persons are killed every year in fires from 2000-2012 [Beredskabsstyrelsen, 2013]. In a report from 1998 the social costs of fires in Denmark are estimated by Danish Emergency Management Agency. The Danish Emergency Management Agency estimated the social costs to be around 1% of the Gross Domestic Product which in 1998 corresponded to 9.8-10.8 billions Danish kroner. The social costs covers both the humans cost, direct cost, administration of fire insurance, cost of rescue service and finally the prevention costs, where the last is estimated to 4.9-5.9 billions Danish kroner and thereby it covers around 50 % of the total social costs. The preventions costs in the analysis covers the initiative which is done on building with the only purpose of reducing the consequence of fires [Møller, 2000]. Therefore, there is a potential for decreasing this costs by using new fire protection strategies which were allowed with the change of the building regulation in 2004 to allow the use of function based fire protection.

From the 1st of June 2004 the building regulations was changed from only being prescriptive to also include a function based option regarding fire protection. The function based fire protection option enables the architect and consulting engineer to exploit new and innovative building designs and fire protection solutions. The prescriptive fire protection is based on many years' experience from building fires and can be used when designing traditional buildings, e.g. houses and stables. After 1st of June 2004 the prescriptive fire protection where compiled into the document in Danish called "Eksempelsamling om

brandsikring af byggeri 2012" (in English: Example collection about fire protection of building 2012). The function based fire protection can be used when new architecture or very high atriums is designed. With the function based fire protection the consulting engineer has to prove the fire protection level through calculation, e.g. CFD calculation.

The advantage of using the function based fire protection is that it allows the architect and consulting engineer to make a new building layout and architecture, they just have to show the fire protection is sufficient with calculation for example CFD calculation. This leads to the main disadvantage of the function based fire protection, because the calculation needs documentation of the fire protection level, but also that the CFD calculation is valid in the case. The opposite advantage and disadvantage are valid for the prescriptive fire protection, because with the prescriptive fire protection the build just have to be designed after some given rules, which makes the documentation more simple on the other hand the architectural freedom is more limited. Both methods can be used in a fire technical documentation, which can be requested by the city council when assessing a building permission.

1.1.1 Fire technical documentation

The purpose of the fire technical documentation is to demonstrate that the buildings fire safety level is obtained and maintained throughout the service life of the building. It contains a description of the buildings [Energistyrelsen, 2012]:

- Presentation
- Application
- Location
- Escape route
- Passive fire protection
- Active fire protection
- Rescue services ability to work
- Operational and maintenance conditions

The escape route and evacuation of persons can be performed with computer based evacuation simulation. Computer based evacuation simulation is used to calculate and visualise the human behaviour during an evacuations in case of an emergency, e.g. fire. There exists different evacuation software, one of which is Pathfinder from Thunderhead Engineering Consultant, Inc. and FDS+Evac from VTT Technical Research Centre of Finland (VTT). In the latter software it is possible to have simultaneous simulations of the fire and the evacuation process [Korhonen & Hostikka, 2009]. Both software treats each evacuee as a single entity, where it is possible to assign each evacuee with its own properties and evacuation strategies [Korhonen & Hostikka, 2009] [Thunderhead Engineering, 2011].

The passive fire protection is the fire safety protections which does not need activation of any kind. Examples of passive fire protection are a fire door, a fire section, a fire barrier, etc. Normally the passive fire protection is shown on the drawings and follows the demands in the Example collection about fire protection of building 2012 [Sørensen, 2004]. The active fire protection is a collective name of fire protection plants which all need activation from a sensor before the plant delivers the fire protection. Examples of active fire protection are an automatic sprinkler system, an automatic fire door closing system, an automatic fire call system, etc. The collaboration between the system and the operational and maintenance conditions is typically described in the technical fire documentation [Sørensen, 2004].

The extent of the fire technical documentation is decided by the city council. The consulting engineer and the city council typical agrees on the level of fire technical documentation in a prior meeting before the building design is decided [Energistyrelsen, 2012]. In the fire technical documentation it is possible to use CFD fire simulation to show the fire protection solution used in the building.

In order to used CFD in the fire technical documentation it is important to know the accuracy of the CFD software and for which fire scenario the software is validated [Erhvervs- og Boligstyrelsen, 2004]. Hence the consulting engineer companies, such as NIRAS Safety, COWI etc., and the public authority represented by Copenhagen and Fredericia fire department have made a industry guideline called: CFD Best Practice. The purpose of the CFD Best Practice is to standardise the implementation and documentation of the CFD fire simulations and it is accepted by both the consulting engineers and the public authority [Jakobsen et al., 2009].

Because CFD fire simulation is a tool in the fire technical documentation it is therefore interesting to look into the state of art of CFD fire simulations, which is done in the next section.

1.2 CFD Fire Simulations and Fire Dynamics

For a fire to burn the following three things needs to be present: oxygen, sufficient high temperature and combustible material. When these three components are present the fire is initiated with an ignition, where the material is heated and starts to gasify. The gas then burns when it comes into contact with the oxygen. The burning of the gas release an amount of heat, which then again heats the combustible material and the fire can continue until one of the three things is not presented any more.

The simple description of a fire given above contains many complex phenomenons, such as the combustion of the combustible gasses, the mass transfer of solid material to combustible gasses, the buoyancy driven fluid flow away from the fire, the heat transfer from the flame to the combustible material and the surrounding. These complex phenomenons can be modelled with the use of CFD.

CFD is a numerical tool to solve the governing equations for fluid flow. The governing equations include Navier-Stokes equations, mass-, energy-, and species conservation which can be applied to both laminar and turbulent flows. The area of interest is divided into many small volumes, where the equations are discretised into algebraic equations. Furthermore the turbulence of the fluid flow must also be solved and this is typically done by using turbulence models, because direct solving of the turbulent structure demands very large computational time. The turbulence modelling used by fire models are evaluated in the next section. The section is based on "Fire Modeling: Where Are We? Where Are We Going?" by Dr. Kevin McGrattan from National Institute of Standards and Technology (NIST) [McGrattan, 2005].

1.2.1 Turbulence model for fire simulation

Within CFD fire simulation three different turbulence CFD techniques are available: Direct Numerical Simulation (DNS), Large Eddy Simulation (LES) and Reynolds-Averaged Navier-Stokes (RANS). The three turbulence models are described in further details in Appendix C.3.

DNS is a direct solving of the governing equations and this requires a very fine spatial and temporal discretisation. Therefore, the DNS technique is not practical for large-scale fire simulations. Both LES and RANS uses models to solve the unresolved dissipative processes. The difference between LES and RANS is that LES attempts to compute as many of the large eddies and estimate the small eddies, whereas RANS make an averages over significantly larger spatial and temporal scales.

To declare a winner between the LES and RANS turbulence modelling would probably be scenario dependent. A scenario where the user is only interested in a "steady state" solution and the turbulence can be assumed "homogeneous" will be handled very well by RANS. At NIST they maintained that LES is better at representing fire-driven flows such as fire plumes, ceiling jets, etc. They also believe that when more sophisticated models for combustion processes within a fire are developed, LES will be better than RANS. The belive this because when a fire is time-averaged to the degree demanded by RANS, this time-averaging will not allow for at modelling of the fire dynamics the allready seen [McGrattan, 2005].

The next section looks into the CFD software currently available for fire simulations.

1.2.2 CFD fire simulation software

A survey performed in 2003 by [Olenick & Carpenter, 2003] lists the CFD software available for fire simulation. Some of the CFD software are listed below. The complete list can be seen on the surveys homepage [Olenick, 2008].

- CFX
- FLUENT
- FDS (Fire Dynamic Simulator)
- JASMINE
- SOFIE
- And many more.

CFX and FLUENT are general purpose CFD software which now is part of the ANSYS software packed, where many different turbulence and combustions models are available. CFX and FLUENT can be purchased from ANSYS.FDS is a low Mach number CFD software developed by NIST specific to fire-related flows, where LES turbulence model is used. FDS is available for free CFD software.

JASMINE can be used for modelling of fire consequences and evaluate design solutions such as for example smoke management. JASMINE uses a standard k-ϵ turbulence model. The JASMINE software is available on request. SOFIE is the contraction of "Simulation of Fires in Enclosures" and it is a CFD code which uses a k-ϵ with incorporated buoyancy modifications. Both commercial and research license is available.

According to the Danish building regulations chapter 1.3 paragraph 2, the authority can make demands about their ability to read the electronic documentation, e.g. the CFD software. This demand from the authorities means that the consulting engineer also must consider this when choosing the CFD software which is used to perform the fire simulations. In Denmark, FDS is the commonly used CFD software for both the consulting engineering companies and the fire preventions authorities [Jakobsen et al., 2009].

Based on the above discussion of CFD fire simulations software it is decided to work on with the FDS because it is the most commonly used software concerning fire simulation in Denmark [Jakobsen et al., 2009]. FDS will therefore be described and analysed in the following section.

1.3 Fire Dynamic Simulator

FDS is a CFD software developed by NIST and VTT to solve fire-driven fluid flow. The software solves numerically a form of the Navier-Stokes equations appropriate for low-speed, thermally-driven flow with focus on smoke and heat transport from fires. To visualise the FDS results with animations the Smokeview program is included [McGrattan et al., 2012c], see Figure 1.1 for a screenshot of smokeview.

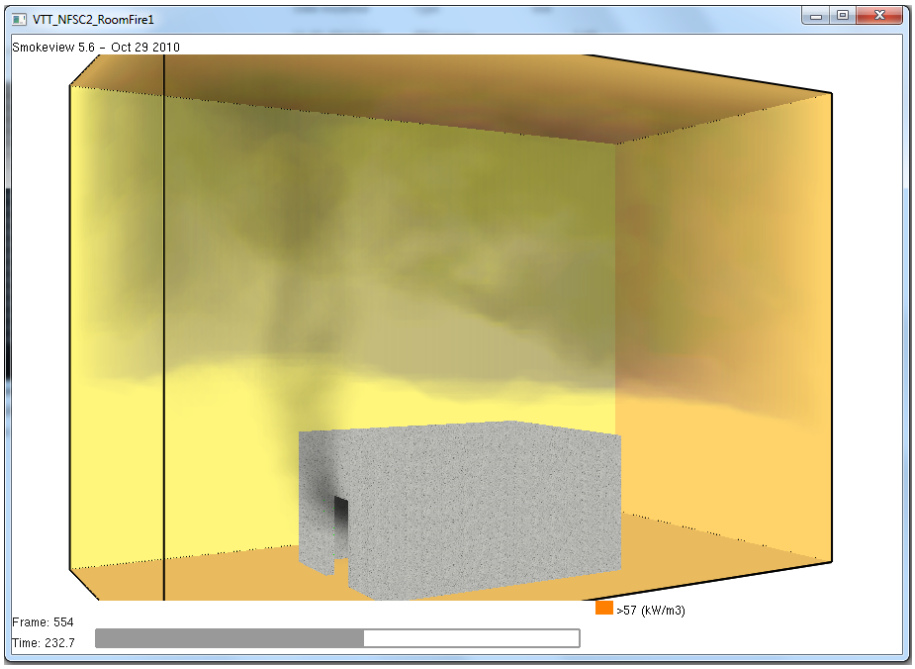

Figure 1.1. A screenshot of the Smokeview application. Smokeview is used to visualise the results from FDS.

FDS version 1 was publicly released in February 2000 at the present time FDS is in version 5.5.4 and version 6 is out in a beta testing version. FDS is developed to solve practical fire problems encountered in fire protection engineering and currently it is possible to use FDS to [McGrattan et al., 2012c]:

- Low speed transport of heat and combustion products from fire
- Radiative and convective heat transfer between the gas and solid surfaces
- Pyrolysis
- Flame spread and fire growth
- Sprinkler, heat detector, and smoke detector activation
- Sprinkler sprays and suppression by water

The governing equations of mass, momentum and energy are approximated with a finite differences method and the thermal radiation solver is computed using a finite volume technique. The solutions of the equations are updated in time on a three-dimensional rectilinear grid. Finally Lagrangian particles are used to simulate sprinkler discharge, fuel sprays, and smoke movement [McGrattan et al., 2012c].

When using a CFD software, two terms are very important for the end user namely the verification and the validation. Verification is checking the mathematical equations whereas validation is to check how good the software models the real world. The user of a CFD software must go through the two terms every time he starts a new simulation. To make this evaluation of the CFD software verification and validation capability, the CFD software must have verification and validation guides. These guides for FDS are made by the developers and the user community.

With the validation guide the end-user can compare his case to the cases in the validation guide and make a judgement if FDS can be used for the current case. Therefore, the more validation cases included in the validation guide the more new design cases can be simulated with FDS. The focus in this report is on performing a validation study of a chosen experiment to increase FDS validation range.

1.3.1 Validation Examples

The former validation work done for FDS, which consists of 40 experiments, are collected in a validation guide [McGrattan et al., 2012b]. The FDS validation guide consists of a collection of fire experiments which have been reproduced in FDS. FDS ability to reproduce the experiments are illustrated by plots where the experimental results and the FDS simulation results arecompared, an example of such a graphical comparison is shown in Figure 1.2.

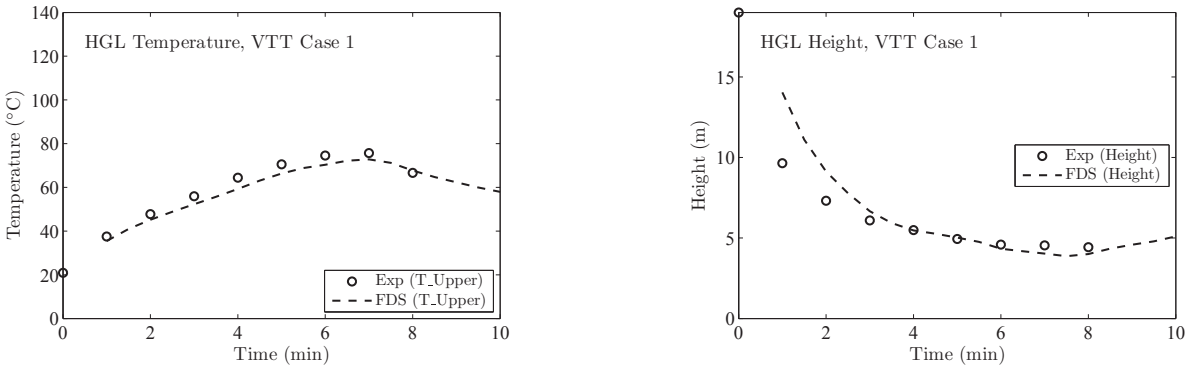

Figure 1.2. Example of graphical comparison of a experiment and the FDS simulation, as it is presented in the FDS validation guide [McGrattan et al., 2012b].

The two validation cases UL/NIST Vent Experiments and FM/SNL Test Series are described next to give an overview of which parameter are validated for the two cases [Floyd et al., 2012]. The UL/NIST Vent Experiments was conducted in 2012 by the Fire Fighting Technology Group at NIST in order to determine how the opening of ceiling vents affects the compartment temperature. The compartment is 6.1 m by 4.3 m by 2.4 m with a single door opening. The compartment temperature was measured with two vertical arrays of thermocouples and the door velocity and temperature were measured with thermocouples and bi-directional velocity probes. The UL/NIST Vent Experiments was used to validate FDS ability to calculate the hot gas layer (HGL) height and temperature and the ceiling jet temperature [Floyd et al., 2012]. In Figure 1.3 the comparison between the experiment and FDS for the ceiling jet temperature is shown.

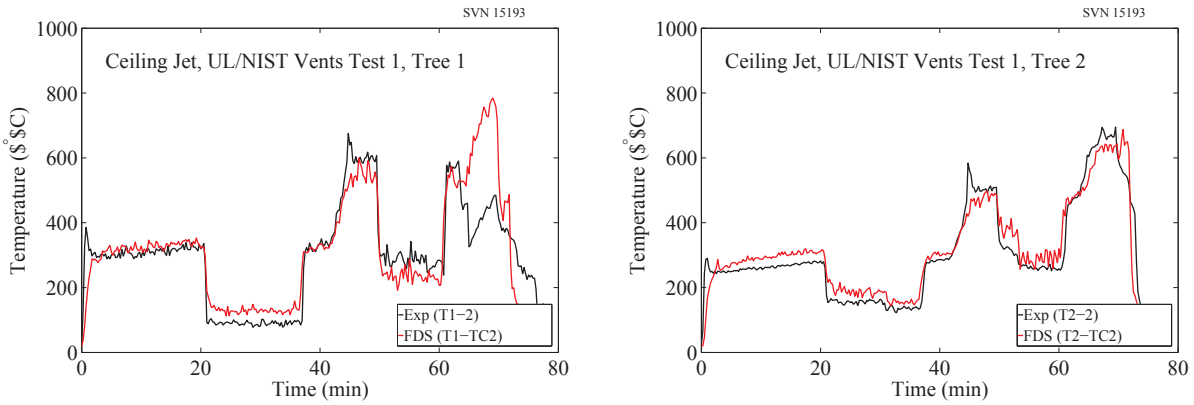

Figure 1.3. Illustration of FDS capability to preproduce the ceiling jet temperature in the UL/NIST Vents experiment [Floyd et al., 2012].

The FM/SNL Test Series were conducted in 1986 by The Factory Mutual and Sandia National

Laboratories and consists of 25 compartment fire experiments. The experiments were conducted in order to provide experimental data which can be used to validate computer models. The test room was 18 m by 12 m by 6 m, with forced ventilation. Thermocouples measured the HGL temperature and height, the ceiling jet temperature and the plume temperatures [Floyd et al., 2012]. The comparison of the plume temperature is shown in Figure 1.4.

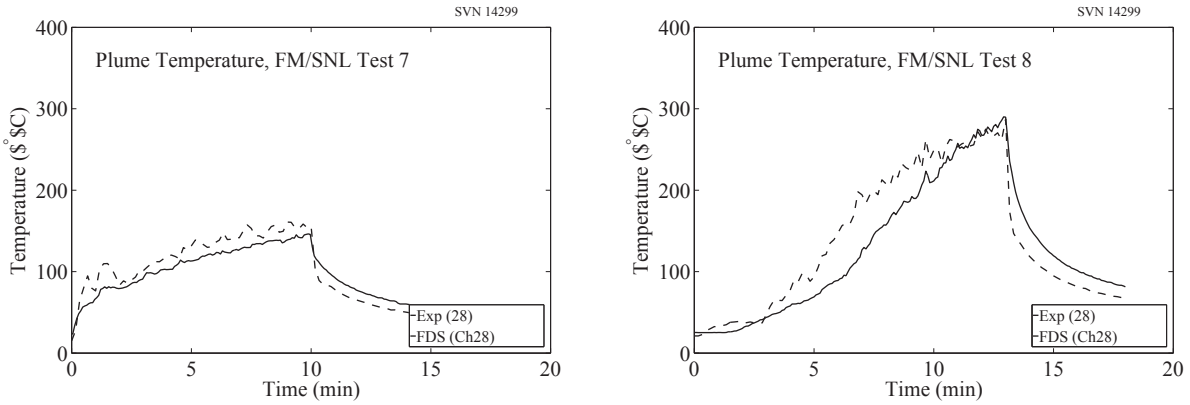

Figure 1.4. Illustration of FDS capability to preproduce the plume temperature in the FM/SNL experiment. [Floyd et al., 2012].

The project manager of the FDS development Dr. Kevin McGrattan tells that many of the experiments found in the validation guide is experiment which were made for other purpose then CFD validation [McGrattan, 2013]. Therefore, many new validation experiments are found by searching for experiments from research labs such as VTT, SP Sweden and NIST. Depending on the experimental data found the experiment is then used to validate many aspect of a fire scenario as possible. In order for an experiment to be used to a validation study it is necessary to know the input to the fire, e.g. the heat release rate (HRR). When the HRR is specified to FDS and the purpose of the simulation is to determine the transport of heat from the fire, then FDS predicts the flow velocities and temperature with accuracy within 10%-20% with the optimal grid solutions. If the HRR is predicted instead of specified the uncertainty is higher [McGrattan et al., 2012c].

The experiment used for validation of FDS in this report is the *"Experimental Study of the Localized Room Fires NFSC2 Test Series"* (NFSC2) from VTT. The NFSC2 is dimensional in between the two above cases and can therefore be used to validate FDS ability to determine the transient fire development when the pool burning rate is prescribed.

Master's Thesis and Delimitation 2

The aim of this project is to perform a validation study with a benchmark test of FDS capability to reproduce the fire induced phenomenons which are experienced during the NFSC2 experiment performed by VTT. Therefore, the Master's thesis is given as:

Can Fire Dynamics Simulator be used to simulated the fire induced phenomenon in the NFSC2 fire experiment.

In order to answer the Master's thesis supplementary questions are stated:

1. Can FDS reproduce the results from the NFSC2 experiment with a prescribed heat release rate
2. How does the FDS results compared with analytical results obtained from plume models
3. What is the sufficient setup of FDS to validate the NFSC2 experiment.

The Master's thesis and the additional questions are answer with the solution strategy presented in the next section.

2.1 Master Thesis Solutions Strategy

Figure 2.1 shows the solutions strategy for answering the Master's thesis stated above.

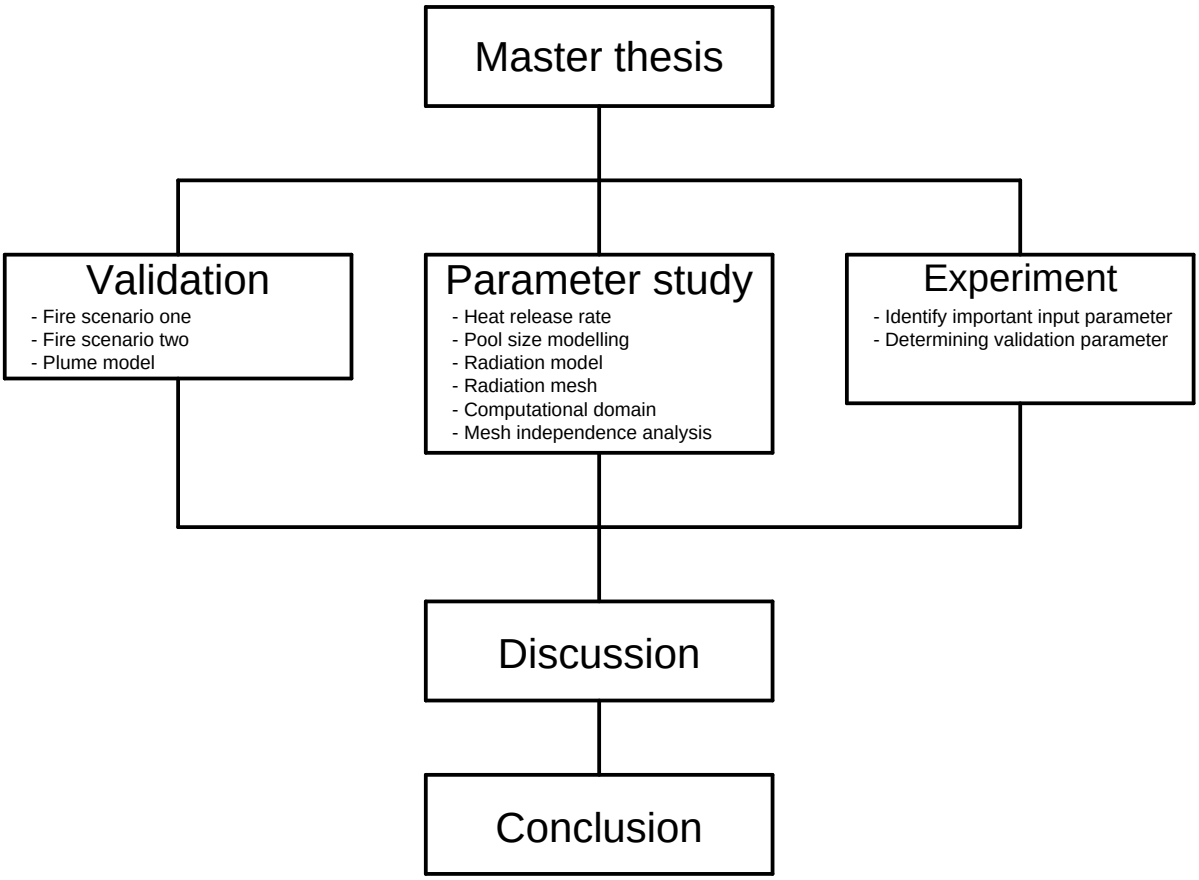

Figure 2.1. The solutions strategy used for answering of the master thesis.

A clarification of Figure 2.1 is described below.

Study of NFSC2 Experiment
The NFSC2 experiment is chosen as benchmark experiment for the validation study of FDS. In order to use the experiment for the validation study the following task is performed:

- Identify important input parameter
- Determining validation parameter

Parameter Study - Setup of FDS
The parameter study is performed in order to determine the sufficient setup of FDS for the validation study. The sufficient setup is determined by the relative difference to the experimental results and the amount of computational time used to obtain the results. In the parameter study the following parameters are investigated:

- Heat release rate
- Pool size modelling
- Radiation model
- Radiation mesh
- Computational domain
- Mesh independence analysis

Validation of FDS with Fire Scenario One and Two
The setup of FDS determined in the parameter study is used to validate two fire scenarios from the NFSC2 experiment. In order to also show FDS capability according to the analytical plume models, their results are compared and discussed.

2.2 Master Thesis Delimitation

In the answering of the Master's thesis, the following limitations are listed in order to limit the extent of the investigation.

Validation parameter: During the test about 150 measurements were made. Therefore, important measurements are chosen as validation parameters.

Transient simulations: All measurements in the experiment are time depending and therefore the comparison with FDS are made transient. Expect when the velocity profile in the door is used.

Standard setup of FDS: The validation study of FDS is performed with the standard setup of FDS and important parameters impact on the results are tested in a parameter study.

Version of FDS: FDS version 5.5.3 is used for all simulations.

Theory 3

This chapter contains a theoretical description of the fire induced phenomenons encountered in enclosed fire scenarios such as the scenarios in the NFSC2 experiment. Furthermore the theoretical backgrounds for analytical plume models are outlined here. The results from the plume models are determined in Appendix B, where one plume model is chosen for comparison with the results obtained from the FDS simulations.

3.1 Enclosure Fire dynamics

Fire in an enclosure can evolve into many different fire scenarios depending on the enclosure geometry, ventilation openings, fuel sources, etc. [Karlsson & Quintiere, 2000]. Therefore, the following description is based on [Karlsson & Quintiere, 2000] and illustrated by the use of fire scenario one from the NFSC2 experiment. The ceiling and one wall of the enclosure are made transparent to visualise the different phenomenons described below.

The heptane pool is ignited and the fuel starts to burn and smokes rises to the ceiling in a fire plume which is illustrated to the left in Figure 3.1. In the plumes the hot smoke rises due to buoyancy. The colder air surrounding the plume is then entrained into the plume. When the plume reached the ceiling the gases are spread on the ceiling as momentum driven ceiling jets, which illustrated to the right in Figure 3.1.

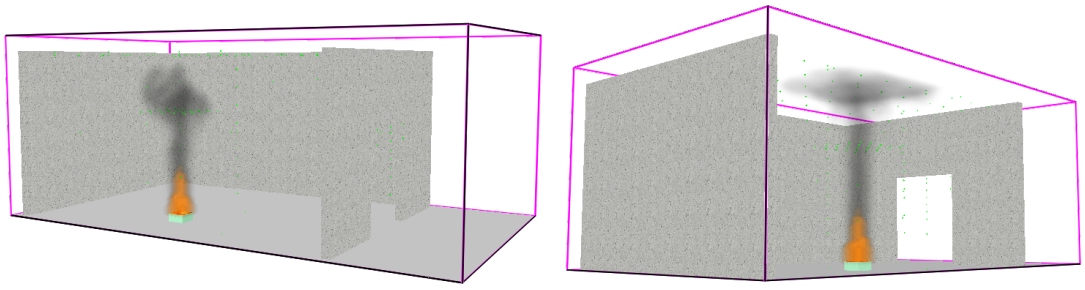

Figure 3.1. To the left is the fire plume shown just after ignition. To the right a ceiling jet is illustrated.

The ceiling jets continue along the ceiling until they reaches the wall where they are deflected downwards the wall. The smoke is still warmer than the surrounding air and again the smoke will rise due to buoyancy and eventual form a layer of hot gases below the ceiling, which is illustrated to the left in Figure 3.2. The hot gas layer continues to grow until it reaches the height of the opening to the ambient and the smoke starts to flow out of the opening. Eventually the hot gas layer reaches a steady state where the amount

of smoke flowing out of the door equals the smoke supplied by the pool fire. This steady state height of the hot gas layer is illustrated to the right in Figure 3.2.

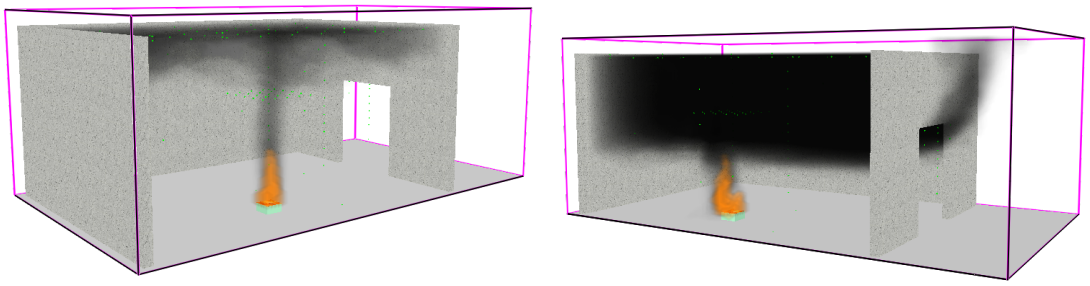

Figure 3.2. To the left it is illustrated how the smoke first moves down the wall and then due to buoyancy rises to the ceiling. To the right it is illustrated how the smoke flows out of the room when the HGL reaches the top of the opening.

As the hot gas layer grows and its temperature increases the heat transfer process is augmented. The hot gas layer transfers heat through convection and radiation to the ceiling and walls. The heat transfer to the lower gas layer and the floor is only through radiation. No further development of fire driven phenomenon is seen in the experimental test due to the experimental configuration.

If instead the fire was in a room with more fuel sources the fire will grow by either increased burning rate, flame spread from the original source or by ignition of other fuel sources. This is termed flashover and it describes the situation where all flammable material in the room contributes to the fire. When a fire is burning the fire is either well- or under-ventilated and these two expressions are described in further details next.

3.1.1 Fuel- or Ventilation-controlled Fire

In compartment fires a fire is either fuel- or ventilation-controlled. A fire is fuel-controlled when there is sufficient oxygen available for the combustion. In this phase the growth of the fire depends only on the fuel and the geometry of the fire source. A compartment fire is typically fuel-controlled after ignition and in the initial stage, the fire can also be fuel-controlled later on. In a ventilation-controlled fire there is not a sufficient level of oxygen available to combust the majority of the flammable fuel gasses. The heat release rate is then controlled by the amount of oxygen that enters the enclosure openings [Karlsson & Quintiere, 2000].

In the validation guide for FDS a global equivalence ratio ϕ is used to describe if a fire is well-ventilated or under-ventilated. The global equivalence ratio is determined with Equation 3.1 [Floyd et al., 2012].

$$\phi = \frac{\dot{m}_f}{r\dot{m}_{O_2}} = \frac{\dot{Q}}{13100\dot{m}_{O_2}} \tag{3.1}$$

where	r	=	stoichiometric ratio	[-]
	$\dot{Q}$	=	peak heat release rate	[kW]
	$\dot{m}_f$	=	mass flux of fuel	$\left[\frac{kg}{s\ m^2}\right]$
	$\dot{m}_{O_2}$	=	mass flux of oxygen	$\left[\frac{kg}{s\ m^2}\right]$

The mass flux of oxygen into the compartment for natural and mechanical ventilation is determined with Equation 3.2 [Floyd et al., 2012].

$$\dot{m}_{O_2} = \begin{cases} \frac{1}{2} 0.23 A_0 \sqrt{H_0} & : \text{Natural Ventilation} \\ \\ 0.23 \rho \dot{V} & : \text{Mechanical Ventilation} \end{cases} \tag{3.2}$$

where	A_0	=	area of the compartment opening	$[m^2]$
	H_0	=	height of the opening	$[m]$
	ρ	=	density of the air	$\left[\frac{kg}{m^3}\right]$
	$\dot{V}$	=	volume flow of air into the compartment	$\left[\frac{m^3}{s}\right]$

A compartment is considered well-ventilated if $\phi < 1$ and under-ventilated if $\phi > 1$. The global equivalence ratio is between 0.03-0.20 for the ten different fire scenarios in the NFSC2 test and thus they are all well-ventilated.

3.2 Plume Models

The purpose with the plume model is to determine the HGL height by the use of Heskestads and Thomas' model. The theoretical background for the plume models are described in this section and the HGL height is calculated in Appendix B. The determined HGL height are then compared with the FDS results in Section 6. Firstly, the concept of two zone models are shortly described before determining the equations for Heskestads and Thomas' plume model

3.2.1 Two Zone Model

The two zone model is a deterministic model used to simulate the fire environment for an enclosure fire. Figure 3.3 illustrates the basic concepts of two zone models.

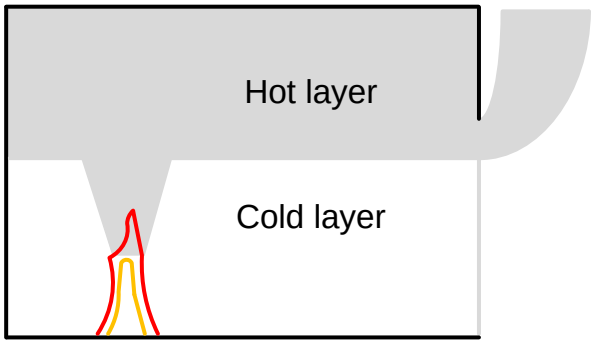

Figure 3.3. Illustration of the two zone model principles. The enclosure is divided into a hot and a cold zone where the conservation equations are setup between these two zones.

In a two zone model the enclosure is divided into two gas zones consisting of a upper hot zone and a lower cold zone, that develops due to buoyancy [Karlsson & Quintiere, 2000]. To solve a two zone model multiple conservation equations are applied to each of the two zones together with mathematical models of reality, such as the plume model. The two zone model can be used to determine the temperatures of the zones, height of the layers, etc. The full two zone model is not investigated further because of limited time. In the following section three different plume models are described.

3.2.2 Plume Models

The plume is defined as the phenomenon illustrated in Figure 3.4.

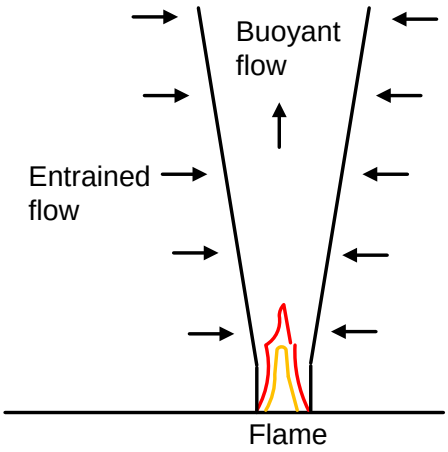

Figure 3.4. Illustration of a plume with a flame, buoyant flow and air entraintment from the cooler surrounding air.

In Figure 3.4 the combustion process makes a visible flame and the hot combustion products are formed in the colder surroundings. Due to buoyancy the hot and less dense combustion product rises upwards [Karlsson & Quintiere, 2000]. The colder ambient air is then entrained into the combustion product and dilutes the combustion products.

The plume is divided into different groups depending on the given scenario. The most commonly used plume in fire safety engineering is the buoyant axisymmetric plume which consists of a diffusion flame. A diffusion flame is when the fuel and oxygen are initially separated and they are mixed by the process of diffusion [Karlsson & Quintiere, 2000].

Ideal Plume Model

The illustration of the characteristics for a buoyant axisymmetric plume are shown in Figure 3.5.

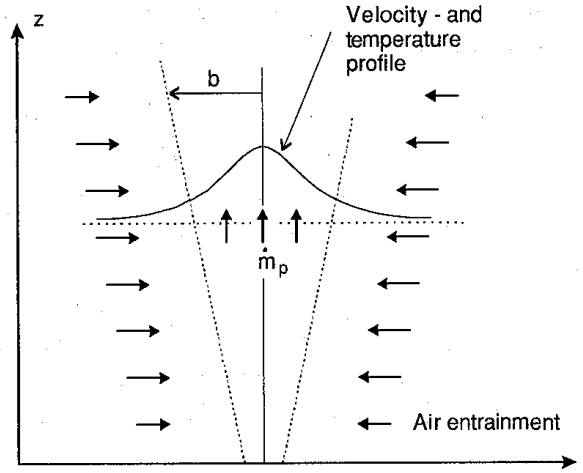

Figure 3.5. Illustration of the parameters used in the development of analytical solutions of an ideal plume [Sørensen, 2004].

The analytical solutions for the plumes temperature, velocity, radius and mass flow is determined based on the below listed assumptions [Karlsson & Quintiere, 2000].

1. All energy from the point fire source is only transported in the plume and no heat is lost due to radiation
2. The density variation through the plume is assumed to be small and is only calculated when the difference $(\rho_\infty - \rho)$ is presented in the equations for the ideal plume.
3. A "top hat" profile is assumed for T and u. Furthermore it is assumed that u = 0 and T = T_∞ outside the plume radius.
4. The entrainment velocity v is assumed to be v = α u, where $\alpha = 0.15$

Based on the continuity equation and the momentum-buoyancy equation, expressions for the ideal plume are derived. The equations for the ideal plume are shown in further details in [Karlsson & Quintiere, 2000]. The ideal plume models equations are not shown in this report because the Heskestad and Thomas plume model are used for comparison with the FDS results.

Heskestads Plume Model

In Heskestads plume model some of the assumptions from the ideal plume model is altered as shown below [Karlsson & Quintiere, 2000]:

1. The point source assumption is replaced with a "virtual origin" at height z_0
2. The Boussinesq approximation is removed so that $\rho_\infty \neq \rho$
3. The convective heat release rate $\dot{Q}_c$ is added
4. The "top hat" profile is replaced with a Gaussian profile and Δ T_0 is reintroduced as the symbols for the centreline plume temperature.

The Heskestad plume properties are illustrated in Figure 3.6 and the equations for Heskestads plume model are given below.

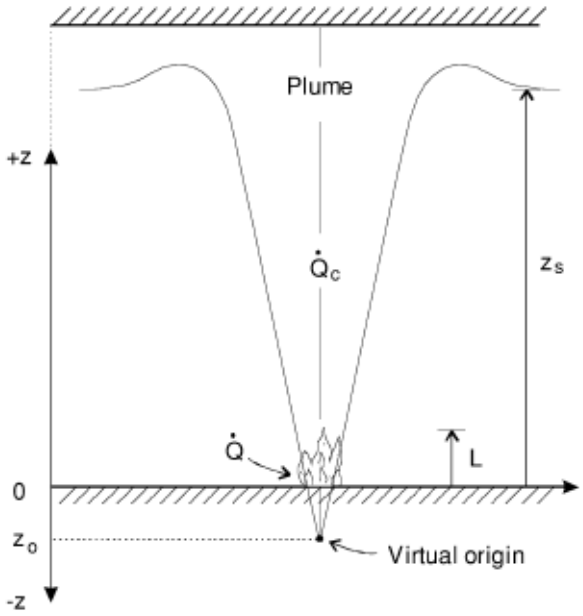

Figure 3.6. Illustration of the parameters used in the Heskestad plume model [Karlsson & Quintiere, 2000].

The height of the virtual origin is determined with Equation 3.3 [Karlsson & Quintiere, 2000].

$$z_0 = 0.083\dot{Q}^{\frac{2}{5}} - 1.02D \tag{3.3}$$

where $\dot{Q}$ = total heat release rate [kW]
D = diameter of the fuel source [m]

To calculate the mass flow rate from the Heskestad model it is necessary to calculate the mean flame height, see Equation 3.4. The flame height is not specific for the Heskestad plume model, but is derived based on the ideal fire plume. [Karlsson & Quintiere, 2000].

$$L = 0.253\dot{Q}^{\frac{2}{5}} - 1.02D \tag{3.4}$$

where L = mean flame height [m]

When estimating the plume mass flow rate the convective energy release rate $\dot{Q}_c$ is used since it causes buoyancy. To determine the convective energy release rate it is necessary to know the energy loss due to radiation which is around 20-40% of the total energy release rate. The convective energy release rate is determined with equation 3.5 [Karlsson & Quintiere, 2000].

$$\dot{Q}_c = 0.6\dot{Q} \text{ to } \dot{Q}_c = 0.8\dot{Q} \tag{3.5}$$

where $\dot{Q}_c$ = convective heat release rate [kW]

The entrainment of air into the plume below the average flame height ($z < L$) is determined by Equation 3.6 [Karlsson & Quintiere, 2000].

$$\dot{m}_p = 0.0056\dot{Q}_c\frac{z}{L} \tag{3.6}$$

where $\dot{m}_c$ = plume mass flow $\left[\frac{kg}{s}\right]$
z = height where the plume mass flow is determined [m]

The entrainment of air into the plume above the average flame height ($z > L$) is determined by Equation 3.7 [Karlsson & Quintiere, 2000].

$$\dot{m}_p = 0.071\dot{Q}_c^{\frac{1}{3}}(z - z_0)^{\frac{5}{3}} + 1.92 * 10^{-3}\dot{Q}_c \tag{3.7}$$

With Heskestad plume model it is also possible to determine the plume radius, centreline temperature and the centreline velocity. The equations for these properties are not shown in this report due to the limited time to perform a thorough comparison with FDS.

Thomas' Plume Model

The Thomas plume model is based on experimental data where the mean flame height, L, was significantly less than the fuel source diameter, D. In the Thomas plume model it was determined that the plume mass flow was independent of the energy release rate in the continuous flame region and instead it is a function of the perimeter of the fire and the height above the fire. The mass flow rate is determined by Equation 3.8 [Karlsson & Quintiere, 2000].

$$\dot{m}_p = 0.188 P z^{\frac{3}{2}} \tag{3.8}$$

where P = perimeter of the fire [m]

Equation 3.8 is only valid for heights up to the flame tip, but the it is especially useful for cases where L/D < 1 [Karlsson & Quintiere, 2000]. The Heskestad and Thomas plume model are used to determine the plume mass flow, which is compared to the mass flow in the FDS simulations and thereby it is possible to compare the HGL height of the FDS results and Heskestad and Thomas plume model. The calculations are performed in Appendix B and the comparison with FDS is performed in Section 6.

Experiment: Experimental Study of the Localized Room Fires - NFSC2 Test Series 4

This chapter contains the description of the experiment used for the validation test of the FDS code. The chapter opens with a description of the literature study performed in order to find the validation experiment, within this literature study the term validation is explained and the demands to the experiment is described. Next the chosen experiment, NFSC2, from VTT is described in order to give the reader an overview of the experiment. Finally the chapter finish off with a description of the input parameter identified to be used in the CFD simulation.

4.1 Determine Experiment for Validation

The term validation in this report refers to the process of evaluating the CFD software ability to reproduce the real world's physics. The validation process can be divided into three steps [McGrattan et al., 2012b]:

1. Comparing model predictions with experimental measurements
2. Quantifying the differences in light of uncertainties in both the measurements and the model inputs
3. Deciding if the model is appropriate for the given application

The user of CFD software, e.g. FDS, needs to go through all three steps every time a new simulation is initiated. To make the process of step 1 and 2 easier for the end-user a validation guide is made from the developers and users of FDS. With the validation guide the end-user can compare his case to the cases in the validation guide and make a judgement if FDS can be used for the current case.

To identify aspect of FDS which needs further investigations a contact to the developer of FDS, Dr. Kevin McGrattan (NIST) was initiated and through these communication three subjects was identified as possible; Flame spread, heat flux to targets and under-ventilated fires. Dr. Kevin McGrattan also suggested that a possible experiment could be found by looking at research labs like VTT, SP Sweden and NIST, as they spend a lot of money on experiments. These experimental results are not used for validation, instead only a paper about the experiment is written or the conclusion is communicated to the sponsors of the experiment [McGrattan, 2013].

From the developer community of FDS, there is a demand to the experiments used for validation purpose. The experiments must have a publicly available test report. The test report must also have a certain quality, such as stated experimental uncertainty, clearly measurement specified with type and locations

and also a discussion of the data procession must be included if the raw data is processed. Finally the experimental data must be able to be included in the FDS validation guide [McDermott, 2013].

It was decided to only search for experiments within the subjects, under-ventilated fires and heat flux to targets. The flame spread was dropped because it was not possible to find quality experiments in this area. Through the communication with Dr. Kevin McGrattan contact with Simo Hostikka was also initiated, he suggested that the room experimenent from VTT named: *"Experimental Study of the Localized Room Fires - NFSC2 Test Sereis"* [Hostikka et al., 2001] was use to validation of FDS. Therefore, the NFSC2 experimen is described in the following section.

4.2 NFSC2 - Experiment

The validation experiment NFSC2 was performed by Simo Hostikka, Matti Kokkala and Jukka Vaari from VTT [Hostikka et al., 2001]. This experimental study consists of two series of full scale fire tests, which were produced in order to produce well-documented data for CFD code verification. The fire test which is used in this report is an experimental series which consist of 21 tests in a 10 x 7 x5 m^3 test room with a 2.4 x 3.0 m^2 opening to ambient. During the 21 tests the fire size and locations were varied to investigate its impact on the burning rates, gas temperature, wall temperature, etc. The experiment is described on more details in Sections 4.2.1-4.2.5 which is based on the experimental report [Hostikka et al., 2001].

4.2.1 Geometry

The experiment consist of a rectangular room with one door opening to the large fire testing hall at VTT, see Figure 4.1.

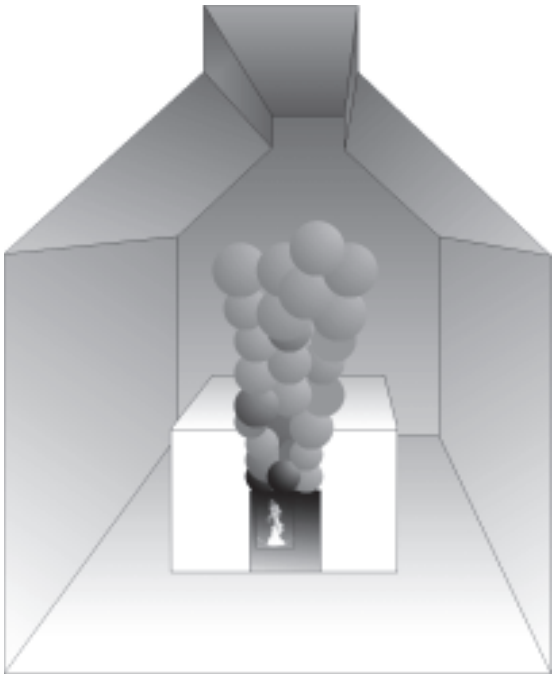

Figure 4.1. Principle drawing of the overview of the test hall [Hostikka et al., 2001].

The inner dimension of the room is 10 m width, 7 m depth and 5 m height. The wall and ceiling of the room were made of lightweight concrete with the properties listed in Table 4.1.

Property	Values	
ρ	475	$\frac{\text{kg}}{\text{m}^3}$
λ	0.12	$\frac{\text{W}}{\text{K m}}$
c_p	≈ 900	$\frac{\text{J}}{\text{kg K}}$

Table 4.1. Material properties of the ceiling and the walls [Hostikka et al., 2001].

The wall and ceiling has a thickness of 0.30 m and 0.25 m, respectively. The door opening has a width and height of 2.4 m and 3.0 m, respectively. However, the door width was reduced by half to 1.2 m for some experiments to study the effect of the opening size. The large fire testing hall has the dimension of 27 m width by 13 m depth by 19 m height where the fire room was approximately placed in the centre of the hall.

4.2.2 Fire Source and Fire location

In 19 of the 21 tests heptane was burned as fuel in a pool fire, in the last two tests wood was used as the fuel. The focus in this report is on the tests with heptane as fuel, because it is easier to specify the HRR as an input parameter to FDS. The heptane was burned in a circular steel pool placed on a load cell, where the mass loss was measured. The size of the pool was varied during the experiment. The HRR was not measured, but it is estimated from Equation 4.1

$$\dot{Q} = \chi \cdot \dot{m} \cdot \Delta H_c \tag{4.1}$$

where	$\dot{Q}$	=	heat release rate	[W]
	χ	=	efficiency of the combustion	[-]
	$\dot{m}$	=	mass loss rate	$\left[\frac{\text{kg}}{\text{s}}\right]$
	ΔH_c	=	heat of combustion	$\left[\frac{\text{MJ}}{\text{kg}}\right]$

From [Hostikka et al., 2001] a value of 0.8±0.1 and -44.6 $\frac{\text{MJ}}{\text{kg}}$ is suggested for χ and ΔH_c, respectively. The location of the heptane pool was varied between four locations during the experiments. The four location is shown in Figure 4.2.

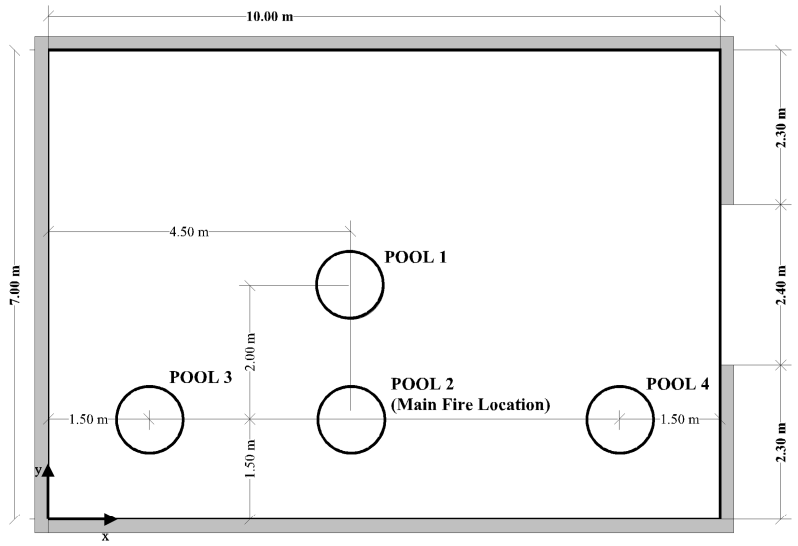

Figure 4.2. Location of the heptane pools during the tests [Hostikka et al., 2001].

The pool size is varied from 0.40 m^2 to 2.0 m^2 and water is used to stabilise the fire. The water amount was chosen such that the free height from the water surface to the pool edge was 0.13 m.

4.2.3 Fire scenario

During the 21 fire tests, 10 different fire scenarios are tested, meaning that the cases are repeated more than once. The 10 fire scenarios are shown in Table 4.2. Information about all 21 fire test are found in the experimental report [Hostikka et al., 2001].

Fire scenario	Pool location	Pool area	Pool diameter	Fuel surface height from the floor	Door width
1	#2 side wall	0.40 m^2	0.71 m	0.2 m	2.4 m
2	#2 side wall	0.61 m^2	0.88 m	0.21 m	2.4 m
3	#3 rear corner	0.61 m^2	0.88 m	0.21 m	2.4 m
4	#1 center	0.61 m^2	0.88 m	0.21 m	2.4 m
5	#4 front corner	0.61 m^2	0.88 m	0.21 m	2.4 m
6	#2 side wall	1.07 m^2	1.17 m	0.44 m	2.4 m
7	#1 center	1.07 m^2	1.17 m	0.44 m	2.4 m
7B	#1 center	1.07 m^2	1.17 m	0.44 m	1.2 m
8	#2 side wall	1.07 m^2	1.17 m	0.44 m	1.2 m
9	#2 side wall	2.00 m^2	1.60 m	0.25 m	2.4 m

Table 4.2. The fire scenario performed in The NFSC 2 Room test serie [Hostikka et al., 2001].

4.2.4 Measuring and Uncertainty

During the experiments about 150 measurements were made with a measurement time step of 1 s. The different measurements are mentioned below and the position of the measurement devices are shown in Appendix A. Some of the measurement points described below are incorporated into FDS, where they are used as validation parameters.

- **Mass loss rate:** The mass loss rate of heptane was measured with a load cell.
- **Room temperature:** The distribution of the temperature is measured with three vertical rakes T1, T2 and T3, with 10 bare thermocouples in different heights. The location and numbering of the thermocouples are shown in Figure A.4 and A.5.
- **Ceiling temperature:** 46 thermocouples were placed 0.1 m below the ceiling to measure the ceiling jet temperature. The location and numbering of the thermocouples are shown in Figure A.6.
- **Plume temperature:** The horizontal temperature in the fire plume is measured with 25 thermocouples in a 5x5 grid. The numbering is shown in Figure A.7.
- **Flame temperature:** The flame temperature was measured with two thermocouples placed in the plume centre line 1.00 m and 1.95 m below the plume temperature grid.
- **Door temperature:** The temperature distribution in the door were measured with 12 thermocouples. The thermocouples were placed in vertical plane with the outer surface of the wall. The location and numbering of the thermocouples are shown in Figure A.8.
- **Plate thermometers:** Ten plate thermometers was placed in the room. Four are placed on the wall, four are placed just below the ceiling and two are placed on the floor. The location and numbering of the thermocouples are shown in Figure A.9.
- **Heat flux:** The heat flux to a body was measured with one Gardon-type (R1) and four Schmidt-Boelter. The location and numbering of the heat flux meters are shown in Figure A.10.

- **Wall temperature**: The temperatures of the walls are measured with three measuring blocks with three thermocouples each in different depth. The location and numbering of the wall thermocouples are shown in Figure A.11.
- **Gas velocity:** Eight bi-directional probes are used to measure the velocity. Two were placed 0.10 m below the ceiling (V1 and V2) and six were placed in the door opening (V3 to V8). The location of V1 and V2 are shown in Figure A.11 and V3-V8 in Figure A.8.
- **Hot gas layer height:** The hot gas layer height is not measured directly, instead it is calculated based on the temperature measurements from the thermocouple trees and calculated based on the method shown in Appendix E.

In a noise test it was determined that the noise generated in the measuring devices only deviated from the mean value with less than 0.5°C for the temperature, 0.1 $\frac{\text{kW}}{\text{m}^2}$ for the heat fluxes and 0.1 $\frac{\text{m}}{\text{s}}$ for the velocities. Based on the duplicated fire scenarios it was determined that the error limits are about 10% for the point measured values such as the temperature, velocity and heat flux.

4.2.5 Conclusion from the Experiment

In the NFS2 experiment the following parameters were varied during the test series [Hostikka et al., 2001]:

- **Pool size:** The pool size was varied with four different sizes, using 0.4 m^2, 0.61 m^2, 1.07 m^2 and 2.0 m^2.
- **Pool location:** Four different pool locations was used, the locations are shown in Figure 4.2
- **Door width:** The door size was reduced from 2.4 m to 1.2 m, during three experiments.

The main conclusions from the experiment are listed below for the three different parameter variations.

Pool Size

The experimental results show that the burning rate is stronger for larger pools, which is suggested to be from increased radiation from the hot gas layer. It is also found that the hot gas layer height is practically independent of the pool size, even though the temperature of the layer increases as the pool size increased [Hostikka et al., 2001].

Pool Location

From variation of the pool location, it is seen that most of the variables seems to be independent of the location of the fire source. The pool locations effect on the heat flux are naturally strong because the measurement location were unchanged [Hostikka et al., 2001].

Door Width

It is observed that a smaller door width causes the temperature inside the smoke layer to increase and the interface height to become lower. The heat flux measurement also increased as a natural consequences of the increased temperature [Hostikka et al., 2001].

4.3 Validation Parameter

From Section 4.2.4 validation parameters are identified from the experimental measurement. Some of the experimental measurements are dropped because of lacking information. The wall temperature and plate thermometers are dropped because the water content in the wall and the thermocouple size are missing. Therefore, based on the missing information and limited time the following parameters are selected as validation parameter.

- HGL height
- HGL upper temperature
- Ceiling jet temperature

Furthermore Table 4.3 contains important setup parameter to FDS from the NFSC2 experiment.

Properties	**Amount**
Fuel	Heptane - C_7H_{16}
Mass loss rate	Is attached to the CD-ROM as excel file
Heat of combustion	44.6 $\frac{\text{MJ}}{\text{kg}}$
Combustion efficiency	0.8±0.1

Table 4.3. Input parameters to FDS identified from the experimental report.

To identify how the above listed validation parameters are affected by different modelling technic, for example the pool size and mesh size, are reviewed in the following chapter.

Parameter Study of Fire Dynamics Simulator

5

This chapter contains the parameter study made in order to obtain the setup of FDS for the validation study. The chapter opens with an introduction of the parameter study, where assumptions, fire scenario and evaluation technic are described. It then continues with separate section about the different parameters, where the parameters are described and the results are stated. An overview of the parameter investigated is shown in Table 5.1. Finally the chapter finish with the recommended setup for the validation study.

5.1 Parameter Study

The purpose with the parameter study is to determine a sufficient setup for the validation study. The sufficient setup is determined with a parameter variation study. The parameter simulation results are compared with the experimental results and based on this comparison a conclusion is made for the particular parameter. The parameter variation study is illustrated in Figure 5.1.

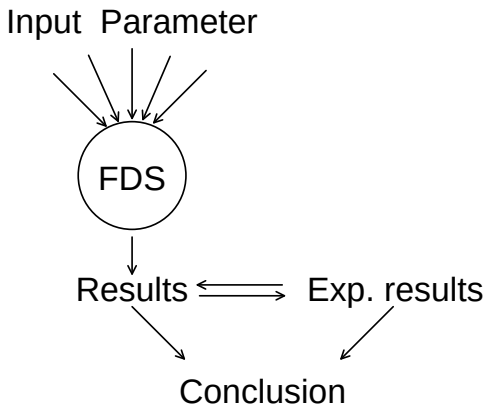

Figure 5.1. Illustration of the parameter variation setup.

In the parameter study the focus is not only on obtaining the setup with the best agreement with the experiment, but also the setup with the ability to obtain a solution within a reasonable timeframe with the current computer available.

5.1.1 Computer Configurations

The available computer is a workstation with the following specification, shown in Table 5.2.

Parameter	Variation	Comparison Parameters	Conclusion
Heat release rate	Combustion eff. 0.8±0.1	HGL - Interface height HGL - Upper temperature Upper thermocouple from thermocouple tree	Combustion eff. 0.85
Pool size	Equivalent area, hydraulic diameter or circumference	HGL - Interface height	Equivalent circumference
Radiation model	1 band (grey gas model) 6 bands 9 bands	HGL - Upper temperature Ceiling temperature Heat flux measurement	1 band (grey gas model)
Radiation mesh	50 angles 100 angles 200 angles 500 angles	HGL - Upper temperature Ceiling temperature Heat flux measurement	100 angles
Computational domain	Hall Room, 0 m extension Room, 1.2 m extension Room, 2.7 m extension Room, 3.2 m extension	Door velocity	Room, 3.2 m extension
Flow mesh/Mesh independence analysis	25 cm cells 12.5 cm cells 8 cm cells 6.25 cm cells	HGL - Interface height HGL - Upper temperature Upper thermocouple from thermocouple tree	8.0 cm

Table 5.1. The table shows an overview of the investigation performed to find the sufficient setup for the validation investigations. The table also gives an overview of the parameters varied in the different investigations. In the most right column, the conclusions from each investigation are listed.

Component	Specification
CPU	Intel core I7-3770 @ 3.40 GHz (Quad-core) and 3.90 GHz turbo frequency
RAM	16 GB DDR3
Operating system	Windows 7 64 bit

Table 5.2. Specification of the computer used.

The CPU has the ability to use a turbo frequency of 3.90 GHz on up to two cores if the right power, temperature and headroom exists [Intel Corporation, 2013]. This means that based on how many parameter studies are ran on the workstation, a difference can be seen on the computational time.

To setup the input file for FDS the graphical user interface PyroSim from Thunderhead Engineering Consultants, Inc is used. With PyroSim it is possible to visualise the input file to FDS and thereby

minimize typing errors in the input file.

5.1.2 Reference Case: Fire Scenario One

In the parameter study fire scenario one is used as reference scenario. Fire scenario one is chosen because the simulation time is the shortest, which makes each parameter study less computational expensive. The parameter variation study is performed on a 12.5 cm cubic single mesh, because initial simulations showed good agreement between the simulation and the experimental results with this cell size.

Fire scenario one consist of two experimental tests (test 0 and test 1), therefore when the experimental results are compared with the simulation results, the experimental results are an average of test 0 and test 1. An example of how the experimental results are average are illustrated by the mass burning rate in Figure 5.2.

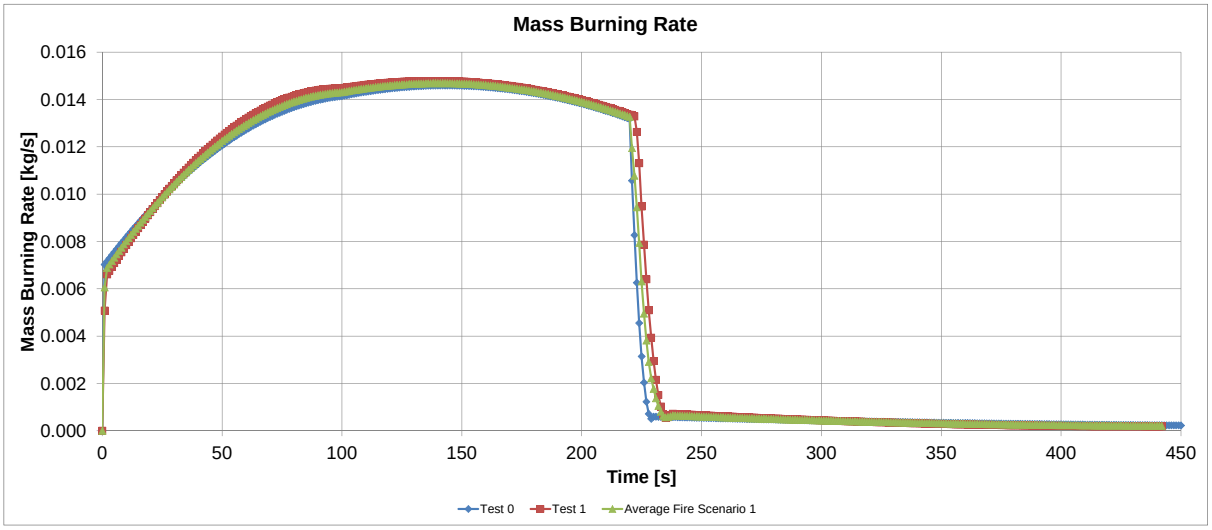

Figure 5.2. The mass burning rate for fire scenario one, which is an average of the test 0 and test 1.

The mass burning rate shown in Figure 5.2 is loaded into the FDS input file where it is converted to a HRR with Equation 4.1. In fire scenario one the pool fire is located in location #2 side wall, see Figure A.3, with a pool size of 0.40 m^2 and a full door width of 2.4 m. The setup from PyroSim is shown in Figure 5.3. In Figure 5.3 the nearest wall and ceiling are made transparent in order to show the location of the pool fire and the measuring point.

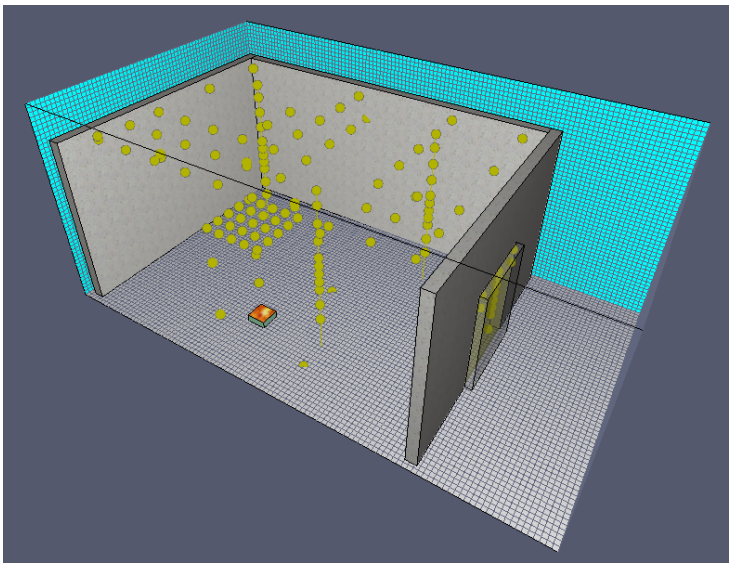

Figure 5.3. Illustration of the setup used in fire scenario one, where the nearest wall and ceiling are made transparent in order to show the location of the pool fire and the measuring point.

5.1.3 Evaluation Parameters

To evaluate the effect of the parameter study the relative difference and the computational time are used as quantities to judge the parameter study. The relative difference ϵ is given in Equation 5.1. The relative difference used in this report is the absolute relative difference, because it makes it easier to judge between different simulations results.

$$|\epsilon| = \frac{\Delta M - \Delta E}{\Delta E} = \frac{(M_p - M_0) - (E_p - E_0)}{(E_p - E_0)} \tag{5.1}$$

where ϵ = relative difference [-]
M_p = model peak value
M_0 = model start value
E_p = experimental peak value
E_0 = experimental start value

From the FDS output file it is possible to obtain the CPU usage time for every 100 time steps. FDS also reports who much of the total computational time is used on the different process, such as velocity and radiation calculations. An example of this reports is shown below:

CPU Time Usage, Mesh 1

	CPU (s)	%
MAIN	23933.60	100.00
DIVG	1526.40	6.38
MASS	3227.50	13.49
VELO	5426.45	22.67
PRES	573.16	2.39
WALL	877.80	3.67
DUMP	127.25	0.53
PART	0.00	0.00
RADI	11871.77	49.60
FIRE	287.50	1.20
COMM	0.19	0.00
SubTot	23918.01	99.93

Thereby it is possible to judge the different parameters impact on the total calculation time and determine if the increase in accuracy is worth the increase in computational time.

5.1.4 Limitations of Fire Dynamics Simulator

Using FDS as CFD software introduces a set of limitation for the use of FDS. The limitation is due to assumptions build into the programs algorithms, by the developers. The most prominent limitations of FDS are listed below [McGrattan et al., 2012c].

Rectilinear Geometry: FDS uses a rectilinear numerical grid and with the use of a fast direct solver of the pressure field it increase the efficiency of FDS. The use of rectilinear grid can cause limitation when the domain is not rectangular and saw tooth domains are created. But for the must cases the increase in grid resolutions because of the pressure solver offsets the saw tooth modelling [McGrattan et al., 2012c].

Low Speed: FDS is developed to low-speed flows (Ma $\leq$ 0.3). This means that FDS cannot be used to modelling flow which involves speed approaching the speed of sound, e.g. explosions [McGrattan et al., 2012c].

Combustion: FDS uses a mixture fraction combustion model in most applications. In the mixture fraction model the combustion between fuel and oxygen is assumed to be mixing controlled and happens infinitely fast and regardless of the temperature. This is a good assumption for large-scale, well ventilated fires. However, in under-ventilated fires a burn no burn criterion is introduced to make it possible for the oxygen and fuel to mix without combustion. The burn no burn criterion is an empirical rule, where the combustion is furthermore a function of the oxygen volume fraction and the gas temperature [McGrattan et al., 2012c].

Radiation: In the radiation models in FDS several limitations are introduced in order to solve the radiation transport in a reasonable time frame. Firstly the radiation transport equation are reduced to include a finite number of bands instead of all the electromagnetic wavelengths. In FDS a grey gas (1 band), 6 bands and 9 bands radiation model are available. In the three models different substances, such as soot, carbon dioxide and water, are included via the absorption emission coefficient. Secondary the radiation transport equation is discretised on a finite number of direction vectors. In FDS the default value are 100 discrete radiation angels. The introduction of discretised radiation angles can lead to a non-uniform distribution of the radiant energy on targets fare away from the fire [McGrattan et al., 2012c].

Turbulence - LES: The LES turbulence model is chosen for turbulence modelling. With the LES model the large eddies are resolved by the numerical grid and the smaller eddies are filtered off and modelled by the Smagorinksy turbulence model. With the use of LES turbulence modelling it is aimed to get a greater spatial and temperoral accuracy of simulated fires [McGrattan et al., 2012c].

5.1.5 Assumptions in the Fire Dynamics Simulator Setup

Setting up the input file for FDS requires assumptions to be made. The assumptions made are listed below:

Square pools: The circular pool from the experiment is modelled as a square pool in FDS. The reason for using square pool is that FDS is optimized for square and cubic elements. In a parameter study in Section 5.3 it is determined if the square pool should have equivalent surface area, circumference or hydraulic diameter.

Thermocouple measurement: In the experiment bare thermocouples are used, which means that the temperature measured is not the gas temperature. Instead it is the thermocouple temperature which also is due to radiation. In the experiment it was found that the radiation can increase the temperature with up to 50°C. To account for this error the thermocouple model in FDS is used where the radiation is accounted for.

Single mesh: The domain is discretised into a single mesh, because the information exchange between meshes are not as good as the information between cells inside a mesh [McGrattan et al., 2012a].

5.2 Heat Release Rate

The HRR is a measure of how the energy release from a material when it is burned, which also can change with time. The unit of HRR is therefore usually given in $\frac{\mathrm{J}}{\mathrm{s}} = \mathrm{W}$ [Karlsson & Quintiere, 2000]. In the NFSC2 experiment the HRR is not measured instead the mass loss rate of the fuel is measured via a load cell. Based on the mass loss rate, the combustion efficiency and the heat of combustion the HRR is estimated with Equation 4.1, shown again in Equation 5.2.

$$\dot{\mathrm{Q}} = \chi \cdot \dot{\mathrm{m}} \cdot \Delta \mathrm{H_c} \tag{5.2}$$

From the NSFC2 experiment a combustion efficiency (χ) of 80%±10% and a heat of combustion ($\Delta \mathrm{H_c}$) of -44.6 $\frac{\mathrm{MJ}}{\mathrm{kg}}$ of heptane is suggested. The combustion efficiency is described as the ratio between the effective heat of combustion and the complete heat of combustion [Karlsson & Quintiere, 2000]. Two important parameters which leads to incomplete combustion are the formation of soot and carbon monoxide. Carbon monoxide is formed when not enough oxygen is presented in the combustion zone. Soot is formed in the fuel-rich core of large hydrocarbon pool fires, where thermal decomposition eventual can lead to soot formation [Drysdale, 2011].

The carbon monoxide peak content in the test room was measured and varied between 0.0095-0.05%, for fire scenario two-nine (no measurement for fire scenario one). To determine the combustion efficiency and thereby the HRR. A comparison between the experimental results and the simulation results are made together with a chemical calculation of the content of carbon monoxide in the smoke. The chemical calculation is made with the chemical equilibrium program CEA-NASA (see Appendix D).

5.2.1 Results and Discussion

By comparing the carbon monoxide measurement from the experiment and the CEA-NASA calculations it is concluded that the combustion efficiency of heptane is very effective therefore a HRR with a combustion efficiency of 80%, 85% and 90% is used as input to FDS. The different HRR are compared to the experiment on the HGL height, the HGL upper temperature and upper thermocouple from the T1 thermocouple tree.

In Figure 5.4 the HGL height comparison is shown for the HRR with 80%, 85% and 90% combustion efficiency and the experiment.

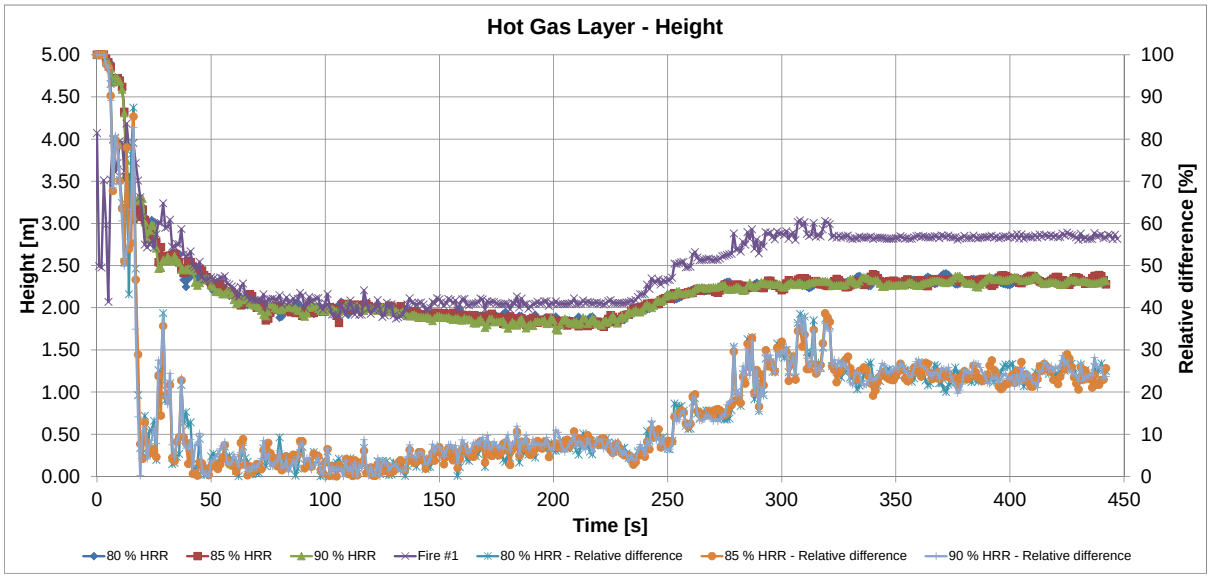

Figure 5.4. Comparison of the HGL height for 80%, 85% and 90% combustion efficiency to the HGL height for the experiment.

The results in Figure 5.4 shows that the HGL height is not depending on the HRR, which corresponds well with for example Thomas plume theory, see Section 3.2.2, where the plume mass flow only depends on the perimeter of the fire. The relative error between the experiment and the CFD simulation is below 10% in the interval from 50-250 seconds where the fire source is dominating and in the last part the relative error is around 25-30% when the hot gas layer stabilizes in the interval from 250-450 seconds. The HGL upper temperature is shown in Figure 5.5, for the experiment and the simulations.

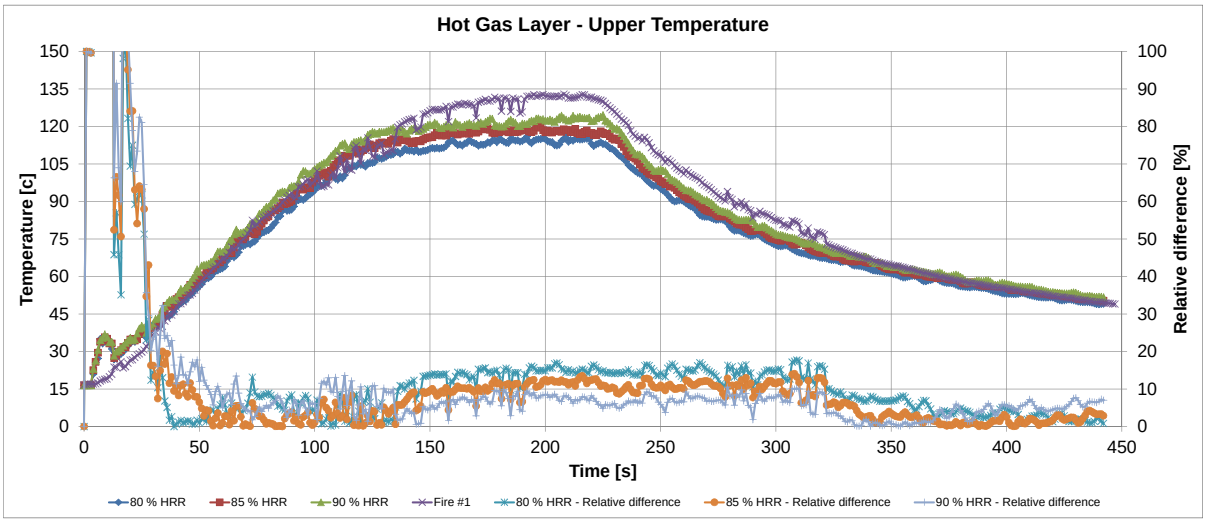

Figure 5.5. Comparison of the HGL upper temperature for 80%, 85% and 90% combustion efficiency to the HGL upper temperature for the experiment.

The comparison in Figure 5.5 shows that all simulations are capable of reproducing the transient increase and decrease of the HGL upper temperature. A small difference between the three HRR are seen. The relative difference for the three HRR are up to around 15%, 12% and 10% for the 80%, 85% and 90% HRR, respectively

Furthermore the HRR impact on the upper thermocouple from the thermocouple tree T1 is shown in Figure 5.6, but the same tendency is also seen in the other two thermocouple trees. The location of the thermocouple tree T1 in the test room is shown in Figure A.4 in Appendix A.

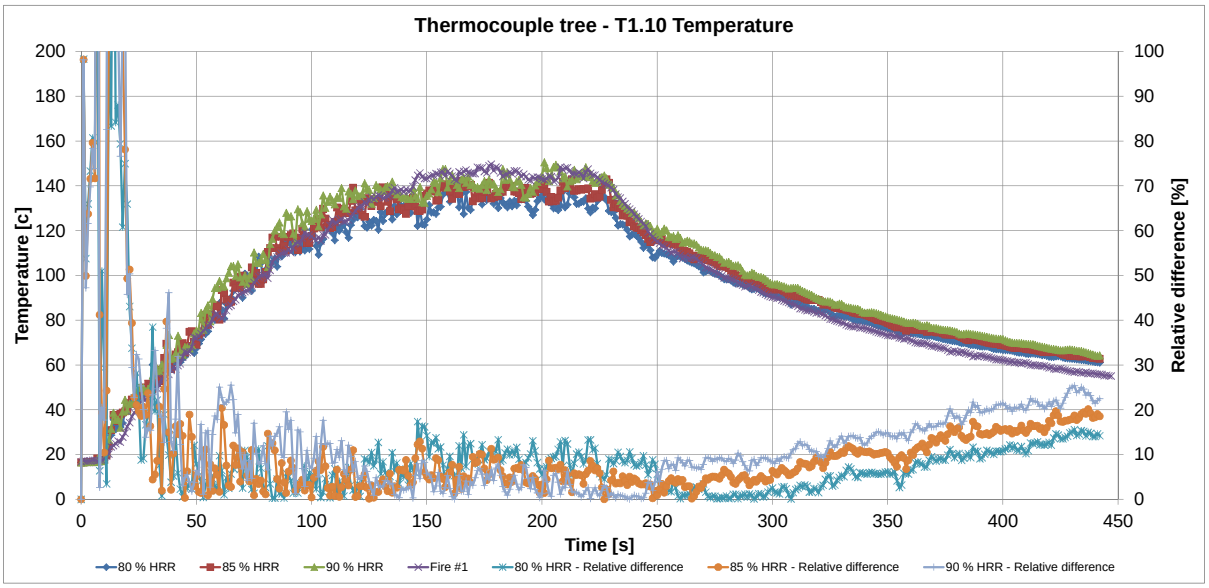

Figure 5.6. Comparison of the temperature of the upper thermocouple in the thermocouple tree T1, the location of the thermocouple is shown in Figure A.4 and A.5.

The comparison of the temperature in Figure 5.6 shows that all HRR is nearly in the same temperature range and that FDS is capable of reproducing the transient temperature development. The relative differences for all three HRR are below 20% after the initial time steps.

From the litterature [SFPE & NFPA, 2002] a combustion efficiency of heptane in a well-ventilated fire is 92%. In the validation study of the hall experiment from the second part of the NFSC2 test series a combustion efficiency of 85% is assumed [McGrattan et al., 2012b]. For the validation study a combustion efficiency of 85% is assumed, because the difference between the results in the HGL height and upper temperature is not very significant. In the temperature comparison of the thermocouple tree all three HRR is in the same temperature range, but the relative difference for the thermocouple tree comparison shows that the 85% combustion efficiency shows the best agreement between the simulations and the experimental results, but the difference between the simulations is not very large.

Therefore, the validation study a combustion efficiency of 85% is used.

5.3 Pool Size

The pool in the NFSC2 experiment was circular and therefore not optimal for FDS. A square pool is modelled instead and in this section it is tested how the pool modelling technic affects the results. Three methods with equivalent surface area, equivalent circumference and equivalent hydraulic diameter are simulated. The dimension of the three pools are listed in Table 5.3 together with the dimension of the circular pool from the experiment.

Pool	Size [m]	Circumference [m]	Area $[m^2]$
Experiment (circular)	0.71	2.23	0.40
Equivalent surface area	0.63	2.52	0.40
Equivalent circumference	0.55	2.20	0.30
Equivalent hydraulic diameter	0.71	2.84	0.50

Table 5.3. Dimension of the pools used in the investigation of the pool size effects on the HGL height.

The three different methods all give different circumference. At the circumference fresh air is drawn into the plume. The entrainment of fresh air into the plume is illustrated in Figure 5.7.

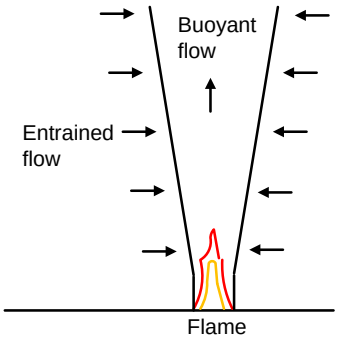

Figure 5.7. Illustration the air entrainment into the plume.

It is expected that a difference will occur between the three methods due to the different circumference length.

5.3.1 Results and Discussion

The HGL height for the three simulation and the experiment are shown in Figure 5.8.

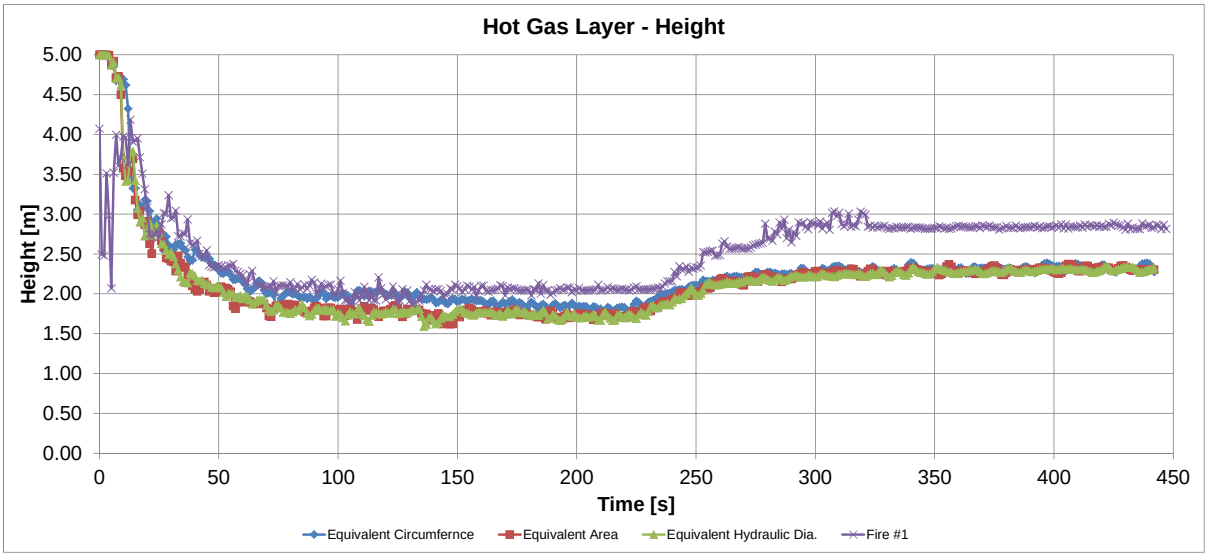

Figure 5.8. The HGL height for the three simulation and experimental data. There are good agreements for all simulation but the equivalent circumference gives the best results compared to the experiment.

It appears from Figure 5.8 that all three pool modelling methods give similar results, but the pool with equivalent circumference shows the best agreement with the experiment. The reason for this must be due to the equivalent circumference, so the same amount of air is entrained in both the experiment and the simulation. The effect from the entrainment is further shown in the interval from 250-450, where no plume is presented and the air entrainment is not occurring and the HGL height is coincident between the three simulations.

Based on the above shown results it is decided to model the pool in FDS with an equivalent circumference.

5.4 Radiation Models

Radiation is energy transfer of heat by electromagnetic waves between surfaces, emission and absorption by various gases and soot. In fire engineering water vapour and carbon dioxide are important substance because they are strong absorbing-emitting, but in most situations the soot radiation is the dominating substance [SFPE & NFPA, 2002].

In the radiation models the goal is to determine the radiant heat flux vector $\dot{q}_r''(x)$. For a non-scattering gas the absorbing and emitting is described with the radiative transport equation, given in Equation 5.3 [McGrattan et al., 2012c].

$$s \cdot \nabla I_\lambda(x,s) = \kappa(x,\lambda)\left[I_b(x) - I_\lambda(x,s)\right] \tag{5.3}$$

where	s	=	unit direction vector of the intensity	
	∇ I_λ(x,s)	=	the derive radiation intensity at wavelength λ in cell x and in the s direction	$\left[\frac{W}{m^3}\right]$
	κ(x,λ)	=	absorption coefficient in cell x for wavelength λ	$\left[\frac{1}{m}\right]$
	I_b(x)	=	radiation intensity source term in cell x	$\left[\frac{W}{m^2}\right]$
	I_λ(x,s)	=	radiation intensity at wavelength λ in cell x and in the s direction	$\left[\frac{W}{m^2}\right]$

An exact solution of the radiation heat transfer is very expensive, because it dependence of the electromagnetic wave length. Therefore, assumptions are made to simplify the radiative transport equation by dividing it into a number of bands and each bands has a separate radiative transport equation, see Equation 5.4 [McGrattan et al., 2012c].

$$s \cdot \nabla I_n(x,s) = \kappa(x,n)\left[I_{b,n}(x) - I_n(x,s)\right], n = 1 \ldots N \tag{5.4}$$

where	∇ I_n(x,s)	=	the derive radiation intensity at band n in cell x and in the s direction	$\left[\frac{W}{m^3}\right]$
	κ(x,n)	=	absorption coefficient in cell x for band n	$\left[\frac{1}{m}\right]$
	$I_{b,n}$(x)	=	radiation intensity source term for band n in cell x	$\left[\frac{W}{m^2}\right]$
	I_n(x,s)	=	radiation intensity at band n in cell x and in the s direction	$\left[\frac{W}{m^2}\right]$

The total intensity is calculated with Equation 5.5, when all the bands intensities are known [McGrattan et al., 2012c].

$$I(x,s) = \sum_{n=1}^{N} I_n(x,s) \tag{5.5}$$

where I(x,s) = total intensity in cell x in the s direction

The radiative heat flux is then found by integrating the total intensity on the radiation mesh. The radiation mesh is described in further details in Section 5.5.

In FDS, three radiation models are available, which all are based on the use of radiation band assumption [McGrattan et al., 2012c].

- **Grey gas assumptions:** Soot is the important product in the most large scale fire scenarios. The reason for this is that the radiation spectrum of soot is continuous. Therefore, it is modelled as a grey medium which means that the spectral dependence is lumped into one absorption coefficient.
- **6 and 9 bands models:** The 6 and 9 bands models are available for fire scenario where the soot content is smaller than the carbon dioxide and water content. Here it is possible to used extra bands in the radiative models to model the radiative effects from the water, carbon dioxide, etc.

In this parameter study the effect from the three radiation models on the simulated results are tested. The results of the parameter investigation are shown in the next section.

5.4.1 Results and Discussion

Figure 5.9 shows the HGL upper temperature for the three radiation models and the experiment. The simulations results of the three radiation models are coincident, which is better illustrated with the relative difference shown in Figure 5.10.

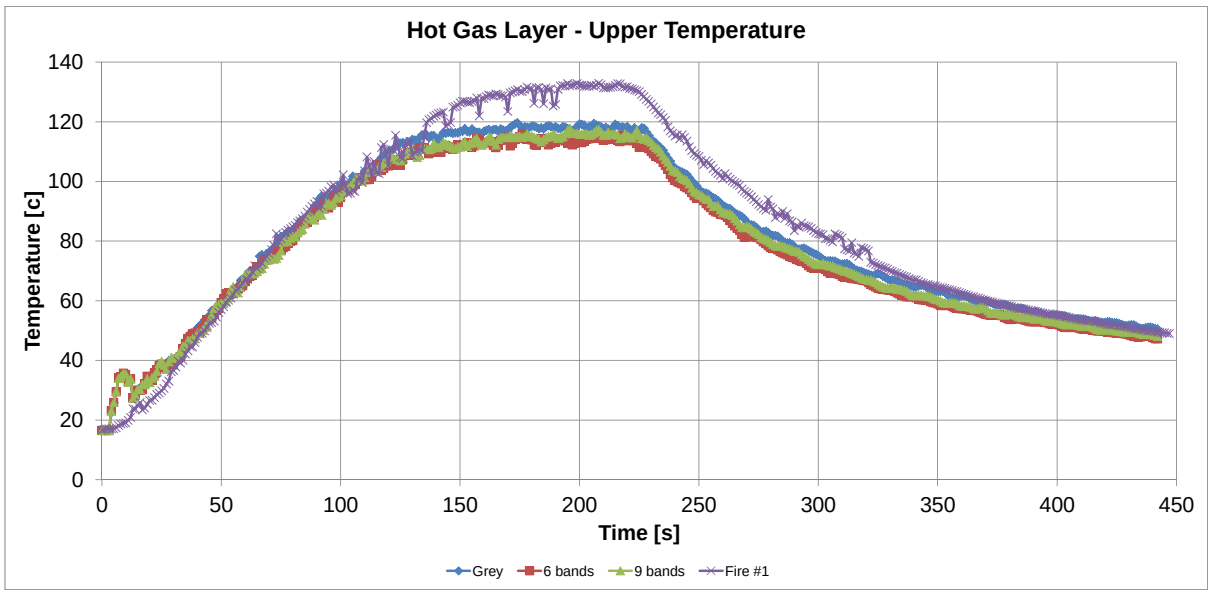

Figure 5.9. The HGL upper temperature for the experiment and the three radiation models, grey gas model, 6 bands and 9 bands.

The agreement between the three radiation models is also seen on the relative difference in Figure 5.10. The grey gas model however obtains a lower relative difference compared to the other two radiation models.

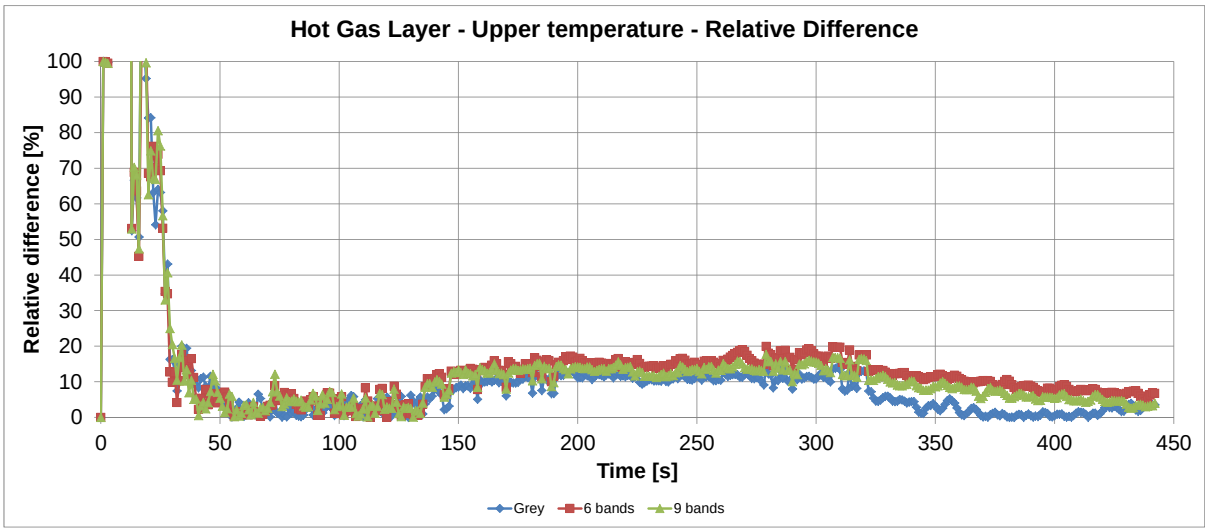

Figure 5.10. The relative difference between the radiation model simulations and the experimental results.

A reason for the good agreement between the radiation models could also be because the air cannot absorb radiation, but only for example the water content in the air. Because of this reason the gauge heat flux from the simulations are compared in Figure 5.11.

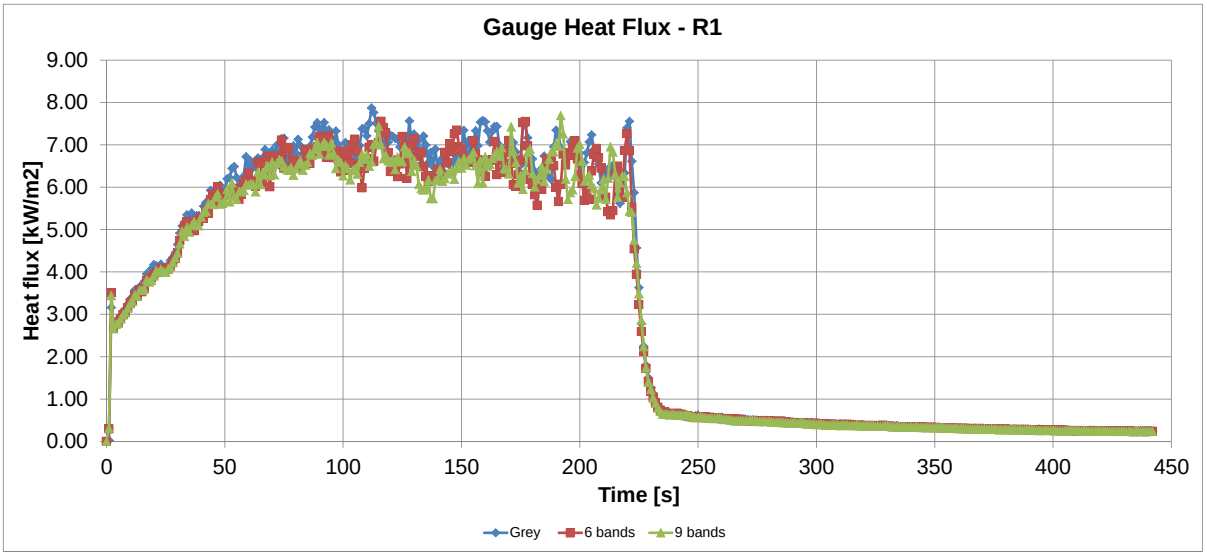

Figure 5.11. Comparison of the gauge heat flux from the R1 measuring point. The position of R1 is shown in Figure A.10.

In Figure 5.11 the gauge heat flux measurement from R1 is compared between the three radiation models. Again convergences between the simulations are seen. The average relative difference between the grey gas model and the 6 bands and 9 bands model is 6.7% and 7.7%, respectively. Based on the results shown here it is possible to concluded that the soot particle is the dominating radiation particle in this case and that the use of more radiation band models does not give significantly better convergence with the experimental results. When the 6 and 9 bands model are enabled the computational time are increased. Therefore it is interesting to see how much the computational times are increased compared to the grey gas model. Table 5.4 shows the computational time needed to perform the simulations and the difference shown in the third column is relative to the grey gas simulation.

Simulation	Time [h]	Difference [%]
Grey	4.74	
6 bands	23.02	485
9 bands	31.86	661

Table 5.4. The total calculation time for the three simulations and the difference in calculation time relative to the grey band model.

Enabling the 6 bands and 9 bands radiation models, increases the computational times with 485% and 661%, and therefore it is not feasible to use in this validation study because the soot yield from the heptane is the dominating radiation particle.

Based on the results shown for this parameter study and the comparison of the computational time it is decided to use the grey gas model in the validation study.

5.5 Radiation Mesh

Thermal radiation from for example a soot particle is emitted in all directions, so to describe the radiation mathematical it would require a infinite number of directions vectors (s) to Equation 5.3 which is not possible to calculate. Therefore, FDS solves the radiations transport equations on a spherical mesh with a finite number of discrete angles, see Figure 5.12.

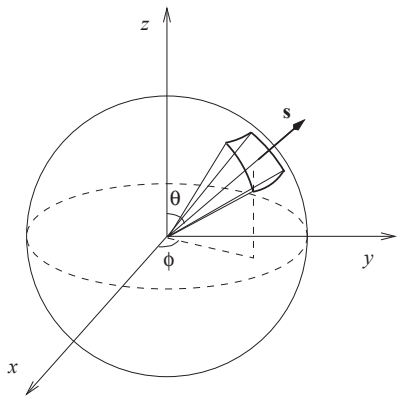

Figure 5.12. Illustration of the radiation sphere where the particle emitting is in the centre of the coordinate system and a random discrete angle is shown [McGrattan et al., 2012c].

The information exchange between the spherical (radiation mesh) and the Cartesian (flow mesh) coordinate system happens by default every third second and the discrete angle are updated by default every fifth second. These two values can be reduced by the cost of more computational power [McGrattan et al., 2012a]. In this study the change of these parameters are not investigated because of limited time.

With this parameter study the effect from the discretisation of the radiation mesh on the results are tested. The radiation mesh is divided into 50, 100, 200 and 500 discrete angles, where 100 angles are the default setting in FDS.

5.5.1 Results and Discussion

Figure 5.13 shows the HGL upper temperature for the four radiation mesh simulations and the experiment. The simulations are coinciding, the level of coinciding are better illustrated with the relative difference

shown in Figure 5.14.

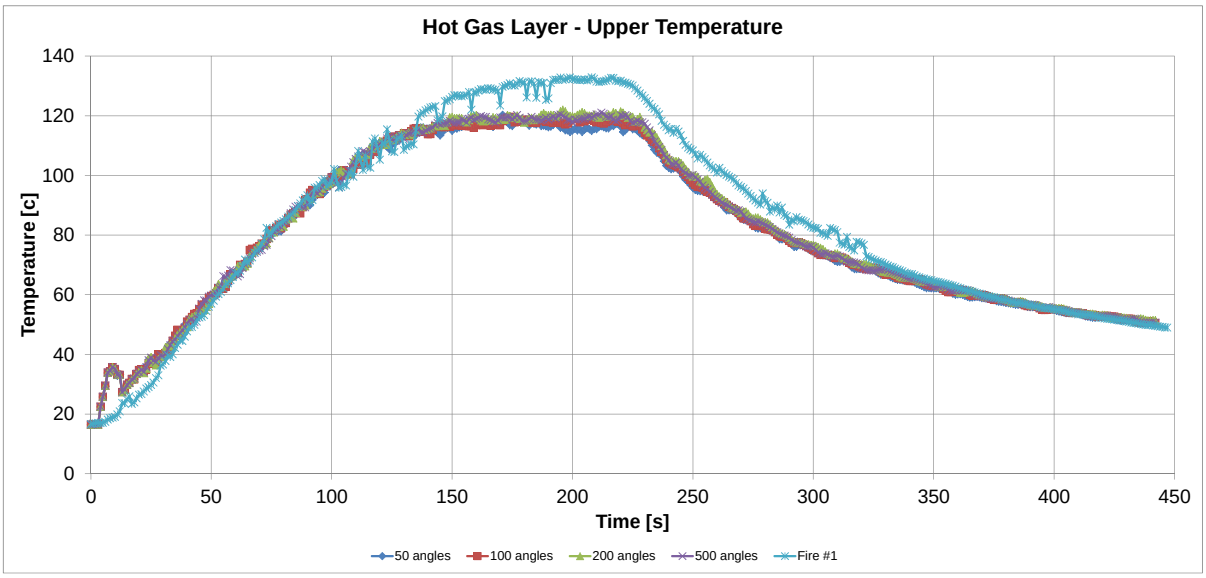

Figure 5.13. The HGL upper temperature for the experiment and the four radiation angles simulations.

The coinciding between the four radiation mesh simulation are also seen on the relative difference between the simulation and the experiment in Figure 5.14.

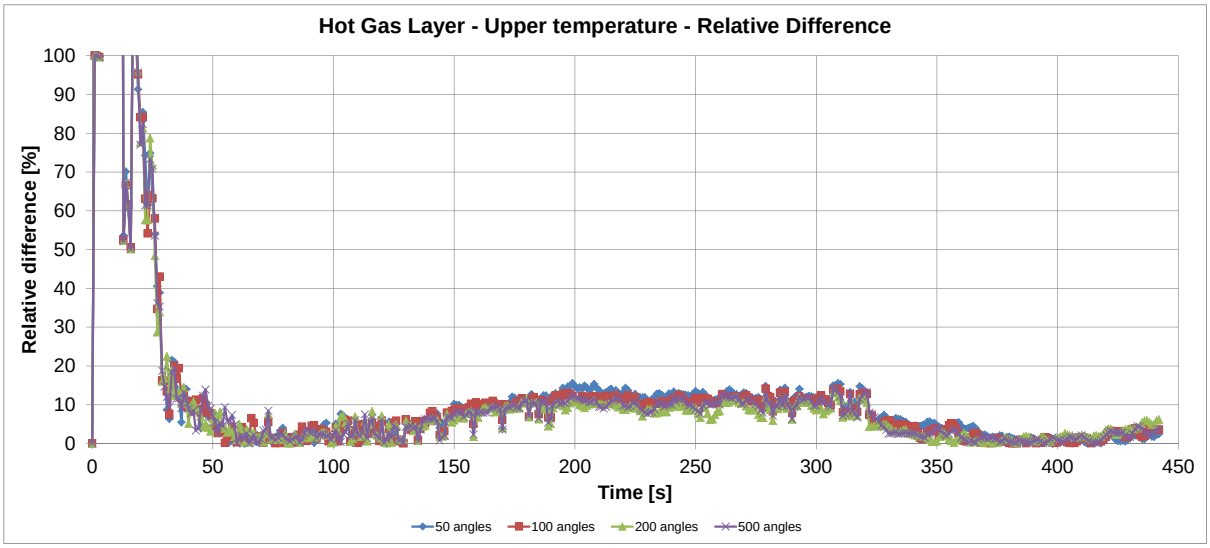

Figure 5.14. The relative difference between the radiation mesh simulations and the experimental results.

As described in the parameter study of the radiation model the good agreement between the radiation mesh is maybe because the air cannot absorb radiation, but only for example the water content in the air. Therefore, the gauge heat flux from the simulations are also compared, see Figure 5.15.

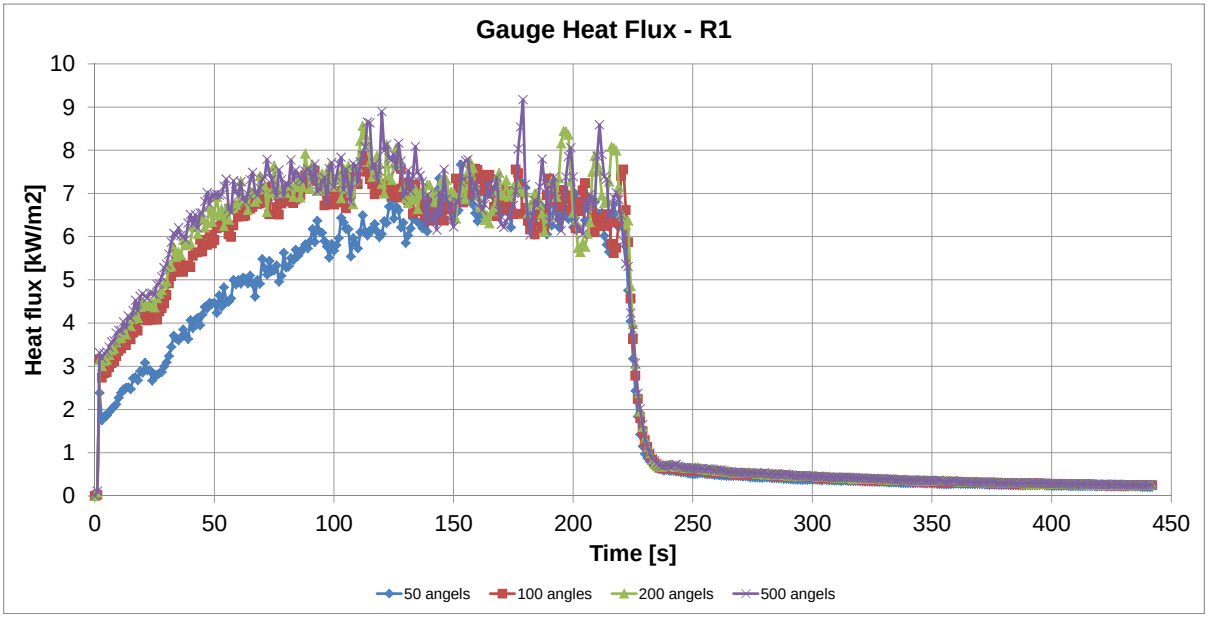

Figure 5.15.

Figure 5.15 shows a agreement between the radiation mesh with 100, 200 and 500 angles, whereas the simulation with 50 angles is below the other simulations in the first 150 seconds of the simulation. Therefore, a choice has to be made between the radiation mesh with 100, 200 and 500 angles. The relative error difference, with the 100 angles as reference is determined to be 7.1% and 8.6% for the 200 and 500 angles, respectively. To make a decision on the number of radiation angles to use, the computational time must also be taken into consideration. Table 5.5 shows the computational times needed to perform the simulations. The difference shown in the third column is relative to the simulation with 100 radiation angles.

Simulation	**Time [h]**	**Difference [%]**
50 angles	4.34	98
100 angles	4.43	-
200 angles	5.10	115
500 angles	6.64	150

Table 5.5. The total calculation time for the four simulations and the difference in calculation time relative to the simulation with 100 angles.

Increasing the number of angles from 100 to 200 and 500 angles increases the computational time with 115% and 150%, respectively. Therefore, based on a small increase in the accuracy at a higher computational cost, it is decided to use the standard setting of 100 discrete angels for the validation study.

5.6 Computational Domain

The computational domain is the actual domain from the experiment. Because the large test hall has large dimension (27 m x 14 m x 19 m), it is desired to reduce the domain down to the test room with a useful boundary conditions. Therefore, a comparison between the two setups shown in Figure 5.16 are made.

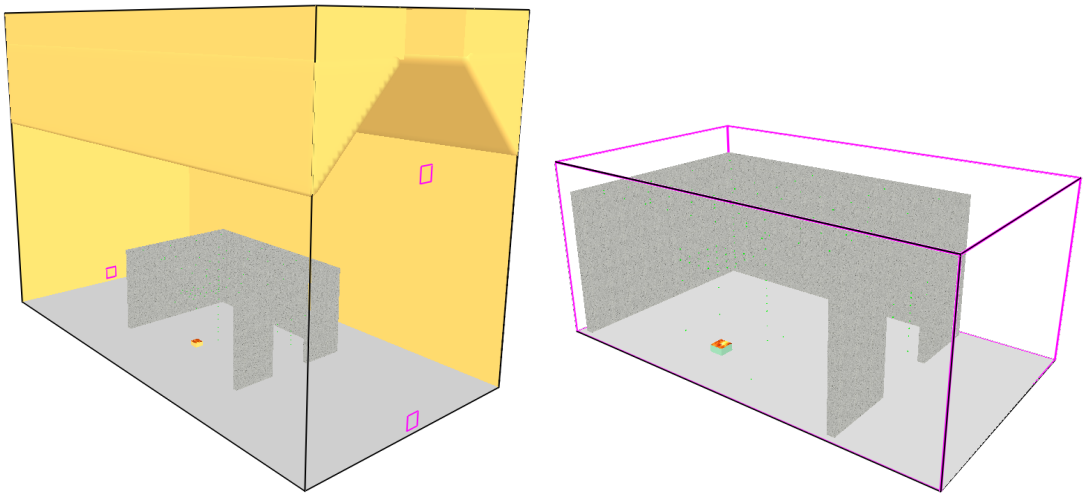

Figure 5.16. Illustration of the test hall and test room domain. The ceiling and side wall is hidden in order to shown the location of the pool fire.

The boundary condition on the test hall simulation, is inert boundary with four 0.6 x 0.6 m^2 opening to the surrounding. In the test room simulation the boundary condition is open. Both simulations have a floor boundary condition on the bottom of the domain. For the room domain it is also tested how far the mesh needs to be extended in order to ensure a good dissolution of the door flow.

In [He et al., 2008] the extending of the domain beyond the wall with a vent opening is studied. The study concluded that the domain should be extended with half the hydraulic diameter and one hydraulic diameter for a fuel controlled and a ventilation controlled fire, respectively. Simo Hostikka suggests that the domain is extended with one door length to ensure a correct door flow [Hostikka, 2013]. The hydraulic diameter of the door is determined to 2.7 m and the height of the door is 3 m.

To study the effect of the door flow, four room domains with different extension and the hall domain are simulated. The different simulations are listed in Table 5.6.

Simulation	**Number of cells outside room**	**Hydraulic diameter**
Room, 0 m extension	0	0
Room, 1.2 m extension	≈ 9	$0.44D_h$
Room, 2.7 m extension	≈ 21	$1.00D_h$
Room, 3.2 m extension	≈ 25	$1.82D_h$
Hall	≈ 65	-

Table 5.6. The five simulations performed for the domain parameter study.

The lengths listed in Table 5.6 are smaller and longer for the domain with half the hydraulic diameter and the door height domain, respectively. The reason for these choices are because the domain will then have the x-length in whole meters, which means that speed optimized number of cells can be used in the simulations.

5.6.1 Results and Discussion

The domain parameter study is evaluated by compare the velocity profile in the door. The velocity profile is found as an average in the interval from 150-200 seconds, where a steady state level is obtained. The door velocity profiles from the simulation and the experiment are shown in Figure 5.17.

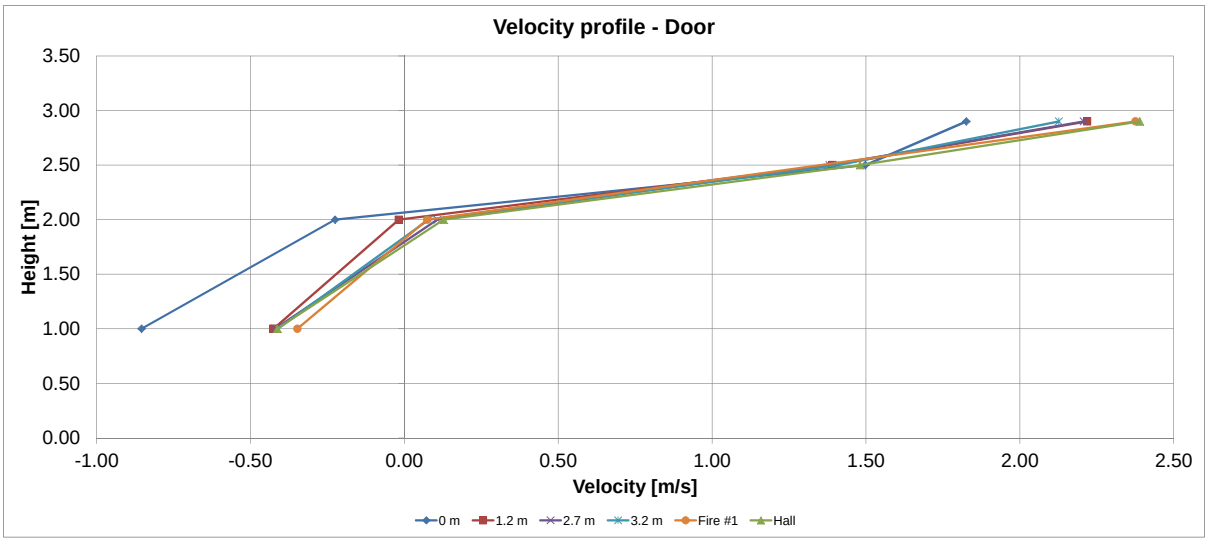

Figure 5.17. The vertical velocity profile of the door flow with the five simulaitons and the experimental velocity profile.

From Figure 5.17 all simulations show the same tendency as seen from the experiment. The simulation with zero extension deviates the most from the experiment. Based on the graph it is not possible to determine which domain obtains the best agreement with the experiment. Therefore, the relative difference between the simulations and the experiment are listed in Table 5.7. Only three measuring points are listed in Table 5.7 which is due to failure of the experimental measurement in 2.5 meters.

	Relative difference [%]		
Simulation	1 m	2 m	2.9 m
Room, 0 m extension	145.77	402.64	23.14
Room, 1.2 m extension	22.36	124.18	6.61
Room, 2.7 m extension	20.81	44.78	7.07
Room, 3.2 m extension	18.38	6.81	10.46
Hall	18.89	72.66	0.59

Table 5.7. The relative difference between the simulations and the experiment in the domain parameter study.

The relative difference in Table 5.7 shows that there is large difference between the simulations and the experiment in 2 m height. The simulation of the room with 0 m extension shows the largest difference from the experimental results in all three measuring points. Whereas the room with 3.2 m extension overall has the lowest total relative difference for all three measurement point. Furthermore the choice must also depend on the computational times used, which is shown in Table 5.8. The difference shown in the fourth column in Table 5.8 is with the 3.2 m extension simulation as reference.

Simulation	Cells	Time [h]	Difference [%]
Room, 0 m extension	267,264	4.32	78.55
Room, 1.2 m extension	294,912	5.11	92.91
Room, 2.7 m extension	331,776	5.37	97.64
Room, 3.2 m extension	344,064	5.50	-
Hall	3,677,184	42.10	765.46

Table 5.8. The computational time of the simulations performed for the domain parameter study. In this parameter study the computational time are higher than normally the reason for this is explained in Section 5.1.1.

Simulation of the hall with the test room in the middle is not feasible, because of the large computational time. The recommendations from [He et al., 2008] are based on purely computational investigation and not corrected for any coherence with experimental data. The recommendation from Simo Hositakka is based on his experience with FDS. From Table 5.7 the lowest difference between the simulation and the experiment for all three measuring points are seen with the room domain with a 3.2 m extension which is the door height extension which also is recommended by the FDS developers. Therefore, it is decided to use the room domain with an extension length of one door height for the validation study.

5.7 Mesh Independence Analysis

The mesh independence analysis is made in order to secure a solution which is not depending on the quality of the mesh. The analysis is performed by starting with a coarse mesh and then gradually refine the mesh until the results does not show any appreciable difference.

In FDS the size of the mesh also decides the time step because the time step is adjusted according to satisfy the CFL (Courant, Friedrichs, Lewy) criterion. The CFL criterion assure that the time step is not larger than allowing a parcel of fluid to move no further than a single mesh cell [McGrattan et al., 2012a].

The domain is discretised with one mesh using cubic cells. A single mesh is chosen because the information exchange between multiple meshes are not as good as the information exchange between the interior cells in the mesh [McGrattan et al., 2012a]. The four different meshes tested are listed in Table 5.9 together with the cell size and the total number of cells.

Mesh	Cell size	Total cells
No. 1	25.00 cm	43,008
No. 2	12.50 cm	344,064
No. 3	8.00 cm	1,312,500
No. 4	6.25 cm	2,752,512

Table 5.9. The four meshes used in the mesh independence study also showing the cell size and the total number of cells in the mesh.

The results for the mesh independence analysis are shown in the next section, where the four meshes are compared to the experiment with the HGL height, the HGL upper temperature and the upper thermocouple in thermocouple tree T1.

5.7.1 Results of Mesh Independence Analysis

Figure 5.18 shows the HGL height for the four mesh simulations and the experiment.

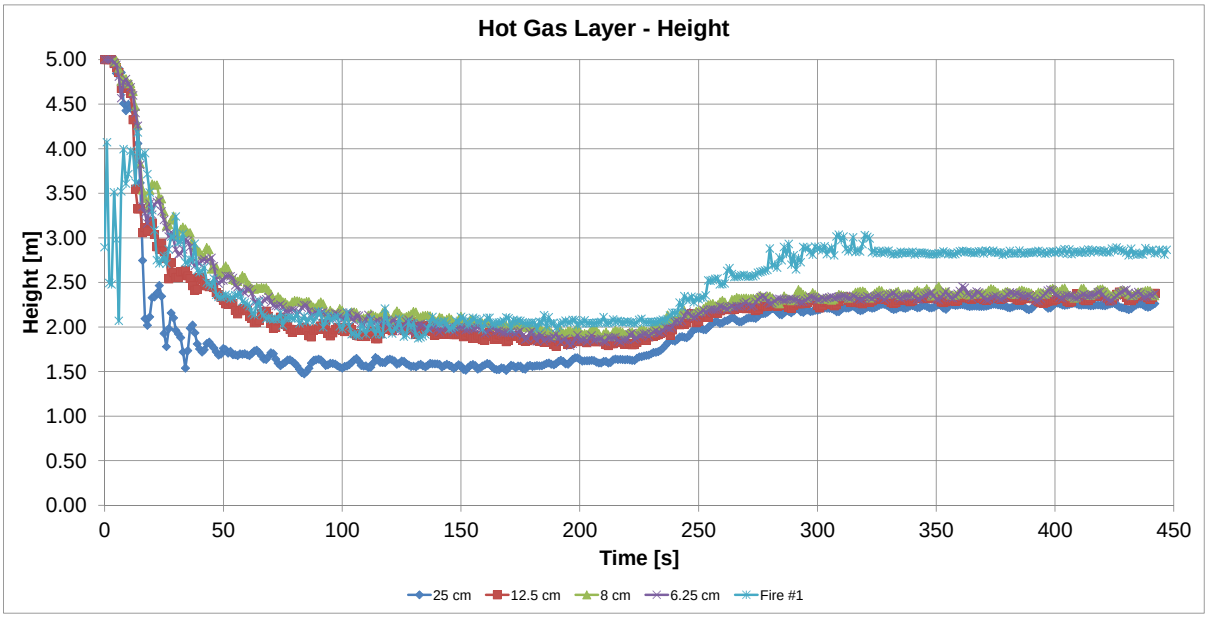

Figure 5.18. Comparison of the HGL height between the four mesh simulations and the experiment.

From Figure 5.18 the mesh simulation with 25 cm cells, over predicts the HGL height when the fire is burning and reach the level of the other simulations when the fire is extinguished. The three other mesh sizes, 12.5, 8 and 6.25 cm cells, shows good agreement between the simulations and the experiment. All three simulations are below 10% in the relative difference when the fire is burning, see Figure 5.19.

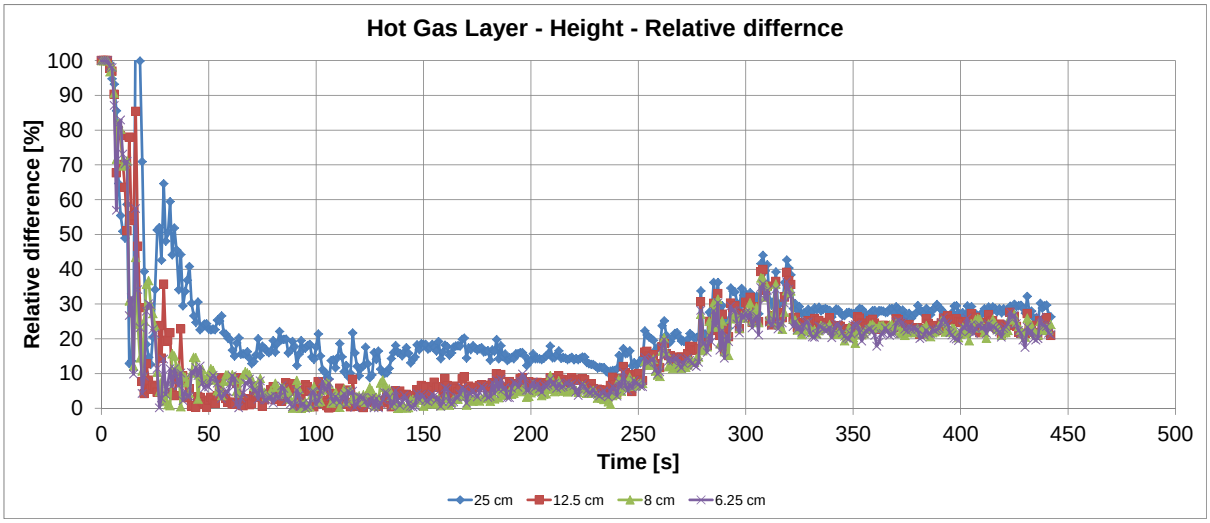

Figure 5.19. The relative difference between the HGL height from the four meshes and the experimental height.

When the fire is extinguished all three simulations has a relative difference to the experiment between 20-30%. The upper temperature of the HGL is shown in Figure 5.20.

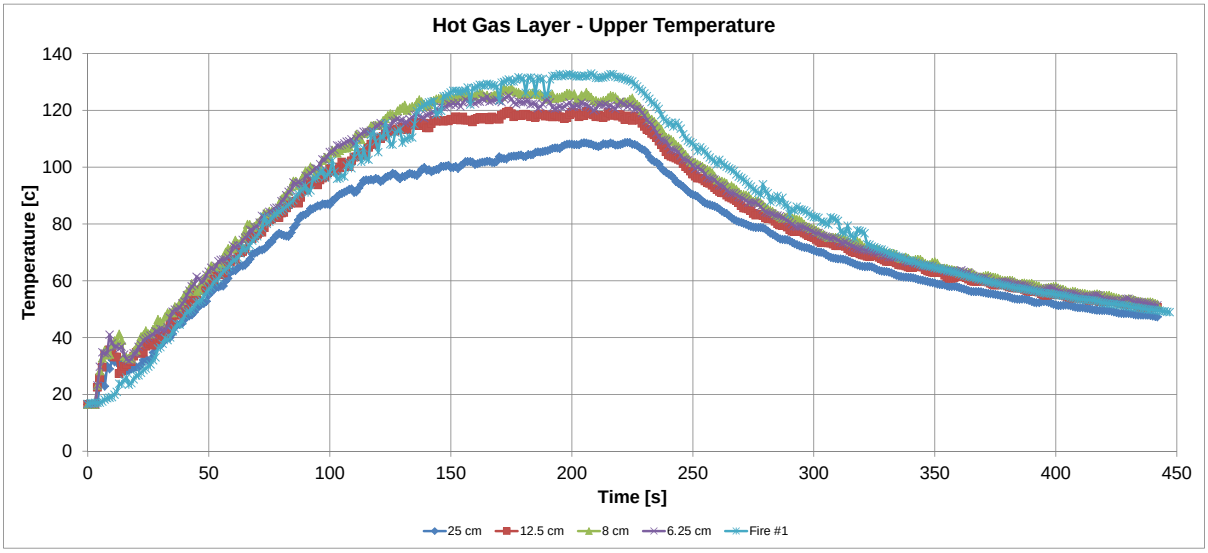

Figure 5.20. Comparison of the HGL upper temperature for the four mesh simulations and the experiment.

Again the mesh with 25 cm cells is not capable of obtaining values in the range of the experimental results when the fire is burning. A slight improvement of the results are seen by reducing the cell size from 12.5 cm to 8 cm. Reducing the cells size from 8 cm to 6.25 cm does not give an improvement, instead it remains approximately the same. The improvement of the relative difference, in the steady state interval 150-225 second, from around 11% for the 12.5 cm cells to around 6% and 7% for the 8 cm and 6.25 cm cells, respectively, see Figure 5.21.

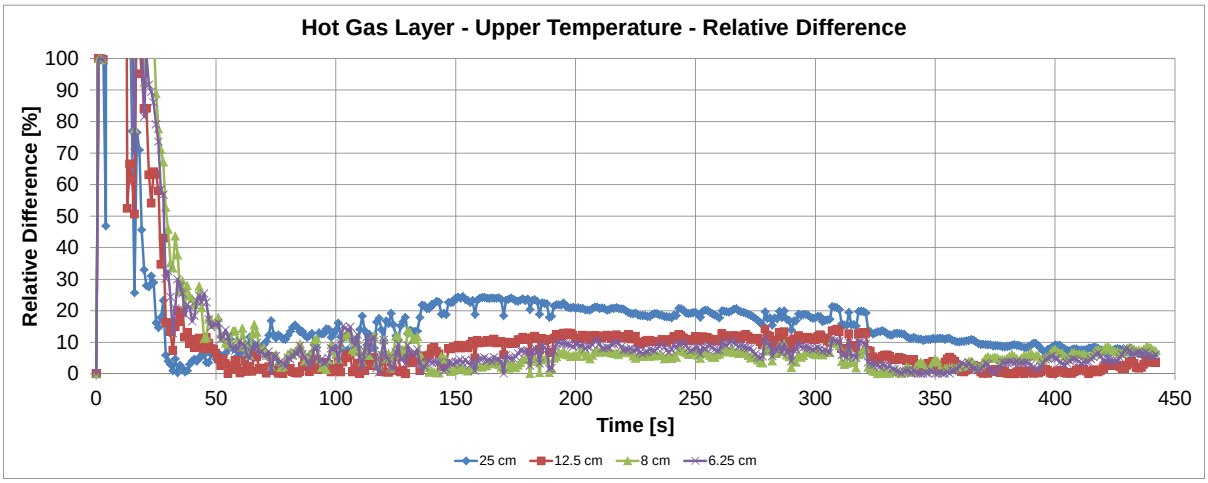

Figure 5.21. The relative difference between the HGL upper temperature from the four meshes and the experimental height.

Finally the comparison of the temperature from T1.10 thermocouple is shown in Figure 5.22.

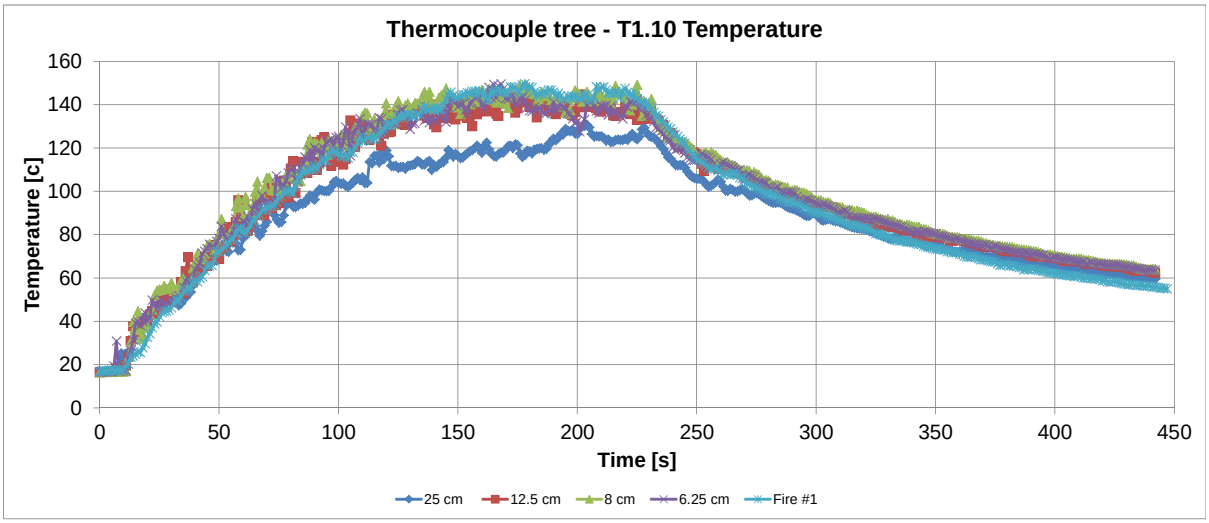

Figure 5.22. The temperature profile of the T1.10 thermocouples from the four meshes simulations and the experimental results.

In the comparison of the temperature from the T1.10 thermocouple the agreement between the three fine meshes and the experimental results are very good. The relative difference for the three fine meshes are all below 10% when the fire is burning and below 20% when the fire is extinguish. Decreasing the cells size means that the total number of cells increases and thereby the computational time increase. Therefore to determine the size of the mesh it is important to know the computational time for each cell size, which are listed in Table 5.10 and the third column shows the difference between the simulations with the 12.5 cm cells simulation as the reference.

Simulation	**Cell size**	**Time [h]**	**Difference [%]**
No. 1	25.00 cm	0.36	5.71
No. 2	12.50 cm	6.31	-
No. 3	8.00 cm	31.00	491.28
No. 4	6.25 cm	65.09	1031.54

Table 5.10. The total calculation time for the four mesh independence simulation and the difference in calculation time relative to the simulation with 12.5 cm cubic mesh.

When the cell size is reduced to 8 cm and 6.25 cm the computational time are increased with approximately 500% and 1000%, respectively. But with the use of cell sized smaller than 10 cm it allows for the validation of the ceiling jet temperature which is measured 10 cm below the ceiling. It is desired not to have measurement point in the adjacent wall cell, because the boundary profile is calculated in this cell [McGrattan et al., 2012c], which is also illustrated in Figure 5.23.

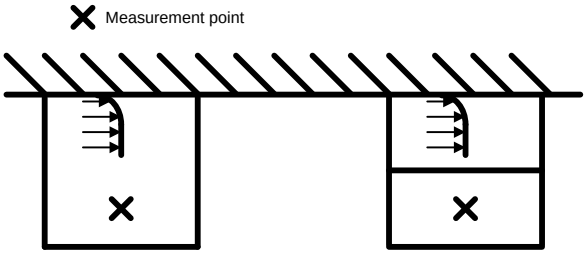

Figure 5.23. Illustration of the use of smaller cells, so the ceiling jet measurement is not in the adjacent wall cell.

Therefore, the cell size of 8 cm is used in the validation study even though the computational time is increased with approximately 500%. The reason for choice is because it enables the use of the ceiling jet temperature in the validation study and a smaller difference is obtained with the 8 cm cells.

5.8 Setup Used for Validation Study

The parameter studies shown above are summarized in Table 5.11, which give a guideline to the setup of FDS for the validation of FDS with the NFSC2 experiment.

	Validation study setup
Heat release rate	85%
Pool size	Equivalent circumference
Computational domain	Room, door length extension
Radiation model	Grey
Radiation mesh	100 angles
Mesh independence	8.00 cm

Table 5.11. The validation setup used in the validation test of the NFSC2 experiment.

The dimension of the domain is shown in Figure 5.24 and 5.25 where the top view and side view are shown, respectively.

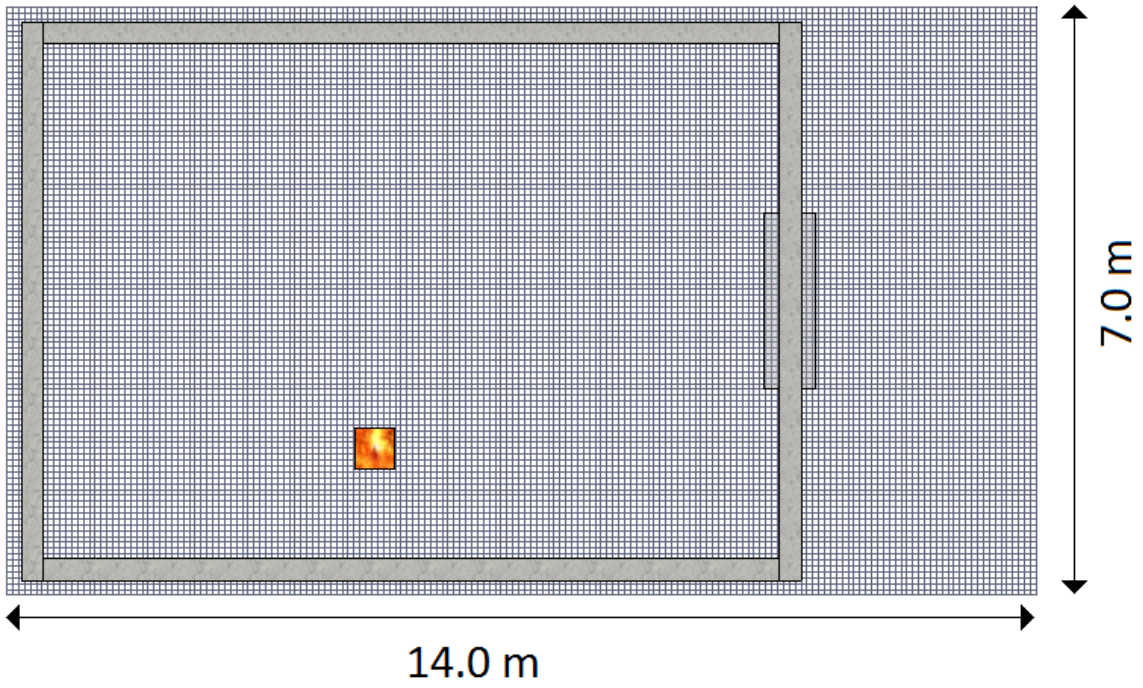

Figure 5.24. Top view of the computational domain with 14 m width in the x-direction and 7 m in the y-direction.

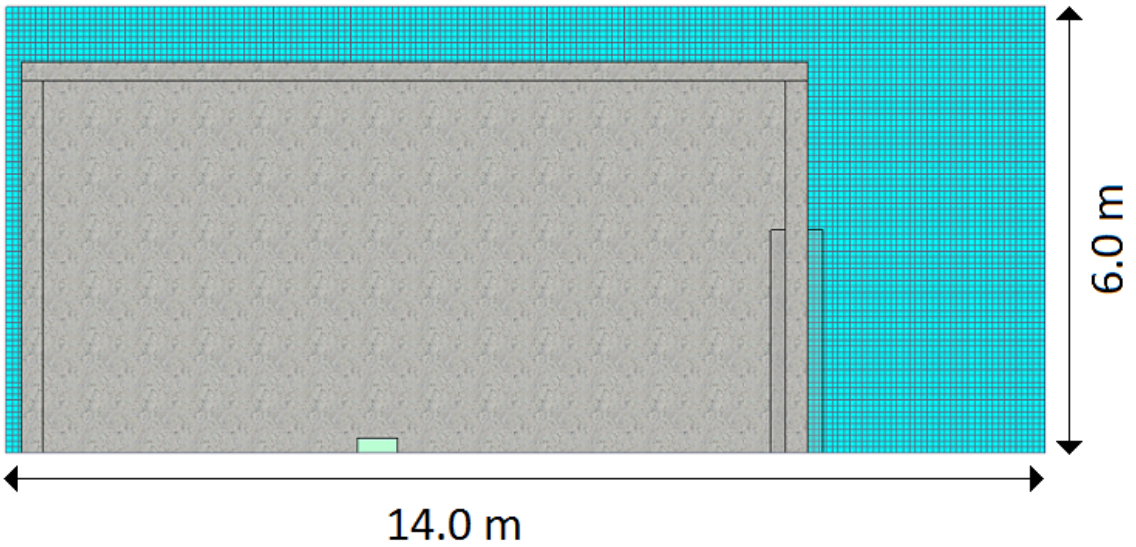

Figure 5.25. Side view of the computational domain with 14 m width in the x-direction and 6 m in the z-direction.

Validation of Fire Dynamics Simulator 6

The validation of FDS with the NFSC2 experiment is presented in this chapter. The chapter consist of the validation study of fire scenario one and two, where the HGL height, HGL upper temperature and ceiling jet temperatures are compared.

6.1 Validation of Fire Dynamics Simulator with the NFSC2 Experiment

The NFSC2 experiment was chosen to validate FDS ability to reproduce the fire driven phenomenons experienced during the experiment. A recommended setup of FDS was determined in the previous section. The recommended setup is then used to validate FDS against fire scenario one and two of the NFSC2 experiment where the transient experimental results are compared to the similar FDS results. The two fire scenarios are compared by the HGL height, HGL upper temperature and the ceiling jet temperature.

For each parameter a graphical plot of the transient development are shown together with the relative difference between the experimental and the simulated results. The results for the HGL height are also compared with the analytical HGL height determined from Heskestads plume model. The calculation of Heskestads plume model is shown in Appendix B. A discussion of the results presented in this section is presented in Section 7.

6.2 Validation of Fire Scenario One

Fire scenario one consist of the experimental test 0 and 1, where an average between the two tests are compared with the FDS results. The fire burns for 240 seconds and burns approximately 3 kg of heptane. The measurement continues to a total simulations time of approximately 440 seconds. The pool fire is located in position two near the side wall with an area of 0.40 m^2 and a circumference of 2.23 m. The door is fully open with 2.4 m width and 3.0 m height during the fire. The other dimensions of the test room are described in Section 4 and Appendix A.

6.2.1 Hot Gas Layer Height

The HGL height describes the location of the interface between the hot smoke layer and the colder lower layer in a burning compartment. Figure 6.1 shows the comparison of the HGL height between fire scenario one and the FDS results. The black line shows the HGL height calculated with Heskestads plume model.

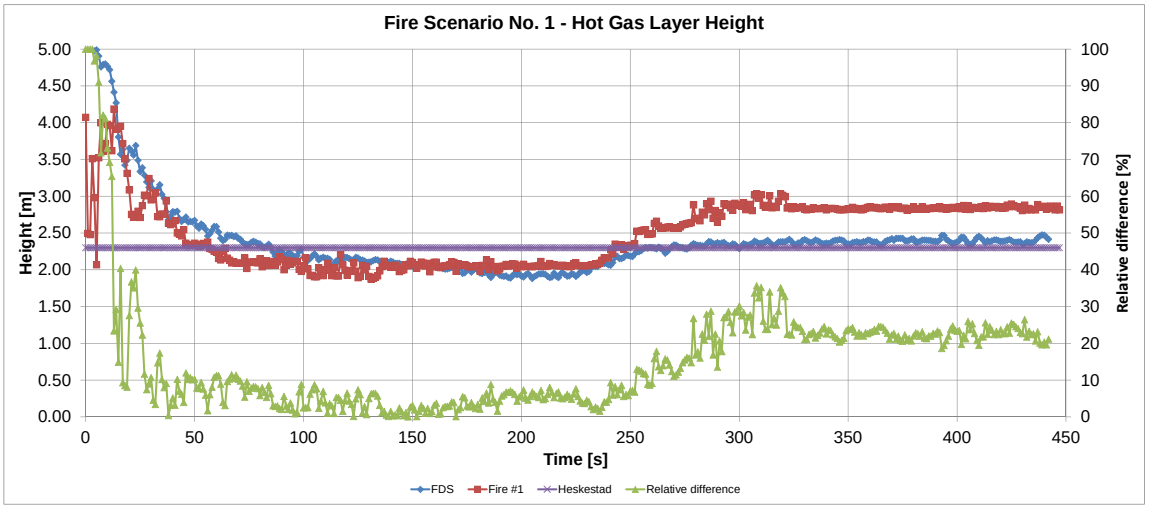

Figure 6.1. Comparison of the HGL height between the experimental results from fire scenario one and the FDS simulations with the relative difference.

The relative difference is below 10% in the first 250 seconds and increase to approximately 20% in the rest of the simulations when the fire is extinguished. The relative difference shows that FDS is capable of reproduce the HGL height of the NFSC2 experiment within the expected difference range of the program and within the experimental uncertainty when the fire is burning.

The Heskestads plume model calculates a steady state HGL height of 2.3 m, which is approximately 12.7% and 11.7% under predictions according to FDS and NFSC2, respectively. Despite these difference, it is shown that using simple assumptions and calculations it is possible to obtain a reliable results for the HGL height in fire scenario one.

6.2.2 Hot Gas Layer Upper Temperature

The HGL upper temperature is the average temperature of the HGL. The comparison of the HGL upper temperature is shown in Figure 6.2.

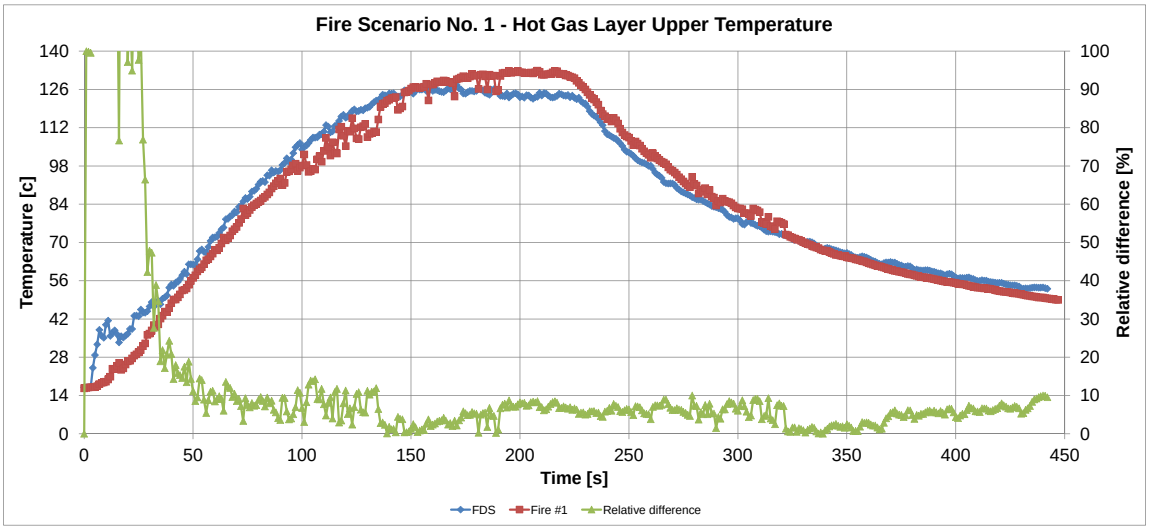

Figure 6.2. comparison of the HGL upper temperature between the experimental results from fire scenario one and the FDS simulations with the relative difference.

After the initial time the relative difference are around and below 10% which shows that FDS is capable of determining the HGL upper temperature for the NFSC2 experiment fire scenario one. The larger relative difference seen in the first 25 seconds of the simulations time is due to the reason discussed in Appendix E, that the calculation of the HGL height and upper temperature are based on temperature difference and the calculation is only valid when a HGL is formed.

6.2.3 Ceiling Jet Temperature

The ceiling jet temperatures in the NFSC2 experiment are measured with 46 thermocouples. In the validation study the C25, C31, C36 and C41 measuring points are selected for comparison. They are selected because they are located perpendicular to the centre of the pool fire where C25 is nearest the fire and C41 furthest away from the fire, see Figure A.6 in Appendix A. The comparison of the ceiling jets temperature are shown in Figure 6.3-6.6.

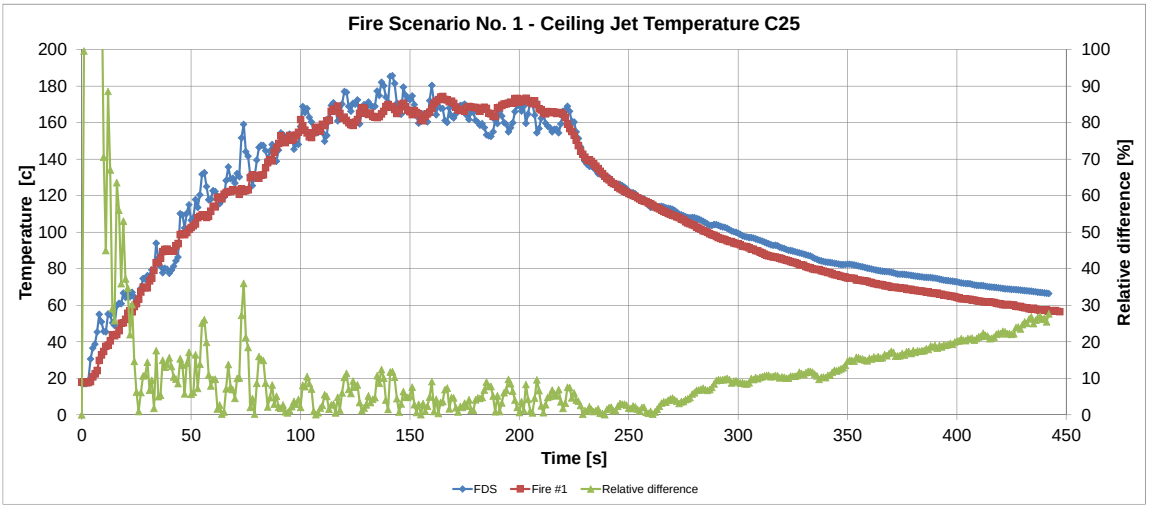

Figure 6.3. Comparison of the ceiling jet temperature in the C25 measuring point. The location of the measuring point in the test room is shown in Figure A.6.

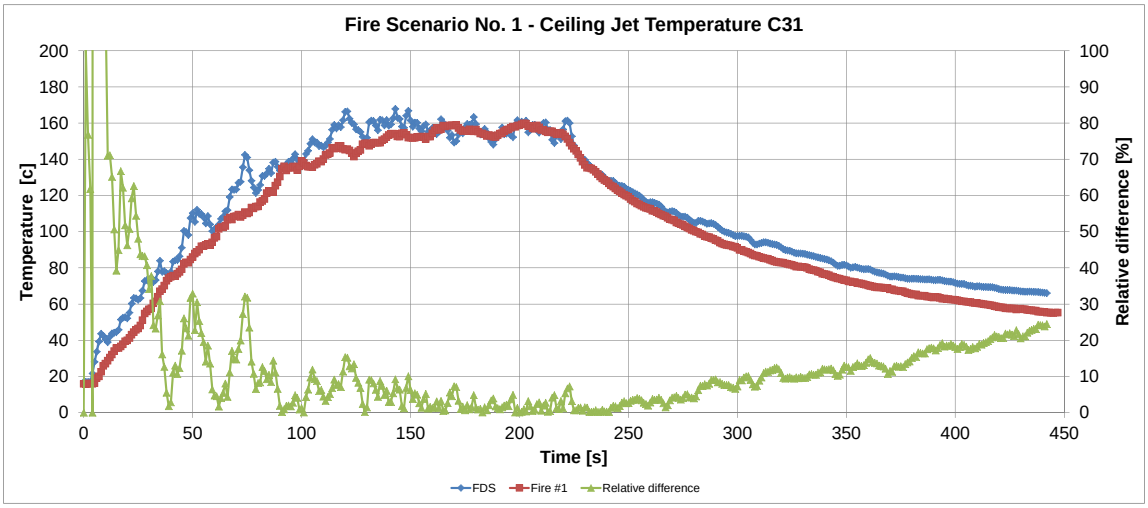

Figure 6.4. Comparison of the ceiling jet temperature in the C31 measuring point. The location of the measuring point in the test room is shown in Figure A.6.

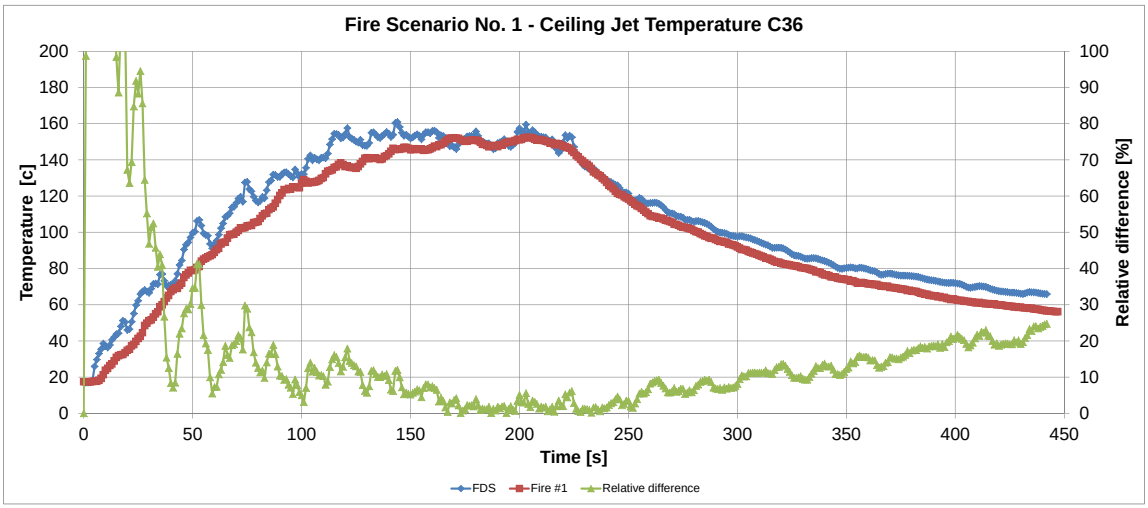

Figure 6.5. Comparison of the ceiling jet temperature in the C36 measuring point. The location of the measuring point in the test room is shown in Figure A.6.

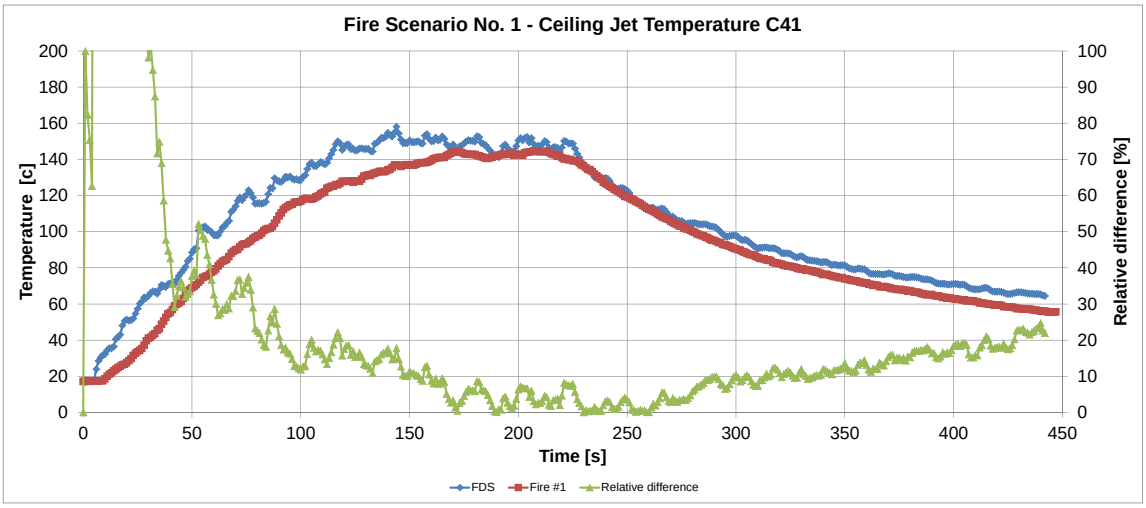

Figure 6.6. Comparison of the ceiling jet temperature in the C41 measuring point. The location of the measuring point in the test room is shown in Figure A.6.

The comparison of the ceiling jet temperature from C25 to C41 shows that FDS over predict the ceiling jet temperature in the first 150 seconds the further away from the fire the measurement comes. The reason for this over prediction is possibly due to the mixing of hot and cold air between the zones which increase the closer the measurement comes to wall. The concept of mixing between the layers are illustrated in Figure 6.7.

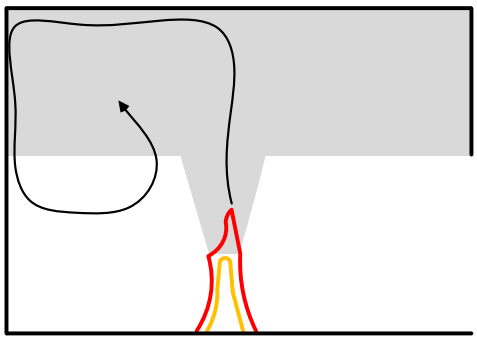

Figure 6.7. Illustration of how the hot smoke moves around inside the enclosure, which causes the over prediction of the ceiling jet temperature in FDS.

The black line shows how the hot smoke raises and follows the ceiling and down the wall before it rises up again due to buoyancy. This movement of the hot smoke is probably the explanation to why the ceiling jet temperatures in FDS are over predicted the closer the measurement is to the wall. Otherwise the relative difference between the FDS results and the experimental results is below 10% until the fire is extinguish and afterwards the relative difference increase up to 25%.

6.3 Validation of Fire Scenario Two

Fire scenario two consist of the experimental test 3, 4 and 5, where an average between the three tests are compared with the FDS results. The fire burns for approximately 480 seconds and burns approximately 11 kg of heptane. The measurement continues to a total simulations time of 600 seconds. The pool fire is located in position two near the side wall with an area of 0.61 m^2 and a circumference of 2.76 m. The door is fully open during the fire. The other dimensions of the test room are described in Section 4 and Appendix A.

6.3.1 Hot Gas Layer Height

The comparison of the HGL for fire scenario two is shown in Figure 6.8.

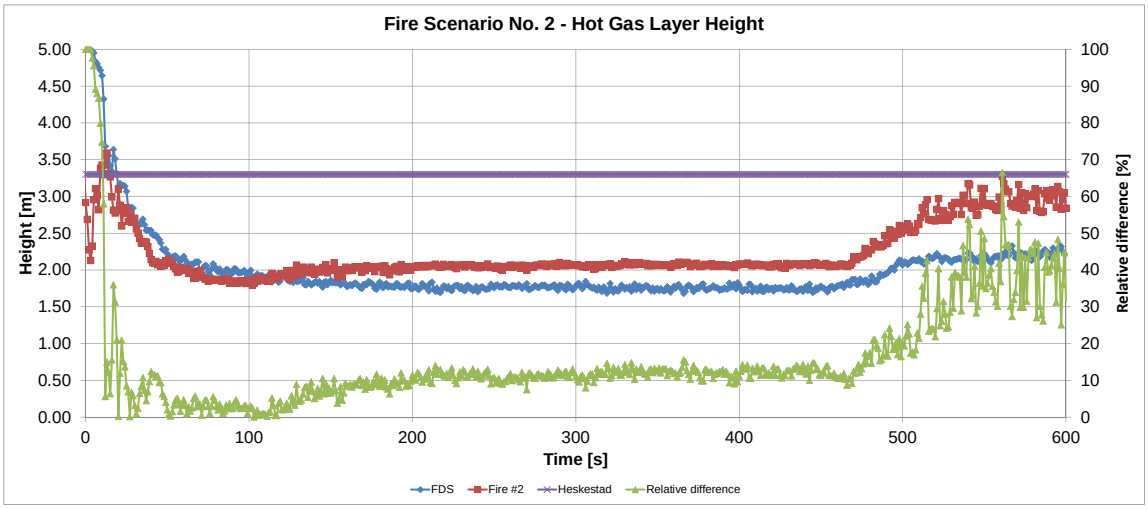

Figure 6.8. Comparison of the HGL height between the experimental results from fire scenario two and the FDS simulations with the relative difference.

The relative difference between the FDS results and experimental results are below 10% after the first initial seconds and until 150, where it increases to approximately 10% in the interval from 150 seconds to 500 seconds. In the last part of the time frame where the fire is extinguish the relative difference increase up to approximately 45%. In this comparison the relative difference is higher than seen in the validation of fire scenario one. This increase could be due to the larger fire and the higher temperature measured in the HGL, which creates a larger temperature gradient between the top and bottom of the test room. To better resolve this temperature gradient a smaller mesh should have been used for this case. Still FDS is capable of reproducing the transient HGL layer and the changes in it, within the expected range of the program.

Heskestads plume model calculates a steady state HGL height of 3.3 which is approximately 80% and 60% under predictions according to FDS and NFSC2, respectively. For fire scenario two Heskestads plume model is not capable of determine the HGL height with in an acceptable range. The reason for this could be that the calculations are made for simple and that the assumptions made for the domain setup is not valid.

6.3.2 Hot Gas Layer Upper temperature

The experimental results and the FDS results are compared in Figure 6.9 for the HGL upper temperature.

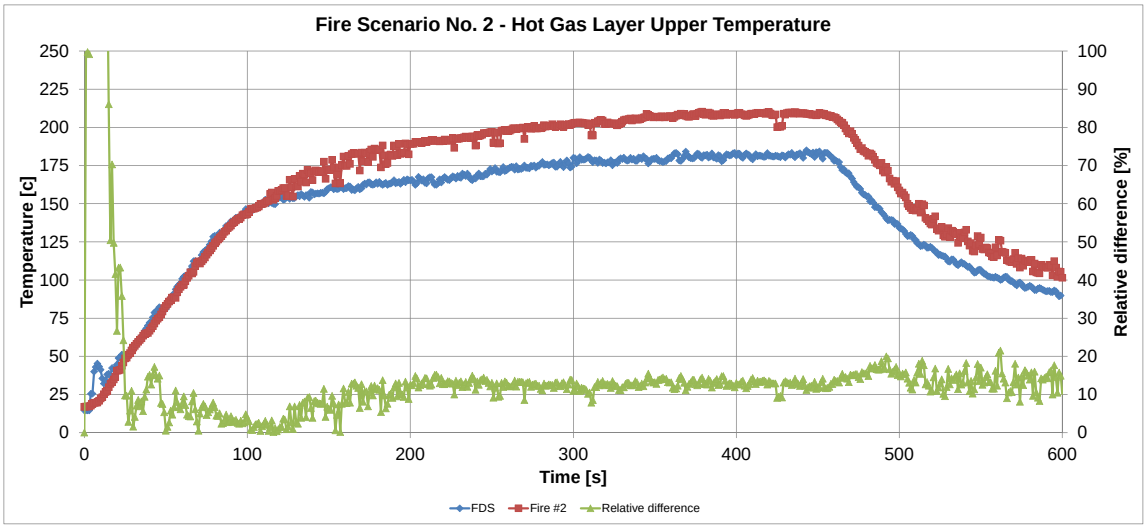

Figure 6.9. comparison of the HGL upper temperature between the experimental results from fire scenario two and the FDS simulations with the relative difference.

Initial the relative difference drops below 10% in the first approximately 150 seconds and afterwards the relative difference is around 15% for the rest of the simulations. This increase in relative difference is possibly due to a larger temperature gradient, which is not fully resolved by the 8 cm cubic cells, but still FDS is capable of reproducing the transient developments of the HGL upper temperature.

6.3.3 Ceiling Jet Temperature

Again, for the validation of the ceiling jet temperature the C25, C31, C36 and C41 measuring points are used. The comparison of the ceiling jet temperatures are shown in Figure 6.10 to 6.13 and the location of the measuring points in the test room are shown in Figure A.6 in Appendix A.

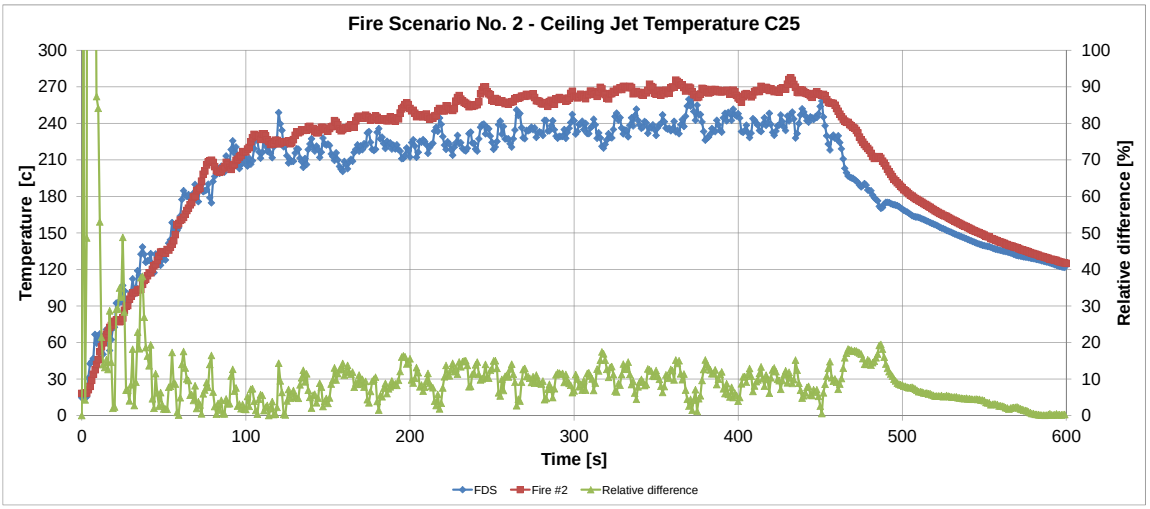

Figure 6.10. Comparison of the ceiling jet temperature in the C25 measuring point. The location of the measuring point in the test room is shown in Figure A.6.

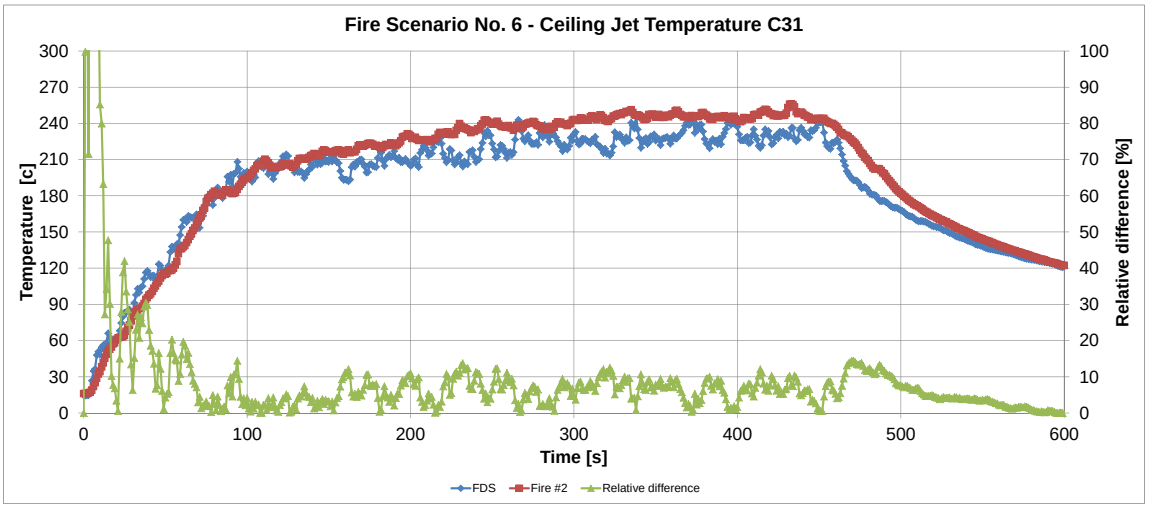

Figure 6.11. Comparison of the ceiling jet temperature in the C31 measuring point. The location of the measuring point in the test room is shown in Figure A.6.

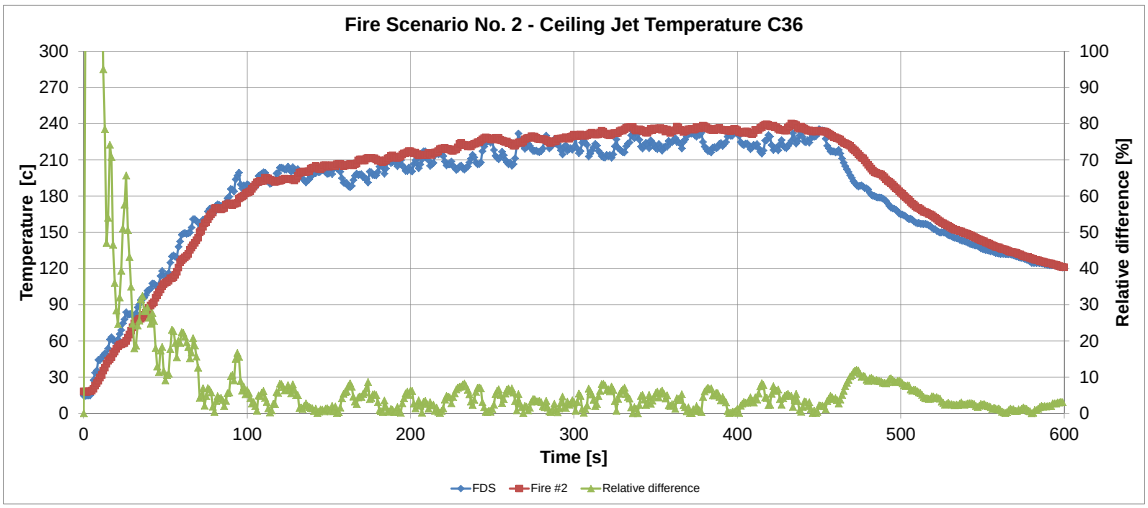

Figure 6.12. Comparison of the ceiling jet temperature in the C36 measuring point. The location of the measuring point in the test room is shown in Figure A.6.

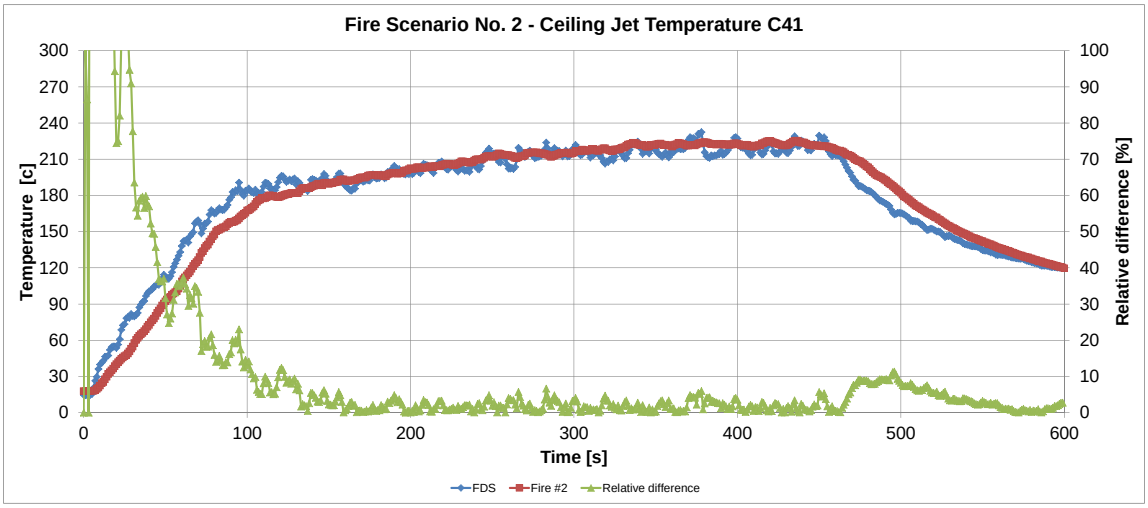

Figure 6.13. Comparison of the ceiling jet temperature in the C41 measuring point. The location of the measuring point in the test room is shown in Figure A.6.

The relative difference in the ”steady state” region from 150-450 seconds is approximately around or below 10% for all four measuring points. The over prediction of the temperature in the first 150 seconds is also seen here, but the over prediction is less significant.

The results presented in the two validation studies are discussed in further details in the following section.

Discussion of Validation Results

7

This chapter contains a discussion of subjects encountered in the parameter and validation study. A discussion is made about the validation of fire dynamics simulator and two zone model compared to computational fluid dynamics model.

7.1 Validation of Fire Dynamics Simulator

In the parameter study in Section 5 an sufficient setup of FDS for the validation studies are determined. In section 6 this setup shows that it has the ability to predict the transient fire induced phenomenon seen in the NFSC2 fire scenario one an two. From all comparison point it is seen that even though FDS under- or over predict a parameter it reproduces the increase and decrease in the parameter at approximately the same time as the experiment.

FDS shows that it has the ability to reproduce the experimental results with in the expected difference of 10-20% and in many cases when the fire is burning the relative difference is below 10%. When the fire is extinguish higher difference between the results are seen for the HGL height in both fire scenario one and two, where the relative difference is up to approximately 45% in fire scenario two.

In fire scenario two the prediction of the HGL height and upper temperature shows that the relative difference is higher than seen in fire scenario one. The reason for this increase is because of a higher HRR from the fire, which creates a higher temperature in the top of the room and thereby creates a stepper gradient between the top and bottom of the domain. Therefore to have the same accuracy of the FDS simulation a smaller cell size should have been used. However, it should be mentioned that the increase in the relative difference is not critical, because the relative difference is still in the expected range of FDS.

Based on the results seen in the parameter studies and in the validation studies, it is found that FDS is capable of reproducing the transient fire induced phenomenon from the NFSC2 experiment, in the most cases within the expected accuracy and in many cases within the experimental uncertainty.

7.2 Two Zone Model Compared to Computational Fluid Dynamics Model

The calculation of the HGL height with Heskestads plume model showed different success for the two fire scenarios. For fire scenario one the HGL height was predicted with a simple difference of approximately 12%. Whereas the difference in fire scenario two are 60% and 80% to NFSC2 and FDS, respectively. Although the results have shown that Heskestad cannot be used for fire scenario two. It is still shown that analytical calculations are capable of providing results that can use and they can be obtained faster

than a CFD calculation.

On the other hand CFD simulations have the ability to give several and more detailed results. For example with CFD it is possible to calculate the composition of the smoke and thereby determine the toxicity of the smoke. Furthermore the CFD simulations also has the ability to simulate the smoke and heat movement in more complex buildings then possible with a two zone models. In the publication "Information about fire safety design" (In danish: Information om brandteknisk dimensionering) it is stated that CFD simulation is only a tool and that it cannot form the foundation of the fire safety design alone. Furthermore they state that it is important that the end user secure that the CFD program does not have mathematical errors and that the program i capable of simulating validation cases [Erhvervs- og Boligstyrelsen, 2004].

Conclusion 8

The object with this report was to determine if FDS could be used to simulate the fire induced phenomenon seen in the chosen experiment. This was tested by performing a parameter study where a sufficient setup for the validation is determined based on the parameters influence on the accuracy and the computational time. The determined setup is then used to perform a validation of two fire scenarios from the experiment, where three parameters are compared.

In the parameter studies it was determined that the combustion efficiency should be 85%, the pool should be modelled with equivalent circumference, the mesh should be extended with a door height beyond the door, that the standard radiation model is sufficient and finally a cell size of 8 cm was chosen. These settings were determined to give an acceptable accuracy of the validation study within a reasonable time frame.

The determined setup in the parameter study was used to perform a validation of FDS according to fire scenario one and two from The NFSC2 experiment. In the validation study FDS shows that it has the ability to reproduce the transient development of the difference parameters within the same timeframe as seen in the experiment. Furthermore FDS was also capable of for the most comparison parameters to determine the its value within the expected range of 10-20% and in many cases the relative difference is below 10%. For some comparison parameter the relative difference increase when the fire was extinguished, for example the HGL height in fire scenario two increase to a relative difference of 45%.

The simple calculation of the HGL height obtained with Heskestads plume showed different success for the two fire scenarios. But still the simple calculations has shown that they can be used. But the CFD calculations has the ability to give many different results and simulate the smoke and heat movement in more complex building design.

Based on the results seen in the parameter studies and in the validation studies, it is found that FDS is capable of reproducing the transient fire induced phenomenon from the NFSC2 experiment, in the most cases within the expected accuracy and in many cases within the experimental uncertainty with a prescribed HRR.

Future Work 9

During the preparation of the validation study of FDS with the NFSC2 experiment different challenges were encountered and in this section two of the challenges are described in more details and suggestion for future improvement are given. The two challenges described are about the difficulties in finding quality experiments and selecting the proper boundary conditions.

9.1 Standard for Fire Experiment

During the search for experiment for the validation study of FDS it soon come clear that it is difficult to find quality experiments, where enough information about the experiment is available in the journal. Also if the experimental journal has the sufficient information and measurement, some of the measurement cannot be used because information is missing. For example in the NFSC2 experiment used in this report, the wall temperature measurement cannot be used as comparison parameter because the moisture content of the walls are not recorded for the experiment.

Dr. Kevin McGrattan has a suggestion to seruce quality data for computer validation: *"You will find that research labs like VTT, SP, NIST, etc, spend millions of dollars/euros on experiments, but for various reasons do not have the time or money or man power to work with the data except to either write a short paper or present their sponsor with some very simple result."* and he continues: *"These labs, including NIST, have talked for years about saving data in some standard format, but all attempts have failed because only us modelers have use for the data after the sponsor has taken what they need."* [McGrattan, 2013].

To avoid the loss of these experimental data the standard format that Dr. Kevin McGrattan talks about should be suggest to the governmental institutions which sponsors the fire experiment. So that the governmental institutions demands the research labs to follow the standard format and thereby secure more quality data for the fire software developers and their communities.

9.2 Boundary Conditions

When setting up FDS it is important to use the correct boundary conditions. This is illustrated by the parameter study in Section 5.3 where the right modelling of the pool is determined. Another example is the missing information about the moisture content of the concrete wall in the NFSC2 experiment which does not gives a correct representation of the walls. This incorrect representation of the wall introduces errors in the FDS results and measurement has to be dropped.

Therefore in future work the focus on obtaining the correct boundary condition should be high prioritised in order to obtain modelling results with minimum errors from the boundary conditions.

Bibliography

Beredskabsstyrelsen, **2013**. Beredskabsstyrelsen. *Dødsbrande og omkomne ved brand - år for år*, 2013. Accessed: 16.05.13.

Drysdale, **2011**. Dougal Drysdale. *An Introduction to Fire Dynamics*. ISBN: 9780470319031, Handbook. Wiley, 2011.

Energistyrelsen, **2012**. Energistyrelsen. *Eksempelsamling om brandsikring af byggeri 2012*, 2012.

Erhvervs- og Boligstyrelsen, **2004**. Erhvervs- og Boligstyrelsen. *Information om brandteknisk dimensionering*, 2004.

Floyd, Forney, Hostikka, Korhonen, McDermott, McGrattan, & Weinschenk, **2012**. Jason Floyd, Glenn Forney, Simo Hostikka, Timo Korhonen, Randall McDermott, Kevin McGrattan, & Craig Weinschenk. *Fire Dynamics Simulator (Version 6) - Technical Reference Guide Volume 3: Validation*. URL: , 2012. Accessed: 03.04.13.

He, Jamieson, Jeary, & Wang, **2008**. Yaping He, Chris Jamieson, Alan Jeary, & Jian Wang. *Effect of Computation Domain of Simulation of Small Compartment Fires*. Fire Safety Science-Proceedings of the Ninth International Symposium, 9, 1365–1376, 2008.

Hostikka, **2013**. Simo Hostikka. *Personal communication*, 2013.

Hostikka, Kokkala, & Vaari, **2001**. Simo Hostikka, Matti Kokkala, & Jukka Vaari. *Experimental Study of the Localized Room Fires - NFSC2 Test Series*, URL: `http://www.vtt.fi/inf/pdf/tiedotteet/2001/T2104.pdf`, 2001.

Intel Corporation, **2013**. Intel Corporation. *Intel core I7 destop processor - Intel turbo boost technology frequency table*, 2013. Accessed: 21.05.13.

Jakobsen, Valkvist, Bennetsen, Carstensen, Madsen, Sommerlund-Thorsen, Hansen, Schmidt, Nygaard, & Sørensen, **2009**. Alex Jakobsen, Morten Birk Sabroe Valkvist, Jens Christian Bennetsen, Rolf Ehlert Carstensen, Gustav Lanng Madsen, Kim Sommerlund-Thorsen, Carsten Stüwing Hansen, Claus Schmidt, Sune Nygaard, & Lars Schiøtt Sørensen. *CFD Best Practice*. URL: `http://www.brand.kk.dk/RaadOgVejledning/~/media/Files/Publikationer/Raad%20og%20vejledning/Best%20Practice%20CFD%20november%202009.ashx`, 2009. Accessed: 16.02.13.

Karlsson & Quintiere, **2000**. Björn Karlsson & James G. Quintiere. *Enclosure Fire Dynamics*. ISBN: 0-8493-1300-7, Handbook. CRC Press, 2000.

Korhonen & Hostikka, **2009**. Timo Korhonen & Simo Hostikka. *Fire dynamics Simulator with Evacuation: FDS+Evac - Technical Reference and User's Guide*. URL: `http://www.vtt.fi/inf/pdf/workingpapers/2009/W119.pdf`, 2009. Accessed: 03.04.13.

McDermott, **2013**. Randall McDermott. *Contribution Guide - Guide on how to contribute to FDS-SMV development*, 2013. Accessed: 06.04.13.

McGrattan, **2013**. Dr. Kevin McGrattan. *Personal communication*, 2013.

McGrattan, **2005**. Kevin McGrattan. *Fire Modeling: Where Are We? Where Are We Going?* Fire Safety Science. Proceedings. Eighth (8th) International Symposium, pages 53–68, 2005.

McGrattan, McDermott, Hostikka, & Floyd, **2012a**. Kevin McGrattan, Randall McDermott, Simo Hostikka, & Jason Floyd. *Fire Dynamics Simulator (Version 5) - User's Guide*. URL: `https://docs.google.com/folder/d/0B-EZ4HlrI6VDUWtRN1N0MmM5c1U/edit?docId=0B_wB1pJL2bFQQzlJVklhSkpoa28`, 2012. Accessed: 11.02.13.

McGrattan, McDermott, Hostikka, & Floyd, **2012b**. Kevin McGrattan, Randall McDermott, Simo Hostikka, & Jason Floyd. *Fire Dynamics Simulator (Version 5) - Technical Reference Guide Volume 3: Validation*. URL: `https://docs.google.com/folder/d/0B-EZ4HlrI6VDUWtRN1N0MmM5c1U/edit?docId=0B_wB1pJL2bFQel91N2prdHVsWjg`, 2012. Accessed: 11.02.13.

McGrattan, McDermott, Hostikka, Floyd, Baum, Rehm, & Mell, **2012c**. Kevin McGrattan, Randall McDermott, Simo Hostikka, Jason Floyd, Howard Baum, Ronald Rehm, & William Mell. *Fire Dynamics Simulator (Version 5) - Technical Reference Guide Volume 1: Mathematical Model*. URL: `https://docs.google.com/folder/d/0B-EZ4HlrI6VDUWtRN1N0MmM5c1U/edit?docId=0B_wB1pJL2bFQTFMtckVGY1FzTjg`, 2012. Accessed: 11.02.13.

Møller, **2000**. Kristian Møller. *De samfundsøkonomiske omkostninger ved brand*, URL: `http://brs.dk/viden/publikationer/Documents/De_samfunds%C3%B8konomiske_omkostninger_ved_brand.pdf`, 2000.

Nielsen, **2010**. Peter V. Nielsen. *DCE Lecture Notes No. 22 - Dimensiionering af Brandventilation*, 2010.

Olenick & Carpenter, **2003**. Stephan M. Olenick & Douglas J. Carpenter. *An Updated International Survey of Computer Models for Fire and Smoke*. Journal of Fire protection engineering, 13, 87–110, 2003.

Olenick, **2008**. Stephen M. Olenick. *Fire model survey*, 2008. Accessed: 12.03.13.

SFPE & NFPA, **2002**. Society of Fire Protection Engineers SFPE & National Fire Protection Association NFPA. *The SFPE Handbook of Fire Protection Engineering*. ISBN: 087765-451-4, Handbook. National Fire Protection Association, 2002.

Sørensen, **2004**. Lars Schiøtt Sørensen. *Brandfysik og brandteknisk design af bygninger*. ISBN: 87-5020959-0, Handbook. Polyteknisk Forlag, 2004.

Thunderhead Engineering, **2011**. Thunderhead Engineering. *Pathfinder*, 2011. Accessed: 03.04.13.

Turns, **2000**. Stephen R. Turns. *An Introduction to Combustion: Concepts and Applications*. ISBN: 0-07-230096-5, Handbook. McGraw-Hill, 2000.

Versteeg & Malalasekera, **2007**. H. K. Versteeg & W. Malalasekera. *An Introduction to Computational fluid dynamics - The Finite Volume Method*. ISBN: 978-0-13-127498-3, Handbook. Pearson Education Limited, 2007.

Experiment - Measurement point A

This appendix contains a description of the measurement points which are recorded during the VTT experiment. This appendix is based on the experimental report by [Hostikka et al., 2001]. The experimental report is also found on the attached CD-ROM.

The benchmark experiment is the "Experimental Study of the Localized Room Fires - NFSC2 Test Series". The experiment is performed by Simo Hostikka, Matti Kokkala and Jukka Vaari from VTT Technical Research Centre of Finland. This experimental study consists of two series of full scale fire tests, which were produced for CFD code verification. The fire test which is used in this report is an experimental series which consist of 21 tests in a 10 x 7 x 5 m^3 test room with a 2.4 x 3.0 m^2 opening to ambient. The test room is placed in the middle of a 27 x 13 x 19 m^3 test hall. An overview of the experimental setup is shown in Figure A.1 and A.2.

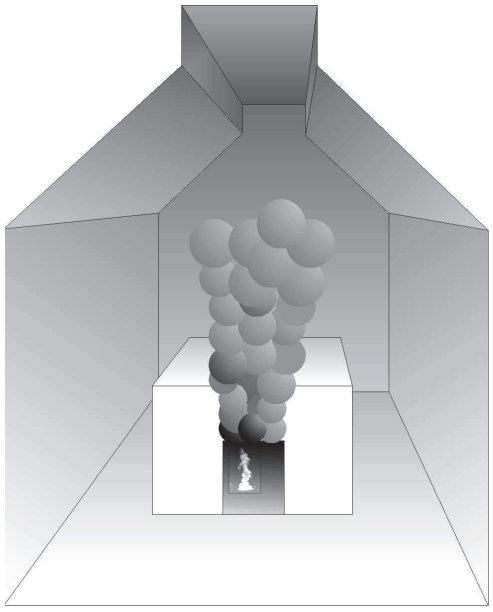

Figure A.1. Principle drawing of the overview of the test hall with the test room in the middle [Hostikka et al., 2001].

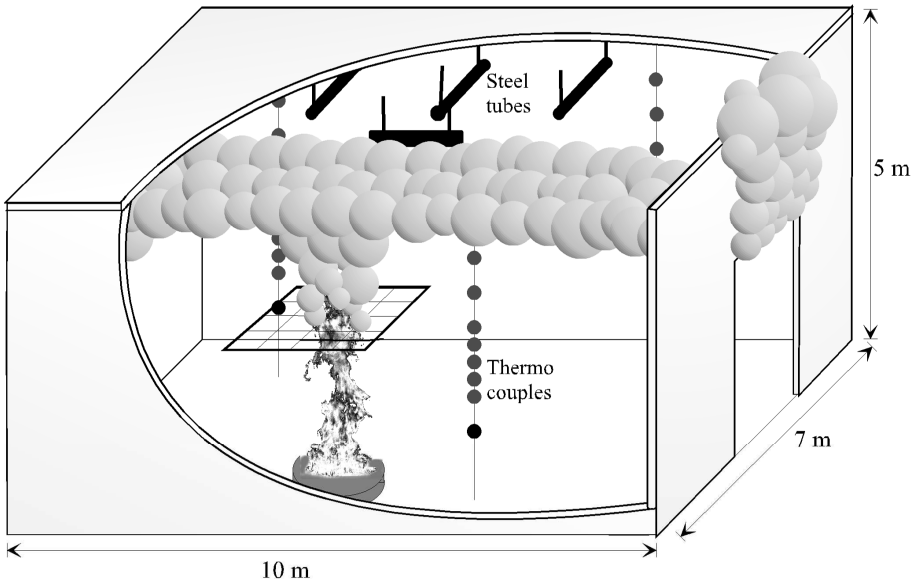

Figure A.2. Principle drawing of the overview of the test room with measurement devices [Hostikka et al., 2001].

Four locations of the fire source were used through the experiments. The locations are shown in Figure A.3.

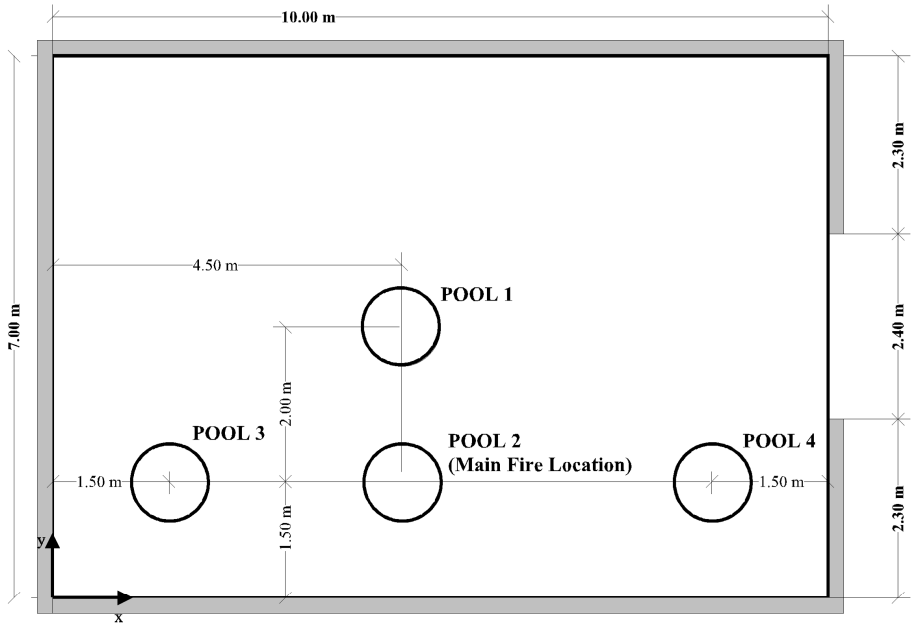

Figure A.3. Illustration of the four pool locations inside the test room [Hostikka et al., 2001].

The gas temperatures of the test room were measured with three thermocouple rakes named T1, T2 and T3. The rakes consisted of 10 bare thermocouples in different heights. During the experiments the thermocouple size were changed from 0.1 mm to 0.5 mm from Test #12 and onwards. The location of the thermocouple rakes are shown in Figure A.4 and in Figure A.5 the spreading of the thermocouples is shown. The numbering of the thermocouples in each rake starts from 1 near the floor to 10 near the ceiling.

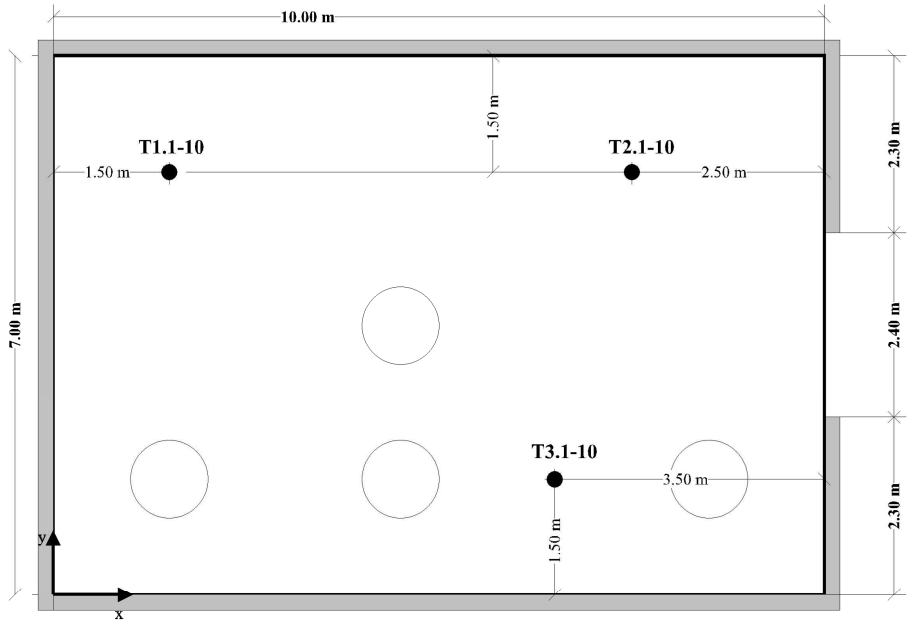

Figure A.4. Location of the thermocouples tree in the test room [Hostikka et al., 2001].

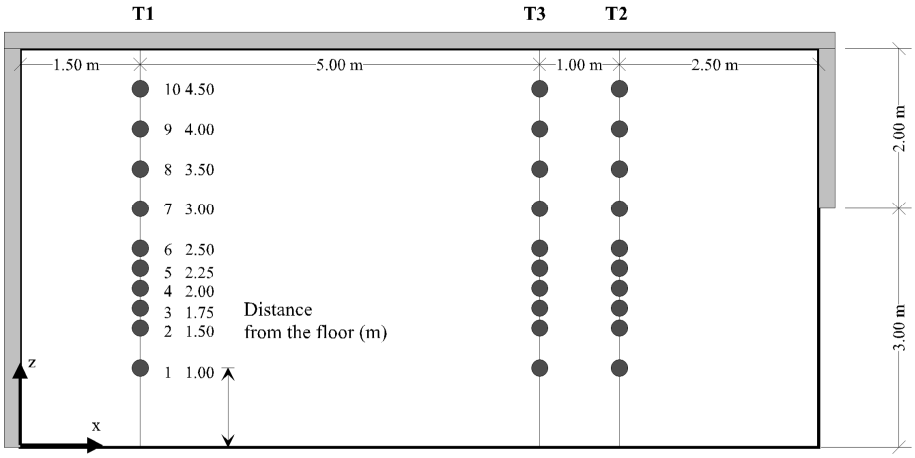

Figure A.5. The spreading of the thermocouples in the thermocouples tree [Hostikka et al., 2001].

The temperature of the smoke layer near the ceiling is measured with 46 0.5 mm thermocouples. The thermocouple is placed 0.1 meter below the ceiling, and the horizontal location is seen in Figure A.6.

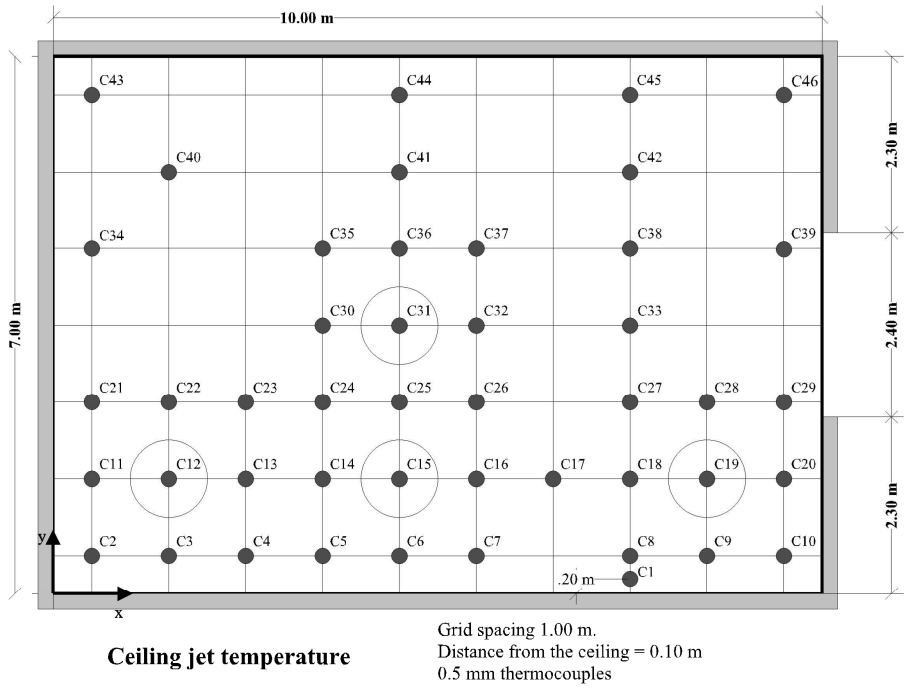

Figure A.6. The spreading of the thermocouples in the ceiling thermocouple mesh [Hostikka et al., 2001].

The horizontal temperature distribution of the plume was measured with 25 0.5 mm thermocouples placed into a 5 x 5 grid with 0.40 m spacing which is located above the fire location. The height of the thermocouple grid was varied to keep the thermocouple grid just above the flame tip, when the fire was in fire location #2. When the fire was in one of the other fire location, the gird was 0.60 m below the ceiling. The numbering of the grid is shown in Figure A.7. The grid height can be found in the experimental journal [Hostikka et al., 2001], which also is found on the attached CD-ROM.

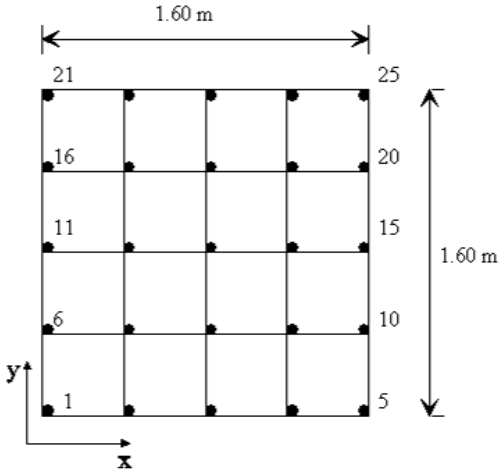

Figure A.7. The thermocouple grid for the horizontal plume grid [Hostikka et al., 2001].

In the door both the temperatures and the velocities were measured in the same vertical plane as the outer surface of the wall. The temperature was measured with twelve 0.5 mm thermocouples. The velocity was measured with six bi-directional probes. The location of the thermocouples and velocity probes are shown in Figure A.8.

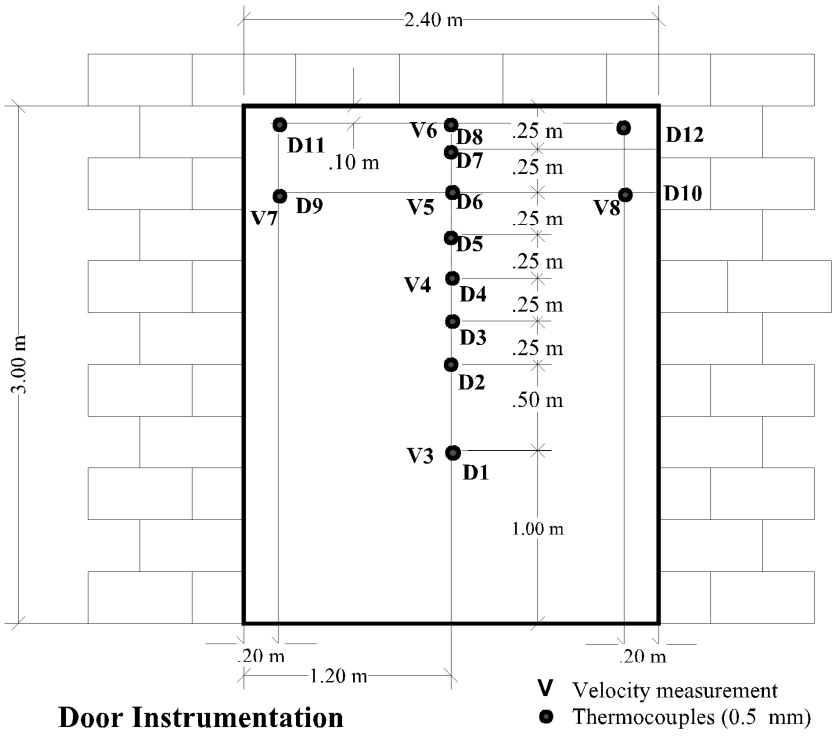

Figure A.8. The location of the thermocouples and velocity measurement in the door [Hostikka et al., 2001].

Ten plate thermocouples were used to measure the heat flux to thin steel objects. Three were placed on the wall, four just below the ceiling and the last two were placed on the floor. The location of the ten plate thermocouples in the test room are shown in Figure A.9.

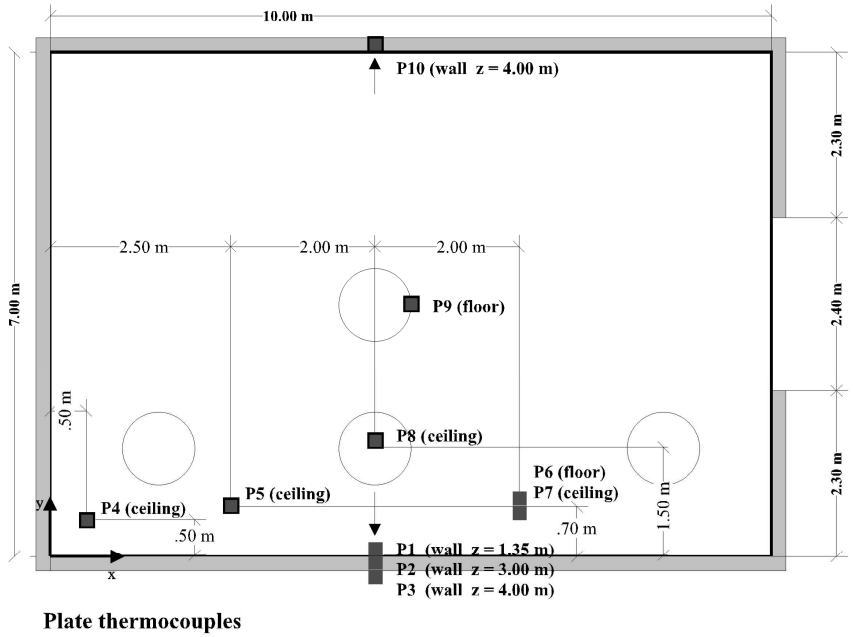

Figure A.9. The location of the plate thermocouples in the test room [Hostikka et al., 2001].

The heat flux to a body was measured with one Gardon-type (R1) and four Schmidt-Boelter. The location

and numbering of the five heat flux meter are shown in Figure A.10.

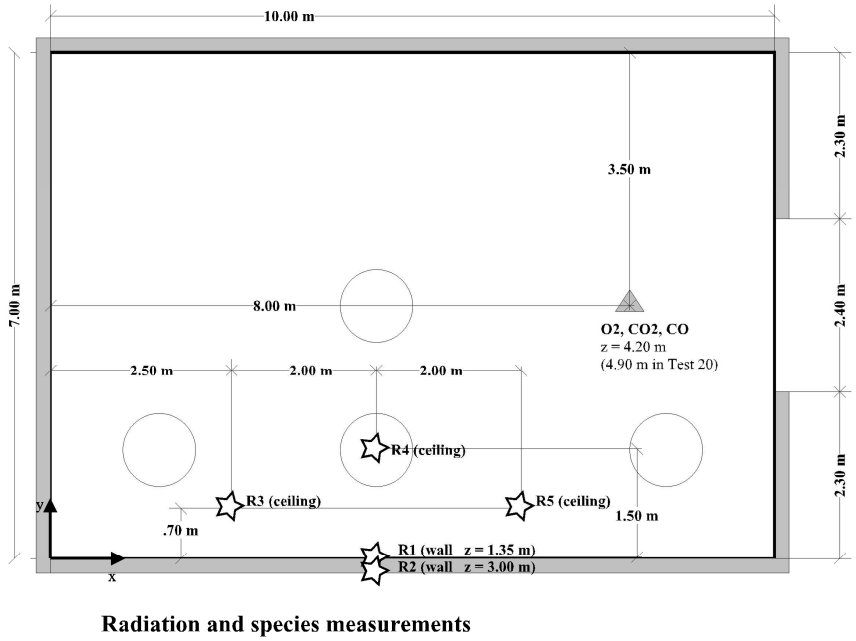

Figure A.10. The location of heat flux meter in the test room [Hostikka et al., 2001].

The heating of the concrete walls were measured by thermocouples which were located at different depths of the walls. The three measuring locations are shown in Figure A.11.

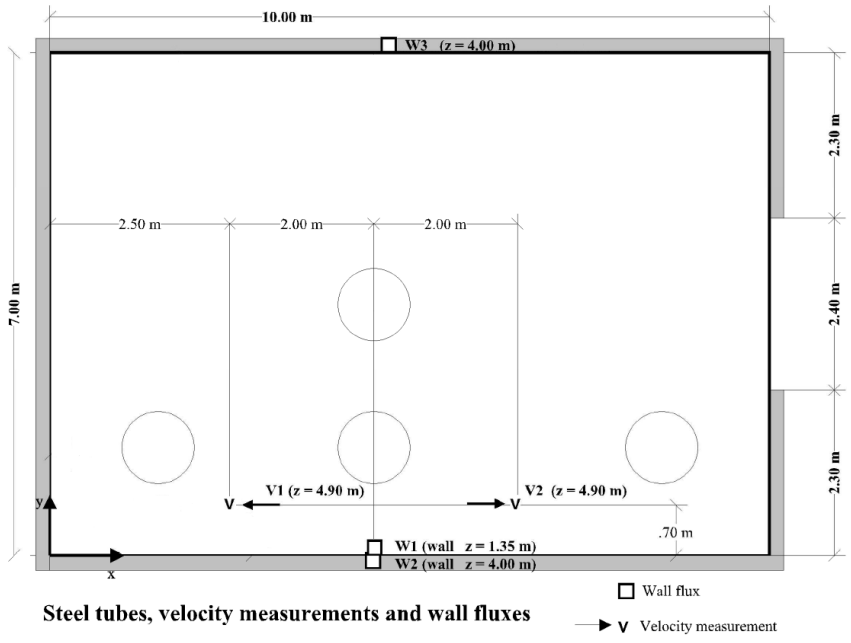

Figure A.11. The location of wall thermocouple and ceiling jet velocity probes in the test room. The picture is modified according to the original picture in [Hostikka et al., 2001] to only show the wall thermocouples and ceiling jet velocity measurement.

The depth of the wall thermocouples are listed in Table A.1.

ID	Depth [m]	ID	Depth [m]	ID	Depth [m]
W1.1	0.0030	W2.1	0.0045	W3.1	0.0050
W1.2	0.0090	W2.2	0.0060	W3.2	0.0070
W1.3	0.0095	W2.3	0.0100	W3.3	0.0095

Table A.1. The depth of the nine wall thermocouples [Hostikka et al., 2001].

Determining Hot Gas Layer Height with Plume Models

B

According to the master thesis in Section 2.2 the results from FDS are compared with results obtained from analytical expression, e.g. the plume models. Therefore the Heskestad and Thomas plume model are used to obtain results of the HGL height.

In order to obtain the results an assumption about the setup of the test has to be made. The assumption is illustrated in Figure B.1

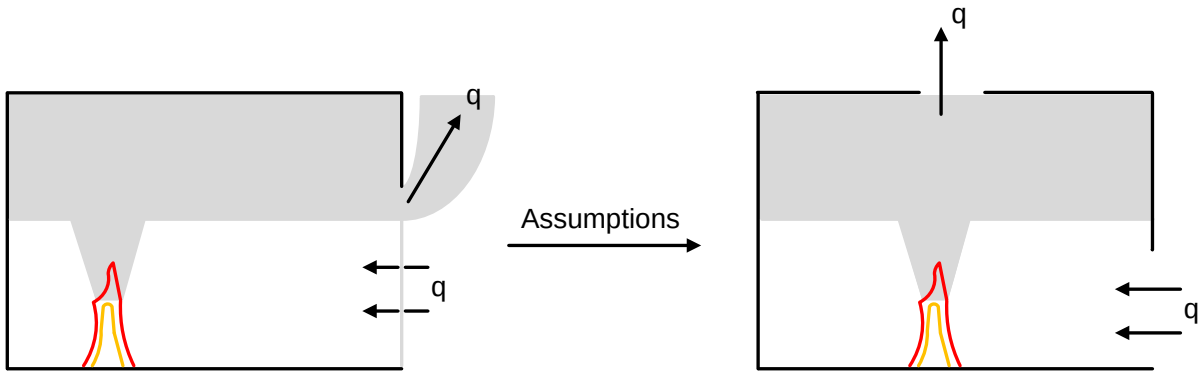

Figure B.1. Illustration of the assumption made in order to use the Heskestad and Thomas plume model to determine the HGL height.

It is assumed that the mass flow of smoke out of the room is equal to the inflow of fresh air, e.g. $\dot{q}_{out} = \dot{q}_{in}$. When the plume mass flow $\dot{q}_{plume}$ also are equal, the height used in Heskestand and Thomas plume equation is assumed to be the height of the HGL height. To calculate the plume mass flow the input parameters listed in Table B.1 are needed.

Parameter		**Fire #1**	**Fire #2**
Total heat release rate	$\dot{Q}$	461 kW	905 kW
Diameter of fuel source	D	0.71 m	0.88 m
Convective coefficient		0.65	0.65
Mass flow of smoke - CFD	$\dot{q}$	2.19 $\frac{kg}{s}$	3.07 $\frac{kg}{s}$

Table B.1. The input parameter for calculation of the HGL height with the Heskestad and Thomas plume model.

The mass flow of smoke out of the domain are obtained from the CFD model where the outflow in the door are measured in the height from 2 m to 3 m, because the HGL height measurement shows the HGL height is two meter above the floor. With Equations 3.3 to 3.8 the following results are obtained for the Heskestad and Thomas plume models, see Table

Parameter		**Fire #1**	**Fire #2**
Virtual origion	[m]	0.24	0.37
Flame height	[m]	2.14	3.46
Convective HRR	[kW]	299.65	588.25
HGL Height	[m]		
- Heskestad		2.3	3.3
- Thomas		3.0	3.3

Table B.2. Results of the plume mass flow calculations for boths fire scenarios.

The HGL height for the two fire scenarios are obtained by using Figure B.2 and B.3 for fire scenario one and fire scenario two, respectively. The black horizontal line in both figures represents the smoke mass flow from the CFD simulation. Thomas plume model is also shown in the figures even though L > D and the models is not valid.

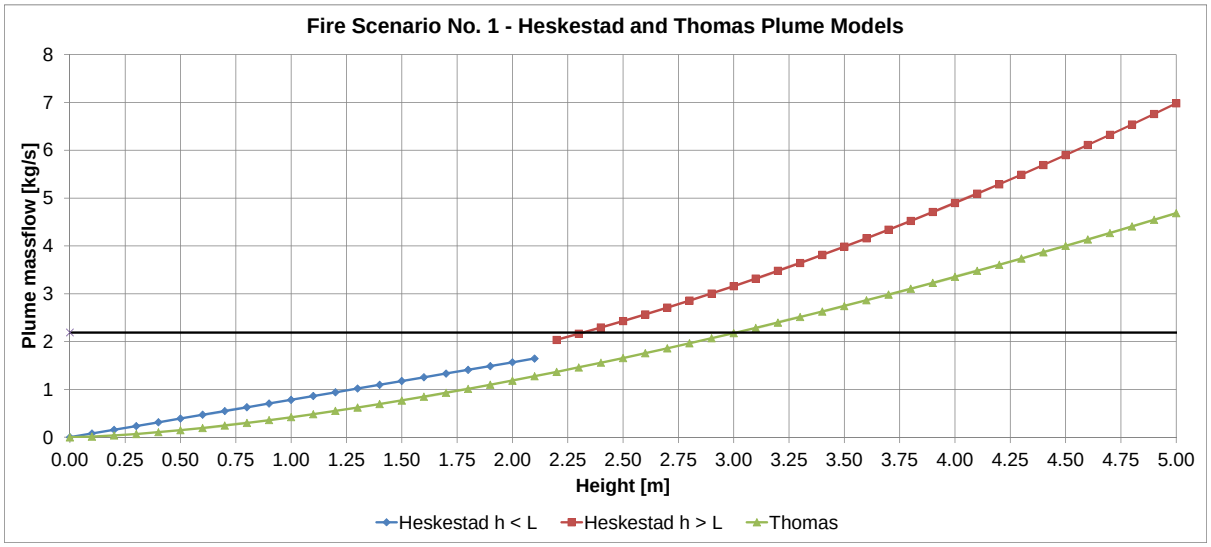

Figure B.2. Illustration of the plume mass flow as a function of the height above the floor for Heskestad and Thomas plume model in fire scenario one. The black horizontal line represents the smoke mass flow from the CFD simulation.

From Figure B.2 the HGL height is found by the intersection between the smoke mass flow and the plume models. For the Heskestad model the HGL height is determined to 2.3 m and for Thomas model it is determined to 3.0 m. The same comparison for fire scenario two is shown in Figure B.3.

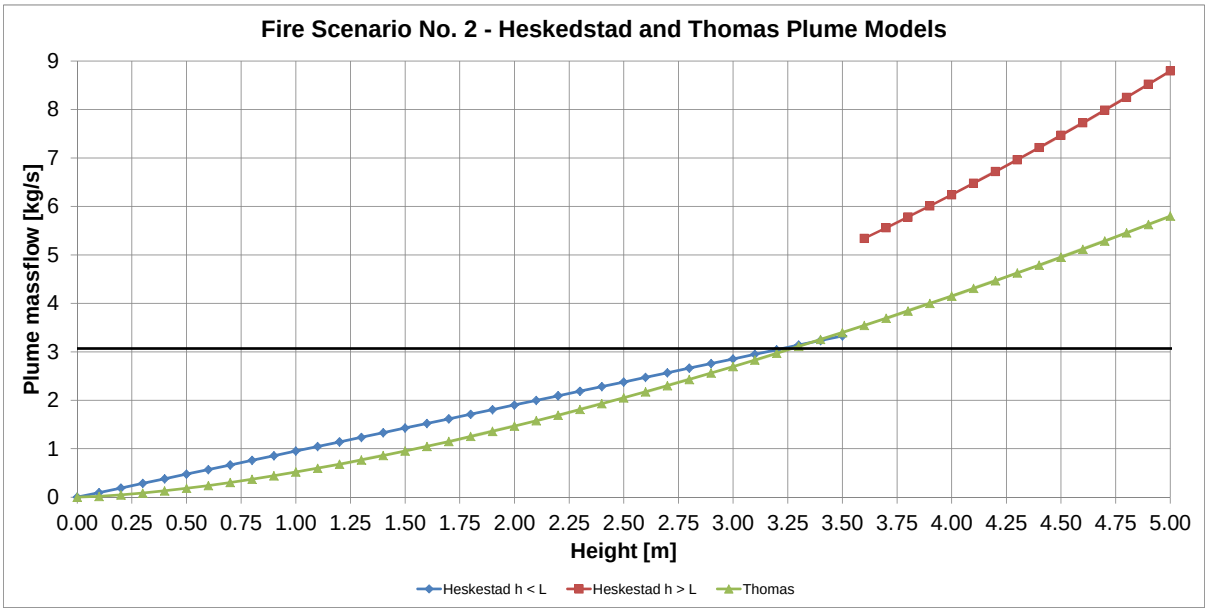

Figure B.3. Illustration of the plume mass flow as a function of the height above the floor for Heskestad and Thomas plume model in fire scenario two. The black horizontal line represents the smoke mass flow from the CFD simulation.

From Figure B.3 the HGL height is found by the intersection between the smoke mass flow and the plume models. The plume mass flow is determined to 3.3 m for both the Heskestad and Thomas plume model.

Because Thomas' plume model is not valid for use in fire scenario one and two, the HGL height of this will not be used for further comparison with the FDS results. Instead the HGL height determined with Heskestad plume model is in Section 6 compared with both the experimental and FDS obtained HGL height. Furthermore in Section 7 a discussion of two zone model and CFD model are given.

Turbulence Modelling C

This appendix contains a short description of turbulence general and a description of the three turbulence models, the Reynolds-Average Navier-Stokes (RANS), the Large Eddy Simulation (LES) and the Direct Numerical Simulation (DNS). In a turbulent flow the flow properties vary in a random and chaotic way. An example of this chaotic random behaviour is shown in Figure C.1.

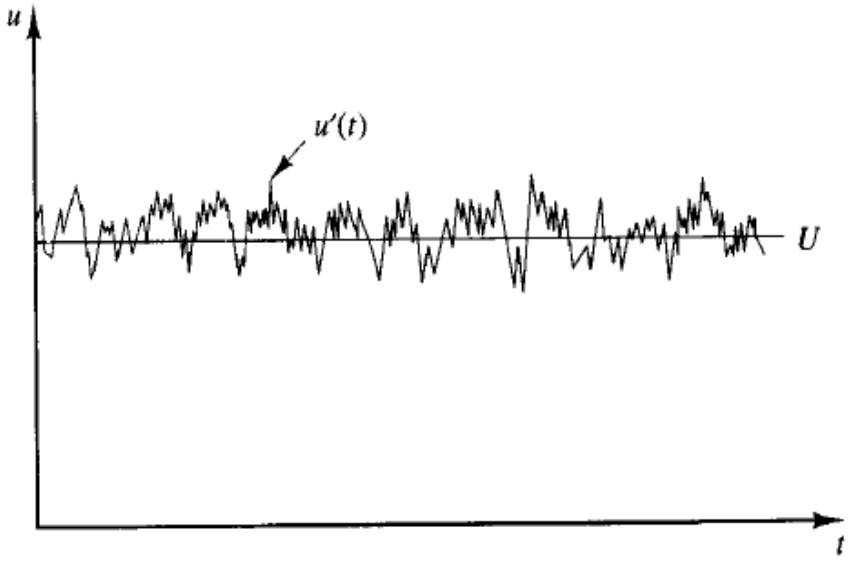

Figure C.1. A point velocity measurement in turbulent flow. The velocity vary in a chaotic manner around a mean velocity [Versteeg & Malalasekera, 2007].

In turbulent flows the rotational flow structure called turbulent eddies are found in a wide range of length scales. In the different method of handling turbulence is the different eddies either resolved or modelled by extra continuity equations. The difference between the three turbulence models ways of treating the chaotic random behaviour is shown in Figure C.2.

Figure C.2 illustrates how the RANS models is an average of the both the large and small fluctuation. The LES solves the larges the large fluctuation and model the small fluctuations. Finally the DNS solves both the large and small fluctuation. The RANS, LES and DNS are described in further details next.

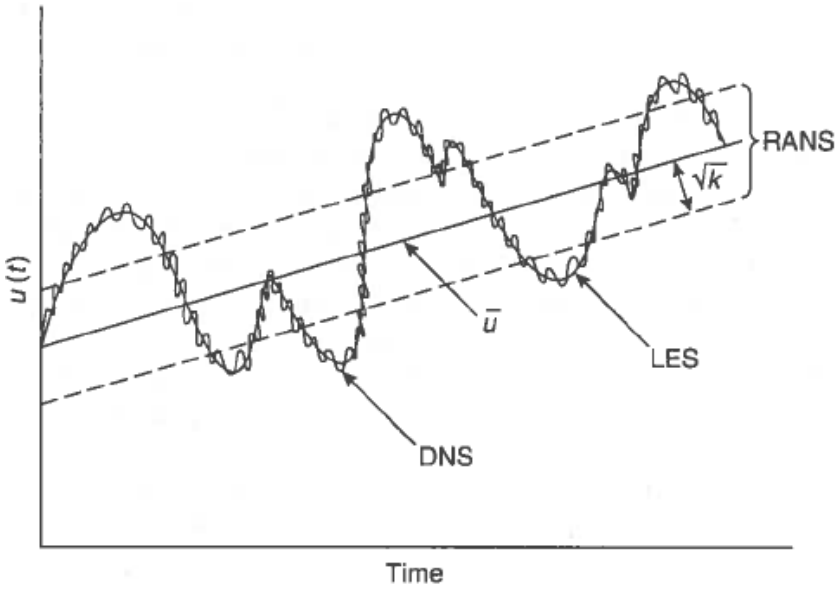

Figure C.2. Illustration of how the three turbulence models treats the turbulence [SFPE & NFPA, 2002].

C.1 Direct Numerical Simulation - DNS

DNS is direct transient solving of the Navier-Stokes equation on a sufficiently fine spatial mesh with an adequate small time step to resolve the smallest eddies [Versteeg & Malalasekera, 2007]. It is possible to perform DNS calculation in FDS if the underlying numerical grid is fine enough [McGrattan et al., 2012c]. Because the DNS method requires very small spatial and temporal discretisation it is very time consuming and not usable for practical engineering purpose [Versteeg & Malalasekera, 2007]

C.2 Large Eddy Simulation - LES

LES is a transient turbulence modelling technique. In large eddy simulation a spatial filtering technique is used to separate the large and smaller eddies. The larger eddies which are resolved by the spatial grid are calculated directly. The smaller eddies which are nearly isotropic and have a universal behaviour are modelled. There exists different filters and their functions together with the cut-off width Δ is to determine which eddies are resolved and which are modelled. The cut-off width Δ can have any size, but for finite volume CFD method it is not recommend to have a cut-off width which is smaller than the spatial grid. Therefore the cut-off width is commonly selected to be of the same order as the grid size [Versteeg & Malalasekera, 2007].

Because the LES is transient it requires large computational resources to storage and calculation, but the technique is begin to be used in more complex geometry [Versteeg & Malalasekera, 2007]

C.3 Reynolds-Averaged Navier-Stokes - RANS

The RANS model focus on the mean flow and the turbulences parameters effects on the mean flow. The RANS model consists of the averaged Navier-Stokes equations. An extra term, named the Reynolds stresses, appears when the Navier-Stokes equation is averaged. This extra term is modelled with extra equation, for example the k-ϵ, k-ω equation, etc [Versteeg & Malalasekera, 2007]. The RANS model is not available in the FDS software.

Estimation of Combustion Efficiency

D

This appendix contains the calculation procedure used to give an estimate of the combustion efficiency. The chemical program CEA-NASA is used to calculate the chemical composition of the products. The calculated carbon monoxide is compared to the experimental recorded carbon monoxide to estimate the combustion efficiency.

Carbon monoxide is a product of incomplete combustion when not enough oxygen is presented in the combustion area. In the experimental report for NFSC2 the author has estimated a combustion efficiency of 80%±10% [Hostikka et al., 2001]. In this investigation it is assumed that the combustion efficiency is due to lack of oxygen in the combustion area, which produces carbon monoxide.

Therefore it is assumed that the 100% combustion occurs with stoichiometric condition, which is shown in Equation D.1.

$$\begin{aligned} C_7H_{16} + n_s\,(O_2 + 3.76N_2) &\rightarrow n_1CO_2 + n_2H_2O + n_3N_2 \\ C_7H_{16} + 11\,(O_2 + 3.76N_2) &\rightarrow 7CO_2 + 8H_2O + 41.36N_2 \end{aligned} \tag{D.1}$$

Therefore is 70%, 80% and 90% combustion efficiency given when the n_s is 7.7, 8.8 and 9.9, respectively for the burning of one mole of heptane. The product composition from CEA-NASA is shown in table D.1.

It is chosen to use only the substance CO, CO_2, H_2, H_2O and N_2, because they together make up 99% of the combustion products. The combustion products are after the combustion mixed with the reaming air in the test room.

In fire scenario number two where an average of 11.32 kg heptane is burned, which results in a release of 3162.92 moles. In the test room there is 350 m^3 of air and with a density of 1.205 $\frac{kg}{m^3}$ the test room contain 421.75 kg of air. With a combustion efficiency of 90 % the air/fuel ratio is from CEA-NASA give to 13.71 which means that burning of 11.31 kg heptane needs 155.2 kg air. Therefore the combustion products mix with the remaining 266.55 kg air which also is equivalent to 9769 moles of air. Based on the number of total moles for the combustion products and the remaining air the mixing estimation for a combustion efficiency of 90% is shown in Equation D.2.

	70%		**80%**		**90%**	
Moles comb.	26.326		27.196		27.941	
	Mole frac. %	Moles	Mole frac. %	Moles	Mole frac. %	Moles
CO	10.087	2.655	6.751	1.836	3.247	0.907
CO_2	5.841	1.538	7.791	2.119	10.022	2.800
H	0.038	0.01	0.065	0.018	0.07	0.020
H_2	4.954	1.304	2.401	0.653	0.842	0.235
H_2O	13.224	3.481	14.157	3.850	14.188	3.964
NO	0.001	0.0003	0.011	0.003	0.079	0.022
N_2	65.843	17.334	68.765	18.701	71.27	19.914
O	-	-	0.001	0.0003	0.01	0.003
OH	0.012	0.316	0.056	0.015	0.199	0.056
O_2	-	-	0.002	0.0006	0.072	0.020

Table D.1. The combustion product mole fraction and mole composition for the three combustion efficiency 70%, 80% and 90%. The data is obtained by use of CEA-NASA.

$$\begin{aligned} &102.7\mathrm{CO} + 317.0\mathrm{CO_2} + 448.8\mathrm{H_2O} + 26.6\mathrm{H_2} + 2254.2\mathrm{N_2} + 9769.8\,(\mathrm{O_2} + 3.76\mathrm{N_2}) \\ &\qquad\qquad\qquad\qquad \rightarrow \\ &102.7\mathrm{CO} + 317.0\mathrm{CO_2} + 448.8\mathrm{H_2O} + 26.6\mathrm{H_2} + 38988.6\mathrm{O_2} + 9769.8\mathrm{N_2} \end{aligned} \tag{D.2}$$

The mole fraction of the different substance from Equation D.2 is given in Table D.2

Substance	Mole fraction [%]
CO	0.21
CO_2	0.64
H_2O	0.90
H_2	0.05
N_2	78.52
O_2	19.68

Table D.2. The mole fraction of the combustion products after mixing with the remaining air with an combustion efficiency of 90%.

In fire scenario two the steady state volume fraction of carbon monoxide is approximately 0.1%. By comparing the figures for carbon monoxide between the CEA-NASA calculation and the experiment, it is possible to conclude that the combustion efficiency must at least be 90% when only carbon monoxide is taken into consideration.

The calculation presented in this appendix is based on a number of assumptions:

- **Incomplete combustion:** It is assumed that the combustion efficiency is due to the lack of oxygen near the combustion area and the formation of carbon monoxide. In real fires the formation of soot, which is unburned carbon, also affects the combustion efficiency.
- **The Boudourad reaction:** It is assumed that the CO is not reacting with the oxygen to form CO_2. This assumption is acceptable because the reaction time for the boudourad reaction is very large compared to the duration of the experiment [Turns, 2000].
- **Closed Room:** The test room is assumed to be closed and new air is not drawn into the test room. The effect of this assumption is not known because in the real fire case smoke and fresh air flows in and out, respectively.

Hot Gas Layer - Height and Upper Temperature

E

This appendix contains a description of how the HGL height and the HGL upper temperature are determined. The method described below is the same method used for both the experiment and the FDS simulations.

The HGL height and the average upper temperature is estimated based on a continuous vertical profile of temperature. A continuous function of the temperature as a function of the height above the floor T_z, where $z = 0$ is the floor level and $z = H$ is the ceiling level. The upper temperature T_{up} and the lower temperature T_{low} are defined as the upper layer temperature and the lower temperature, respectively. Finally z_{int} is defined as the interface height. Then the quantities are determined with Equation E.1 and E.2 [Hostikka et al., 2001] and [McGrattan et al., 2012a].

$$(H - z_{int})\, T_{up} + z_{int} T_{low} = \int_0^H T(z)dz = I_1 \tag{E.1}$$

$$(H - z_{int})\, \frac{1}{T_{up}} + z_{int} \frac{1}{T_{low}} = \int_0^H \frac{1}{T(z)}dz = I_2 \tag{E.2}$$

The interface height z_{int} is then determine from Equation E.3 when T_{low} is taken from the lowest measuring point.

$$z_{int} = \frac{T_{low}\left(I_1 I_2 - H^2\right)}{I_1 + I_2 T_{low}^2 - 2T_{low}H} \tag{E.3}$$

The T_{up} is calculated as an average of the vertical temperature distribution $T(z)$ for $z > z_{int}$. The layer height and upper temperature are obtained via the device (DEVC) line, with the commands shown below, which finds the layer height, lower temperature and upper temperature at the x,y location 1.5,5.5 from 0-5 meter heights [McGrattan et al., 2012a].

```
&DEVC ID='NAME->HEIGHT',    QUANTITY='LAYER HEIGHT',         XB=1.5,1.5,5.5,5.5,0.0,5.0/
&DEVC ID='NAME->LTEMP',     QUANTITY='LOWER TEMPERATURE',    XB=1.5,1.5,5.5,5.5,0.0,5.0/
&DEVC ID='NAME->UTEMP',     QUANTITY='UPPER TEMPERATURE',    XB=1.5,1.5,5.5,5.5,0.0,5.0/
```

With the above described method the HGL height and HGL upper temperature are determined based on the vertical temperature distributions which means that the method is only valid when a HGL is formed. This is illustrated by looking at the ten seconds before and after the fire is started in fire scenario one, see Table E.1.

Time [s]	HGL height [m]	Time [s]	HGL height [m]
-10	3.75	0	4.07
-9	2.48	1	2.94
-8	3.12	2	2.48
-7	2.56	3	3.51
-6	2.12	4	2.98
-5	2.38	5	2.07
-4	3.39	6	3.51
-3	2.98	7	4.00
-2	3.59	8	3.61
-1	2.90	9	3.72

Table E.1. Experimental calculation of the HGL height in the first ten seconds before and after ignition.

From Table E.1 it is seen that before the fire is ignited and just after the HGL height varied between 2.12-4.07 m, which is not the reality. Therefore this method should be used with caution, in the initial stage of the fire, before a HGL is established.

In the NFSC2 the vertical temperature distribution has to be extrapolated in the area below the T_{low} thermocouple in the thermocouple rack. This also introduces an error in the calculation of the HGL height. In FDS the same method for calculating the HGL height and HGL upper temperature are used, but here the calculation is performed in the hole height of five meter corresponding to the calculation in NFSC2 where it is only caluclated from 1-4.5 m above the floor. This difference in the method of obtaining the HGL height gives a minor difference in calculation of the HGL height, which is illustrated in Figure E.1.

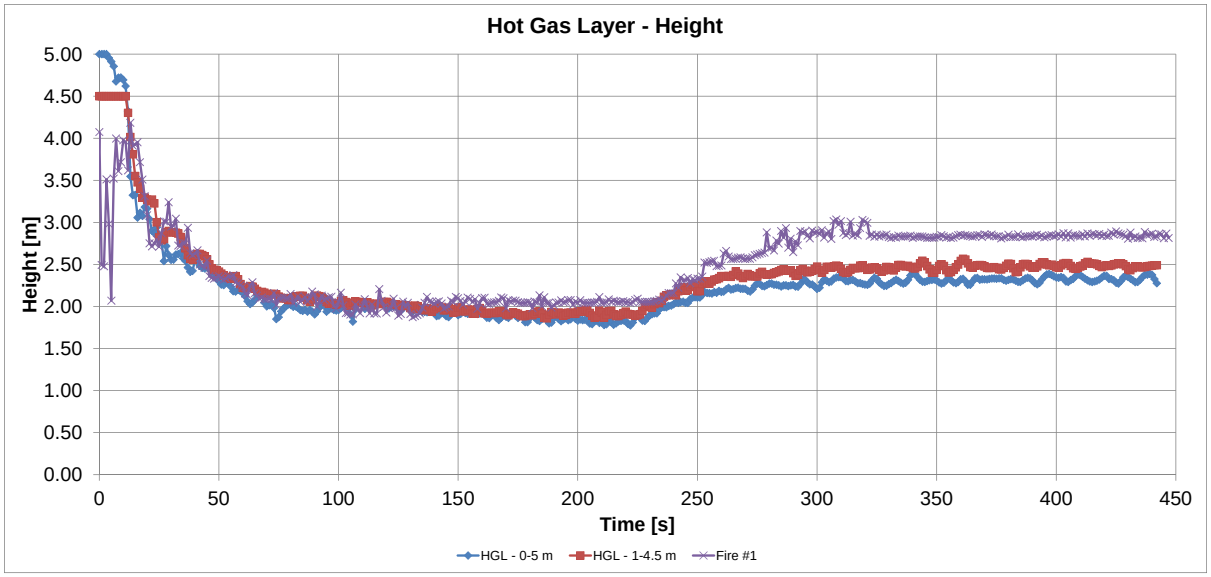

Figure E.1. Comparison of the difference between the HGL height obtained with calculation of the HGL height from 0-5 m or 1-4.5 m.

Because of the small difference between the two methods it is decided to calculated the HGL height and HGL upper temperature in FDS, where it is calculated on the vertical temperature distribution from 0 m to 5 m height.